

Pázmány Péter Catholic University

Faculty of Information Technology and Bionics

Bálint Péter Kerekes

**COMBINED TWO-PHOTON IMAGING,
ELECTROPHYSIOLOGICAL AND ANATOMICAL
INVESTIGATION OF THE HUMAN NEOCORTEX IN
VITRO**

Ph.D DISSERTATION



Budapest

2015

Contents

| | |
|---|----|
| Contents..... | 2 |
| List of abbreviations..... | 4 |
| 1 Introduction..... | 6 |
| 2 Main goals..... | 8 |
| 3 Brief overview..... | 10 |
| 3.1 The Cerebral Cortex..... | 10 |
| 3.2 Cell types..... | 13 |
| 3.2.1 Excitatory cells..... | 13 |
| 3.2.2 Inhibitory cells..... | 14 |
| 3.3 Electrophysiology..... | 15 |
| 3.3.1 Electrical properties of the brain..... | 17 |
| 3.3.2 Brain electric recording techniques..... | 18 |
| 3.3.3 In vitro and in vivo human brain tissue preparations for electrical recordings..... | 20 |
| 3.3.4 EEG graphoelements..... | 21 |
| 3.4 Epilepsy..... | 23 |
| 3.4.1 Tumor based epilepsies..... | 25 |
| 3.4.2 Cortical dysgenesis..... | 26 |
| 3.4.3 SPA and interictal activity..... | 26 |
| 3.5 Two-photon microscopy..... | 28 |
| 3.5.1 Theoretical background of two-photon microscopy..... | 29 |
| 3.5.2 Hardware of a two photon microscope..... | 31 |
| 3.5.3 Laser Sources..... | 32 |
| 3.5.4 Scanning Methods (x-y plane)..... | 33 |
| 3.5.5 Objectives..... | 34 |
| 3.5.6 Detectors..... | 34 |
| 3.6 Neuronal calcium signals..... | 35 |
| 3.6.1 Calcium indicators..... | 37 |
| 3.6.2 Calcium Imaging..... | 37 |
| 4 Materials and methods..... | 39 |
| 4.1 Patients..... | 40 |
| 4.2 Tissue preparation..... | 41 |
| 4.3 Electrophysiology recordings..... | 42 |
| 4.3.1 Laminar recordings..... | 42 |
| 4.3.2 Data transmission systems..... | 43 |
| 4.4 Micropipettes..... | 44 |
| 4.4.1 Local field potential..... | 44 |

| | | |
|-------|--|----|
| 4.4.2 | Intracellular | 45 |
| 4.5 | Multiphoton imaging | 46 |
| 4.6 | Multiphoton glutamate uncaging | 49 |
| 4.7 | Data analysis | 50 |
| 4.8 | Cell morphology..... | 51 |
| 4.9 | Electron microscopy..... | 52 |
| 5 | Results | 53 |
| 5.1 | Recording the spontaneous network activity by simultaneous Ca ²⁺ imaging and field-potential measurements | 53 |
| 5.2 | Intracellular recordings..... | 58 |
| 5.3 | Anatomy..... | 60 |
| 5.4 | Electron microscopy..... | 62 |
| 6 | Conclusion..... | 65 |
| 7 | Future plans | 68 |
| 8 | Acknowledgements..... | 69 |
| 9 | References..... | 70 |
| 10 | Publications..... | 80 |
| 10.1 | Papers | 80 |
| 10.2 | Posters | 80 |
| 10.3 | Presentations | 81 |

List of abbreviations

2P – two-photon

ACSF – artificial cerebrospinal fluid

AM – Acetoxymethyl

AMPA – α -amino-3-hydroxy-5-methyl-4-isoxazolepropionic acid

AO – acousto-optic

AP – action potential

BAPTA – 1,2-bis(o-aminophenoxy)ethane-N,N,N',N'-tetraacetic acid

BPAP – backpropagating action potential

BP5AP – 5 backpropagating action potential

CSD – current source density

DMSO – Dimethyl sulfoxide

ECoG – electrocorticography

EEG – electroencephalography

EPSP – excitatory postsynaptic potential

fMRI – functional magnetic resonance imaging

FRB – fast rhythmic bursting

FS – fast spiking

GABA – γ -amino-butyric acid

GECI – genetically encoded calcium indicator

IB – intrinsic burst

IC – intracellular

IP3R – inositol trisphosphate receptors

IPSP – Inhibitory postsynaptic potential

LFP – local field potential

LFPg – local field potential gradient

mGluR – metabotropic glutamate receptors

MR – magnetic resonance

MTLE – medial temporal lobe epilepsy

MUA – multi-unit activity

NA – numerical aperture

nAChR – nicotinic acetylcholine receptors

NCX – sodium-calcium exchanger

NMDA – N-methyl-D-aspartate

OGB-1 – Oregon green BAPTA-1

PMCA – plasma membrane calcium ATPase
PMT – photon multiplier tube
Pt - patient
ROI – region of interest
RS – regular spiking
RyR – ryanodine receptors
SC – stellate cells
SD – standard deviation
SERCA – sarco-/endoplasmic reticulum calcium ATPase
SNR – signal to noise ratio
SPA – Spontaneous synchronous population Activity
SR101 – Sulforhodamine 101
SUA – single-unit activity
TLE – temporal lobe epilepsy
TRCP – transient receptor potential type C
VGCC – voltage-gated Ca²⁺ channel

1 Introduction

Epilepsies are one of the most common neurological disorders in humans. According to the definition of the WHO, epilepsy is a chronic brain disorder, with different etiology, characterized by spontaneous recurrent seizures emerging from the excessive and pathologically hypersynchronous firing of a large amount of neurons [1] [2].

Though a large variety of antiepileptic drugs are available nowadays, a significant number of patients are pharmacoresistant [3]. In those cases, where the epileptic focus can be precisely localized epilepsy surgery is a possible solution for blocking seizures [4].

Healthy neocortical tissue is also routinely removed due to surgical technical reasons from patients with tumor but without epilepsy, when the pathological mass is localized in the subcortical areas. Comparing the morphology and activity of epileptic and non-epileptic human brain tissue offers an excellent possibility to investigate the normal and impaired neuronal mechanisms at the network, single cell and subcellular levels [5] [6] [7] [8].

Spontaneous synchronous population activity (SPA) can be observed in vitro during extracellular electrophysiological recording of local field potentials (LFP) in epileptic human neocortical slice preparations in physiological bathing medium (according to our unpublished observations, [6] [9] [10]). These synchronous population bursts consist of rhythmically recurring extracellular LFP deflections associated with high frequency oscillations and an increased neuronal firing [6]. Both glutamatergic excitatory and GABAergic inhibitory signaling is involved, pyramidal cells show either depolarizing or hyperpolarizing and even mixed responses during SPA (according to our unpublished observations).

Calcium imaging of neurons is widely used to monitor cellular activity in animal slice preparations (for review see [11]) however, we have only limited knowledge about Ca^{2+} concentration changes in human neurons. Calcium imaging of human neurons was investigated in cells differentiated from induced pluripotent stem cell lines [12], and in cultured neurons of the enteric nervous system [13]. Furthermore, a recent study shows spontaneous Ca^{2+} elevations in human neocortical and hippocampal astrocytes [14], but nothing is known about the intracellular Ca^{2+} properties of neurons derived from native human tissue of the central nervous system.

While two-photon Ca^{2+} imaging technique has high spatial resolution ($<1 \mu\text{m}$), it can cover only a relatively small area of interest ($<1 \times 1 \text{ mm}$). On the other hand, multiple channel extracellular electrophysiology can cover large cortical areas (3-4 mm) at the expense of its low spatial resolution (100 μm). The activity of neurons restricted to one or two cortical layers (<1

mm) can be monitored with two-photon imaging, whereas multiple channel extracellular electrophysiology is needed to record the activity of neurons in the entire depth (3-4 mm) of the human neocortex. The temporal resolution of the two techniques is also different: electrophysiological changes reflecting neuronal activity are considerably faster (<1 ms) than changes in intracellular Ca^{2+} (usually more than 100 ms). Combining these two methods has several advantages. First, it helps us to gain more information on the role of different neurons in the emergence of population activity. Recording with the aid of the linear multielectrode gives information about the fast electrophysiological properties of SPA, detected in all neocortical layers, whereas Ca^{2+} imaging reveals the activity of a relatively large group of neighboring neurons (tens of bulk loaded cells), and their contribution to the generation of SPA. In addition, two-photon microscopy can detect inactive neurons, which are unnoticed in extracellular electrophysiological recordings. Second, the simultaneous use of Ca^{2+} imaging and whole cell patch clamp recording helps us to correlate electrophysiological activity and Ca^{2+} signals in human neurons. One can simultaneously observe and manipulate the membrane potential fluctuations of neurons with intracellular patch clamp recordings and relate to changes in their Ca^{2+} concentrations. Completing these measurements with the detection of extracellular activity we can relate electrophysiological and Ca^{2+} signals of neurons active during SPA. In addition to Ca^{2+} imaging, two-photon uncaging can be used to investigate neuronal input-output functions and postsynaptic signal integration. Cell filling and anatomical reconstruction at the light and electron microscopic level may add important morphological information about the subcellular, cellular and network properties of human neocortical neurons.

2 Main goals

SPA can be detected with electrophysiological methods in cortical slices of epileptic patients, maintained in physiological medium *in vitro*. With EEG, and LFP measurements we can only have informations about the summarized activity of a group of neurons. We can't show how many of the neurons (and which type) were active, and especially how many weren't even involved in the discharge in the LFP. We wanted to gain additional spatial information about the network mechanisms, and the cells which are involved in the SPA generation, so we needed a new methodology.

The aim of the thesis was to develop a method combining multiple channel extracellular electrophysiology, simultaneous intracellular recording, and two-photon Ca^{2+} imaging or uncaging supplemented by fine scale morphological analysis, to make it possible to understand what is going on in the individual cells behind the LFP.

Here we report for the first time the two-photon Ca^{2+} imaging of human neocortical neurons derived from epileptic and non-epileptic brain tissue.

Neocortical slices prepared from postoperative tissue of epileptic and tumor patients were maintained in a dual perfusion chamber in physiological incubation medium. SPA was recorded with a 24 channel extracellular linear microelectrode covering all neocortical layers. After identifying the electrophysiologically active regions of the slice, bulk loading of neuronal and glial markers was applied on the tissue. SPA related Ca^{2+} transients were detected in a large population of neighboring neurons with two-photon microscopy, simultaneously with extracellular SPA and intracellular whole cell patch clamp recordings. The intracellularly recorded cells were filled for subsequent anatomy. The cells were reconstructed in three dimensions and examined with light- and transmission electron microscopy.

This complex method -combining high spatial resolution two-photon Ca^{2+} imaging techniques and high temporal resolution extra- and intracellular electrophysiology with cellular anatomy- is suitable to reveal subcellular, cellular and network properties of human neocortical neurons engaged in spontaneous population activity and may permit a deeper understanding of the structural and functional properties of the human neocortex. The methodological difficulties we faced during the experiments will also be described.

This work is structured around the following theses on the basis of the above-mentioned aims.

Thesis I: A method has been developed for the two-photon Ca^{2+} imaging of human neocortical tissue (see in the Materials and methods section).

Thesis II: The extracellular recording system was successfully combined with the two-photon microscope system. This way the epileptic and non-epileptic human neocortical neurons Calcium responses during SPA was compared.

Thesis III: The functional coupling of LFP, Calcium responses and intracellular activity in human neocortical interneurons and pyramidal cells during SPA will be demonstrated.

Thesis IV: The electrophysiological and imaging measurements were successfully combined with anatomical reconstruction of the intracellularly loaded cells, to gain more information of the morphology of the loaded cells.

Thesis V: The electron microscopic ultrastructure of the filled and reconstructed pyramidal cell will be described at electron microscopic level.

3 Brief overview

There will be an overview of the fields necessary to understand the research.

The anatomy and physiology of the cerebral cortex will be presented.

The electrical properties of the brain and the different electrophysiological measurement types will be introduced.

We will present the necessary informations about epilepsy and some pathophysiology, which were involved in this study.

We will provide the LFP signals which upon this study is started, and the principles of Spontaneous synchronous Population Activity. How the LFP signal was defined first, and how its understanding developed. Based on these foundations the importance of the method described in the “Materials and methods” section will be discussed.

We will discuss the field of two-photon microscopy, its phenomenon, and the calcium imaging’s significance in this study.

3.1 The Cerebral Cortex

In this chapter, there will be an overview of the structure and function of the cerebral cortex, because in this research we focus mostly to this part of the brain. The basic cell types, and their role in the system will be also presented.

The cerebrum is covered by the cortex which is the largest portion of the brain. The cortex width is between 2-4 mm in humans, (depending on which area we take). The cortex takes a key part in many higher order processes, like remembering, attention, speaking, learning, and so on. Its surface is around 220.000 mm², 560 cm³ volume, and 581 g weight in humans [15] [16].

The cortex contains around 14-16 billion neurons, and each of them can connect to more than 10.000 neurons. The phylogenetically older part of the cortex cerebri called allocortex, it contains the archicortex (hippocampus and dentate gyrus) and paleocortex (parahippocampal gyrus, olfactory cortex), the other part called isocortex (neocortex).

There are two distinct compartments of the brain, one is the white matter which contains mostly long myelinated fibers, the other is the gray matter, which contains the cell bodies, a high amount of short fibers, and most of the synapses [17].

In the brain development the cortex grows quicker than the white matter, this is how its fissures (deep ditches), sulcuses (shallow ditches) and gyruses (bossings between the grooves) are formed, and this is how the skull can contain this huge amount. However, this gyrification brings more than functional advantages, for instance, the connection between areas are much shorter. The two hemispheres of the cerebrum are severed by the fissure longitudinalis [18].

In the cortex, we can differentiate 4 major lobes, the frontal, the parietal, the occipital, the temporal lobes, and there are a little part in the lateral cerebral sulcus, the insular cortex.

The frontal lobe is bordered by the lateral cerebral sulcus, and the sulcus centralis. In the frontal lobe, we can find the area of voluntary movement, higher intellectual functions, pain, Broca's motor speech, and well-being.

The parietal lobe is bordered by the sulcus centralis in the front, the parietooccipital fissure in the back, and the lateral cerebral sulcus in the lower side. The parietal lobe integrates sensory information among various modalities.

The occipital lobe is bordered by the parietooccipital fissure in the front, in the convex, and the basal surface, the occipital lobe is not separated harshly by the parietal, and the temporal lobes. The occipital lobe is the primer visual area of the brain.

The temporal lobe is severed from the frontal, and parietal lobes by the lateral cerebral sulcus. Its major role is auditory, but has other functions as well, like process sensory input into derived meanings, the retention of visual memories, language comprehension, and emotion association [19].

We can part the cortex based on cytoarchitectural differences into 52 areas [20]. There was a more detailed division some years after Brodman's work [15] which made 109 different area, and there are some newer detailed division nowadays (see in [21] [22] [23]), but the Brodman nomenclature is the most commonly used by scientists.

In the depth of the neocortex the neural cells forms 6 layers (Figure 1.):

Layer I. stratum zonale (plexiform): mostly fibers, stellate cells

Layer II. stratum granulosum externum: small granule cells, small pyramidal cells

Layer III. stratum pyramidale: small pyramidal cells

Layer IV. stratum granulosum internum: granule cells

Layer V. stratum gangliosum (stratum pyramidale internum): big pyramidal cells

Layer VI. stratum multiforme: spindle-, pyramidal cells

It is suggested [19] that the basic structural and functional component of the neocortex is the cortical column, which extends the whole cortical depth and 200-300 μm in diameter.

The cortex has 2 millions of these columns or modules, each contains 5000 cells. All of the modules sends axons to 50-100 other modules, and receives the same amount of afferents, which shows us the complexity of the neocortex [19].

Every region of the cortex has the same types of neurons, and in the connections between the different types of neurons are alike.

The neurons in the cortex can be separated by many aspects, like neurochemical and electrophysiological nature, or morphology. There are cells which use γ -amino-butyric acid (GABA) neurotransmitter molecules for inhibition, or others which use glutamate for excitation [24].

Based on morphological classifications, the pyramidal cell got its name from the shape of the soma. The pyramidal cells are responsible to form the most of the associational, commissural and projection pathways. The stellate (granular) cells, which makes short local networks. The basket cells axons go around the pyramidal cells bodies, while the chandelier cells connect mostly the axon initial segment of the pyramidal cells, and they make a local network. The disinhibitory cells axons go through all the layers of the cortex to cause inhibition on inhibitory cells.

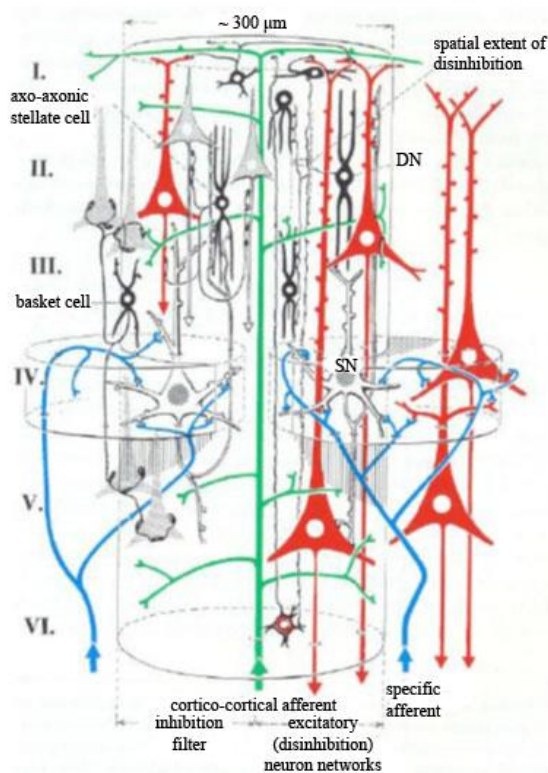


Figure 1. A schematic of a cortical column. How the cells are arranged in the depth of the 6 layer (roman numerals refer to the layers), how the afferent and efferent connections are, and how the disinhibitory network is arranged. The red cells are pyramidal cells, black cells are inhibitory neurons, the green is a cortico cortical afferent fiber, blue lines are specific sensory afferents, (DN = disinhibitory neuron (axon reaches through all the layers), SN = spiny neuron (transmits excitatory nerve impulses)) [19].

A third partition can be made based on the spines (spines are the dendrite buttons, where the synapses are). Pyramidal cells and spiny stellate cells have a lot (mostly communicate via glutamate), but smooth stellate cells (mostly communicates via GABA) have few of the spines.

We can separate the cells by their electrophysiological properties as well. With intracellular current injections we can depolarize the cells in vitro or in vivo and they show different kinds of responses. [25] [26] [27] [28]. Some are fast spiking (FS) some regular spiking (RS), intrinsic burst (IB), and fast rhythmic bursting (FRB) neurons. [28] [29]. The firing can

be adapting, then the firing rate changes by the continuous excitation, or non-adapting, then the firing rate does not change.

The FS neurons can hold a high firing rate (tonic firing) without frequency adaptation, and the action potentials (AP) are short (~0.3 ms). There are inhibitory cells mostly in FS type.

The RS neurons respond quickly or slowly adapting AP sequences to the excitation (most of the pyramidal cells are RS type).

The IB cells respond with bursts for threshold current excitation, and they are followed by relatively long after hyperpolarization (these cells have many spines on their apical dendrites, and they can be found in each layer, except the first) [30] [31].

The FRB cells respond with frequently emerging (30-50 Hz) high frequency bursts (300-600 Hz) for depolarizing current. A portion of these cells are in the deep layers of the cortex, other types are local network making and have a lot or few spines [29].

The classification of the cells by firing rate can be problematic, because by the change of the membrane potential, the modulatory systems activity or the level of alertness can change from one firing type to another [32].

3.2 Cell types

3.2.1 Excitatory cells

The most commonly known cell type in the neocortex is the pyramidal cell, it is easily detectable in Nissl-stained slices. From the cone like soma's tip (tip points to the surface, bottom to the white matter) one big dendrite goes towards the cortex surface (apical dendrite), there are some dendrites all around their base.

Almost every pyramidal cell's apical dendrite reaches the layer I. Only exceptions are the pyramidal cells in layer VI. they reach just to layer IV. [33]. The basal dendrites of the layer III. pyramidal cells go towards the layer IV., where they get thalamocortical synaptic inputs. In layer IV. the pyramidal cells have diverse morphology: pyramidal cells with horizontal dendrite tree, bipolar pyramidal cells (they got a main dendrite to towards the surface of the cortex, and one towards the white matter), upside-down pyramidal cells (the tip of their soma looks in the direction of the white matter) [33]. The apical dendrite have many branches in the layer I. called dendritic tuft. The dendrites of the pyramidal cells have many spines. The axon starts from the base of the cell, with only a few collaterals in the beginning till the white matter.

By the electron microscopy terminology there are asymmetrical and symmetrical synapses. Symmetrical synapses are mostly inhibitory, asymmetric synapses are excitatory.

Synapses of the pyramidal cells are mostly asymmetric, but on their soma, axon initial segment, and proximal dendrites they get symmetrical synapses from inhibitory neurons. On the

distal dendrites the synapses are mostly on the spines, and they are asymmetrical, and both types can be found on the dendrite body. This gives rise to the opinion that the main role of inhibition of the pyramidal cell is total inactivation, and AP-s can only occur by a sum of many excitatory synaptic inputs [33].

There are 4 different sizes of pyramidal cells, small (1-12 μm), medium (20-25 μm), big (45-50 μm) and giant (70-100 μm) (for example Betz cells in the layer V.) [33]. The pyramidal cells are either RB or IB type firing. The RS type pyramids in layer V. are slender tufted, with little branching in layer I., the IB cells on the other hand are thick tufted, and have a large branching near the surface of the cortex [30] [34]. Star pyramidal cells are in between pyramidal cells and stellate cells. They have an apical dendrite (they do not reach to layer I., and just a few branches), and the basal dendrites are symmetrical [35]. Their soma are not pyramid like. The axon of the star pyramidal cell goes to layer II., III., and IV. of the cortex, some branches reach layer V., VI.

Stellate cells (SC) are separable by spine density in two distinct group: smooth, and spiny.

The spiny stellate cells have multipolar star-like cell body (mostly in layer IV.), the dendrites go from that in each direction, and the branching starts quite close to the soma, and densely spined [33]. Their axon reaches towards the white matter, but branches the close to the soma (sometimes it gives a collateral which ends in the upper layers). They give excitatory asymmetrical synapses. The spiny SC-s get symmetrical synapses to their soma, and proximal dendrites. On the distal dendrite tree, they get a few symmetrical synapses, but mostly excitatory asymmetrical presynaptic connections to the spines. There are big and small sized spiny SC-s [36]. The axon goes through the white matter to other cortical areas in case of the big size Spiny SC-s, the small type has only local branches. In some cortical areas, where there are minimal Spiny SC, this way there is no real layer IV. (like in motor cortex) [19].

3.2.2 Inhibitory cells

The smooth stellate cells and the spiny SC-s have a morphological similarity in soma (10-30 μm diameter), and dendrite tree. Smooth SC's axon branches locally in the cortex, it uses symmetrical GABA synapses. Smooth SC get different pattern input from those of pyramidal, and spiny SC. On the soma they have some excitatory, and mostly symmetric inhibitory synapses. On the distal dendrites it is almost the same, but the synapses are mostly asymmetrical. Due their locality, they are often called interneurons. Smooth SC-s are the most heterogeneous group of the above cell types. There are at least 7-8 or even more different inhibitory cell groups by morphology [37]. According to dendrite morphology, there are bipolar, and bitufted. The axon endpoint also can be a basis for classification.

Chandelier cells axons go to the axon initial segment of pyramidal cells. Basket cells make synapses on pyramidal cell somas (with big or small basket). The others innervates mostly the dendrites [37] [38] [39]. The Martinotti cells which are multipolar interneurons with short branching dendrites, with an axon going to the cortex surface. The Cajal-Retzius cells, which are small neurons, the axon goes parallel with the surface (the Cajal-Retzius cells are rare in adults, if there are any).

By staining immunohistochemical agents the different cells stains differently, by these markers the inhibitory cells can be differentiated as well: by calcium-binding proteins (calbindin, calretinin, parvalbumin), or by neuropeptides (vazointestinal peptide, cholecystokinin, and somatostatin). For communication with other interneurons, they use gap junctions as well.

The electrophysiological properties of the interneurons are very diverse too. In general, they are non-adaptable FS cells, or low threshold firing adaptables, but there are more than 10 other type as well according to their spontaneous, and evoked firing pattern [40]. In the cortex, 85-90% of the cells are excitatory (75% pyramidal, 10% stellate cell), and 10-15% inhibitory [33].

3.3 Electrophysiology

In this chapter, we will introduce the principles of the bioelectric signals in the brain, and the electrophysiological measuring methods. Biological information is processed and communicated by various physical modalities, but the electrical behavior e.g. action potentials, synaptic and intrinsic membrane currents and underlying mechanisms of cells and tissues are studied by electrophysiology.

It is well known that the electrophysiological signals are based on the ion composition (and its alteration) of the two sides of the cell membrane. Inside the cell the concentration of K^+ and negatively charged proteins are higher, outside the Na^+ , and Cl^- concentration is higher. The transport of the ions are made by ion channels, and transporter proteins. The ion channels current state (open-closed), the permeability and the concentration gradients of the different ions can alter the membrane potential. The membrane potential can be calculated by the following equation in a steady state (Hodgkin-Katz-Goldman) [41]:

$$U = \frac{RT}{F} \ln \frac{P_K[K]_k + P_{Na}[Na]_k + P_{Cl}[Cl]_b}{P_K[K]_b + P_{Na}[Na]_b + P_{Cl}[Cl]_k}$$

R is the gas constant [8.413 J/ (mol*K)], T is the absolute temperature (310 K), F is the Faraday constant ($9.649 \cdot 10^4$ C/mol), P is the permeability of the fitting ion. Typically the resting membrane potential of a neocortical pyramidal neuron is ~ -65 mV.

If the membrane potential (by some stimuli or by the effect of some presynaptic cell) moves in the positive direction, it is called depolarization, if it goes more into the negative than the process is called hyperpolarization. Chemical or electrical signaling between cells are made by synapses. If some information (for example action potential) comes from the presynaptic cell then Ca^{2+} flows into the presynaptic terminal and neurotransmitters are released to the synaptic gap, then the neurotransmitters connects to the receptors of the postsynaptic cell. If it is an excitatory neurotransmitter like glutamate, then the postsynaptic cell depolarizes (Excitatory postsynaptic potential occurs (EPSP)) by the Na^+ inflow, if it is an inhibitory neurotransmitter like GABA then it hyperpolarizes (Inhibitory postsynaptic potential occurs (IPSP)) by the Cl^- channels opening. If these potentials reach the soma, and the summarized EPSP-s and the IPSP-s go beyond a threshold depolarization level, then action potential (AP) occurs, and thereafter the AP is transmitted towards the axon terminal [19] [42] [43] [44]. The axon initial segment is the place of the AP initiation, because of the vast amount of voltage dependent Na^+ channels. The AP conduction on the axon is described by the Hodgkin Huxley equation:

$$C_m \frac{dV_m}{dt} + I_{ion} = I_{ext}$$

C_m is the membrane capacitance, V_m is the intracellular potential, t is time, I_{ion} is the current going through the membrane, I_{ext} is the external current applied. The ion current which goes through the membrane channels consist of the Na, K, and leaking currents (Figure 2.).

$$C_m \frac{dV_m}{dt} = I_{Na} + I_K + I_L + I_{ext}$$

The membrane can be modeled by a circuit. In this model there are some conductances which should be the result of open membrane channels. Many ion channel has gates which can block the ion flow through. If these gates are open then by the in- or outflow of the corresponding ion (depending on the concentration gradient) the membrane potential alters closer to the corresponding ions equilibrium potential.

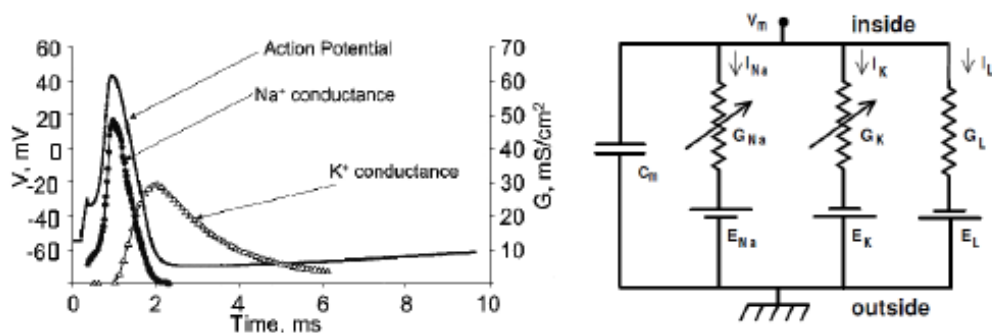


Figure 2. Left) The different channel conductance changes during the action potential. Right) The axon's (membrane, channels) replacement wiring diagram. G = conductance, I = ioncurrent, E = reverse potential, L = leaking [41] [45].

3.3.1 Electrical properties of the brain

In this chapter the basic properties of bioelectric field potentials and characteristic brain rhythms emerging during different vigilance states in humans will be described. The electric fields generated by neuronal activity can be measured with various electrophysiological methods. Electroencephalography (EEG), which is one of the most widely used techniques to record the potential changes in the brain, will be the main method through which the features of the different neuronal oscillations are demonstrated in this chapter.

Field potentials recorded with the EEG on the scalp represent the summation of the synchronous synaptic activity of a myriad of cortical neurons which have similar spatial orientation. On the level of the single neuron, excitatory postsynaptic activity originating on the dendrites generates an inward current flow into the cell (active sink) at the site of the origin, with a simultaneous outward current on the soma (passive source), latter acting as a return current [46]. The electric field generated by this current dipole can be detected with voltage recording electrodes. In a simplistic view, the field potentials registered with the EEG are the resultant of thousands of spatially and temporally superponed dipoles. If the activity of the neurons is temporally synchronized, then the recorded EEG signal contains high amplitude waves with low frequency (synchronized activity). On the other hand, if the activity is temporally asynchronous, low amplitude waves with high frequency can be detected (desynchronized activity). However, the amplitude and frequency content of the EEG signals depends on various factors: e.g. the age of the patient, the vigilance state, and certain diseases can alter these properties as well.

Based on the frequency of the recorded bioelectric field potentials, we can characterize different brain rhythms or oscillations, including the first-discovered and well-known alpha waves [43].

1. Delta (1-4 Hz): Delta waves belong to the brain rhythms with the lowest frequency. The activity of neuronal populations is highly synchronized during delta oscillations, therefore high amplitude waves can be recorded on the entire scalp. This particular brain rhythm arises in the thalamus and neocortex during the deepest stage (slow-wave sleep) of the non-rapid eye movement (NREM) sleep in adults. High amount of delta waves recorded in the awake state usually refers to pathological conditions (e.g. brain tumor).
2. Theta (4-8 Hz): Theta waves are faster compared to the delta rhythm. In humans theta rhythm can be recorded with the EEG during stage 2 of the NREM sleep, but it can occur in meditation in the limbic cortical areas as well [43]. There is another type of theta rhythm which was observed in the hippocampus of rodents during exploration of their environment and during rapid eye movement (REM) sleep [46].

3. Alpha (8-13 Hz): The alpha waves were discovered by Hans Berger, the inventor of the EEG. This brain rhythm can be recorded on the occipital sites of the EEG during periods of eyes closed, but they are present during stage 1 of the NREM sleep as well [46].
4. Beta (13-30): Desynchronized activity with higher frequency oscillations (>13), such as beta and gamma rhythms are the characteristic features of the awake state. Beta waves are present in adults on the frontal and central cortical areas and are associated with active thinking, attention, focusing and problem solving [46].
5. Gamma (30-80 Hz): The neuronal mechanism underlying the gamma waves is actively researched, and this phenomenon may have a major role in the conscious perception (e.g. the binding problem, see ref. [32] [46] [47] [48] [49]). These waves are the hallmark of the awake and attentive brain, where desynchronized activity with low amplitude EEG signals can be observed.

3.3.2 Brain electric recording techniques

Measurements of brain electrical properties require a connective medium between the tissue and the recording device. The connective medium is called electrode, which is formed by an electron conductor placed in an electrolyte [50] [51]. In order to measure potential differences, such as brain electric potentials, at least two electrodes are needed. One electrode is always placed over active tissue. Placement of the other electrode can be also over active tissue, in which case the recording is bipolar. When the second electrode is placed over a zero potential area as a reference electrode, the recording is called monopolar. Both arrangements are widely used in research, so several different properties should be carefully taken into account when choosing one of them for a specific experiment [50].

Brain electric potentials can be both recorded from outside and from inside the brain (Figure 3.). EEG recorded from the scalp and ECoG recorded from the brain surface are the two typical recording techniques for measuring potentials outside the brain. Extracellular and intracellular recordings are the two main types of electric potential measurements performed in the brain.

Extracellular recordings are carried out by placement of a recording electrode in the extracellular medium. Recording electrodes can be metal wires, silicon microprobes with metal recording contacts or glass micropipettes filled with electrolyte solution and connected to an Ag/AgCl electrode. Extracellularly, local field potentials (LFP), multiunit (MUA) and single unit activity (SUA) can be measured. SUA is obtained from MUA recordings when the electrode arrangement, such as tetrode configuration, allows for sorting of recorded spikes based on their

waveform characteristics [50]. MUA and SUA are only recorded from neurons in close proximity of the electrode, since action potential waveforms quickly vanish in the highly conductive extracellular medium [50] [52]. Using multichannel extracellular electrodes enables recording activity from larger brain areas, such as several cortical layers or multiple subcortical nuclei simultaneously. Extracellular recordings can be performed both *in vitro* in prepared brain slices or tissue cultures and *in vivo* in anesthetized or freely moving subjects. Potentials recorded extracellularly are in the μV range.

Intracellular recordings are performed inside a single cell. For this purpose glass micropipettes are always used. The two main types of intracellular recording electrodes are sharp and patch electrodes. A sharp electrode has a tip less than 1 μm thick which can easily penetrate the cell membrane [53] [54]. Sharp recordings are mostly performed in brain slices and carried out in current clamp mode. Current clamp mode means injecting constant current into the cell and measuring resulting membrane potential changes, which are in the mV range. Sharp recordings are used to measure whole-cell membrane potential dynamics but are not able to record single channel potential changes [53] [54]. For this purpose the patch recording technique is widely used. Patch electrode tips are thicker than the tips of sharp electrodes; their thickness is about 1 μm [53] [54]. In contrast to the sharp electrode technique, patch electrodes do not penetrate the cell membrane but form a tight seal on a small patch of the membrane. There are four different types of patch recording [53] [54]. Firstly, cell attached technique means that the patch pipette is tightly attached to the intact cell membrane with negative pressure. In contrast, whole-cell patch recordings are carried out by attaching the recording micropipette to the cell membrane and then ripping the membrane patch inside the micropipette. The other two patch clamp techniques, inside-out and outside-out patch clamp, are performed on membrane patches ripped off the cell. The difference between the two techniques is the side of membrane facing the electrolyte solution in the micropipette. In patch clamp recordings, both current and voltage clamp modes are used. Opposed to current clamp mode, in voltage clamp mode the amount of injected current required for keeping the voltage of the membrane patch at a constant level is measured [53] [54]. Single cell recordings during hippocampal SPA described in this dissertation were made using whole-cell patch clamp in current clamp mode.

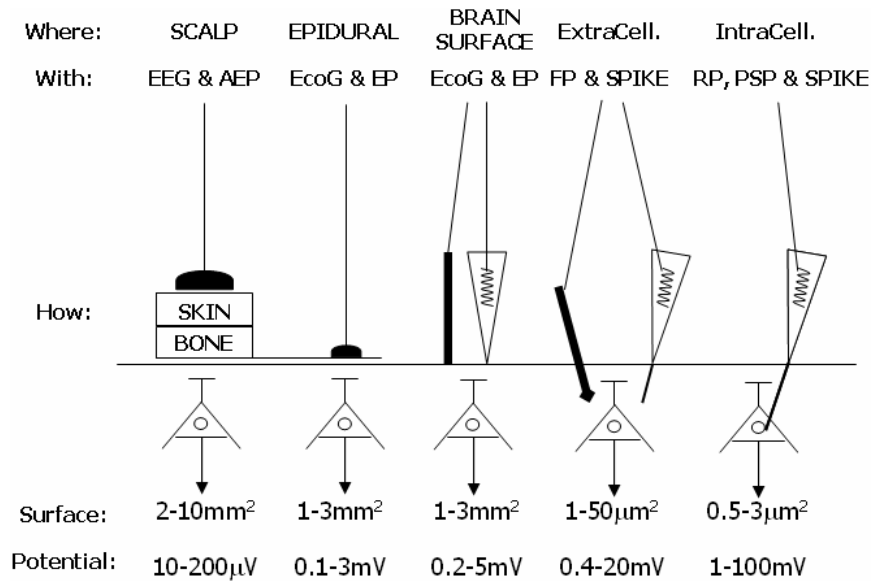


Figure 3. Recording techniques (EEG: Electroencephalogram, AEP: Auditory Evoked Potential, EcoG: Electroencephalogram, EP: Evoked Potential, FP: Field Potential, RP: Resting Potential, PSP: Post-synaptic Potential [51])

3.3.3 In vitro and in vivo human brain tissue preparations for electrical recordings

Electrical recordings from human brain tissue can be either made from different tissue preparations or from the brain of a living patient. In vitro preparations have the advantage of easy manipulation but provide limited access to mechanisms in an intact brain [53]. The easiest way to measure electrical potentials from brain cells is the recording from isolated brain cell cultures. These cultures can be tested in many different conditions by just changing the ingredients of their bathing solution. Heterologous expression systems are cell cultures that express a foreign gene coding for example an ion channel [53]. These systems allow for easy testing of different ion channels in a controlled way. However, in vitro tissue preparations closest to the intact brain are acute brain slices. These slices are kept in a solution called ACSF, which closely resembles the cerebrospinal fluid in the brain. Acute brain slices contain small networks of neurons so that measurements of these slices can reveal valuable information about functions of neuronal networks in the brain [53]. Results of this dissertation were obtained from recordings performed on human acute brain slices.

While all of the previously described extracellular and intracellular recording techniques can easily be used in in vitro tissue preparations, in humans in vivo only extracellular recordings can be performed. However, in vivo recordings have the great advantage of recording from a tissue in its whole physiological environment. Human in vivo recordings are always carried out in subjects undergoing therapeutic brain surgery [55] [56]. Brain surgeries are

preceded by simultaneous video and EEG recordings and also by different brain imaging sessions to localize the area for surgery. During surgery, different recording electrodes are implanted onto the surface of the brain, such as grid and strip electrodes, or into the brain, such as the thumbtack electrode [55] [56](Figure 4.). Recordings by such electrodes are of great value since they are obtained from tissue that is later removed and used in *in vitro* recordings. This allows for direct comparison of data recorded from different tissue preparations [55] [56].

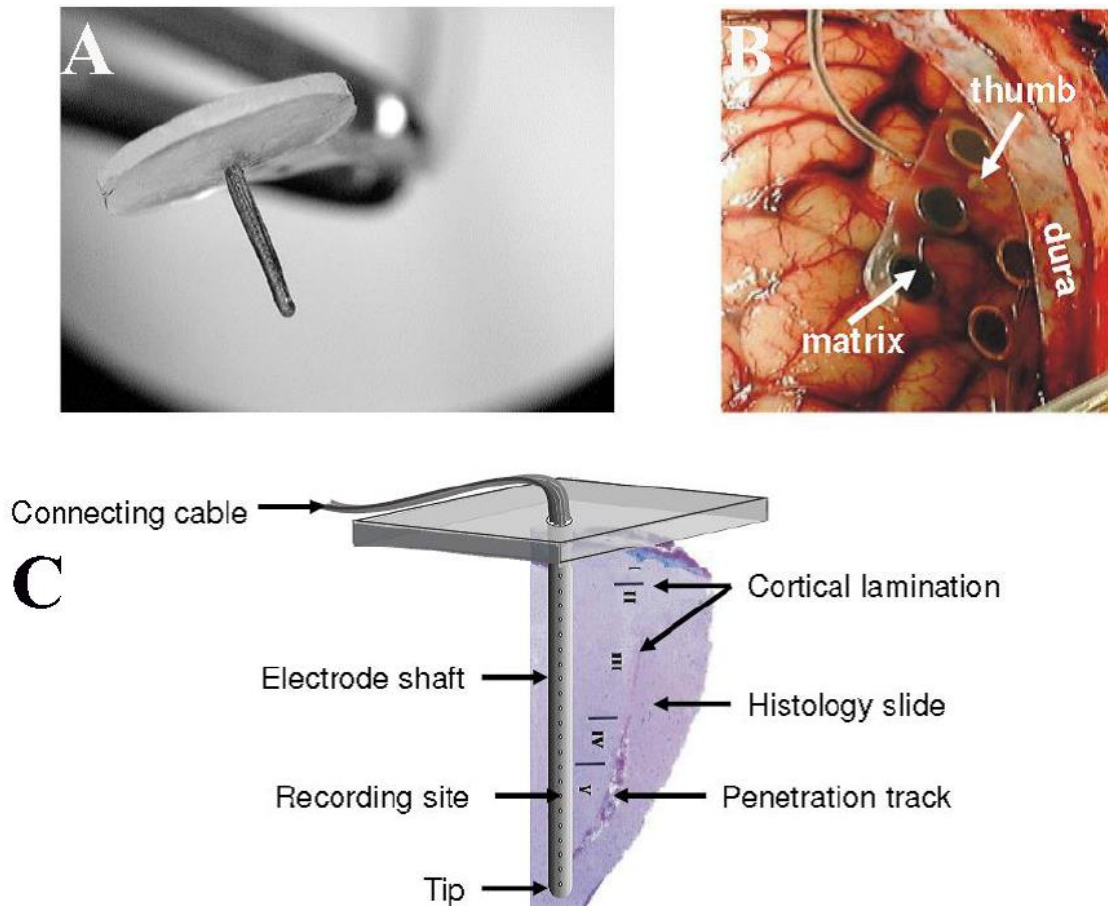


Figure 4. Subdurally implantable thumbtack- (A and C), and grid electrode (B) [55].

3.3.4 EEG graphoelements

EEG graphoelements are manifestations of brain electrical activity recorded on the scalp. These elements are results of both spontaneous and evoked potential changes in the brain. Graphoelements help in categorizing and describing EEG recordings, thus providing a powerful tool for both researchers and clinicians. In 1924, Hans Berger described the first EEG graphoelement as the alpha wave, which is measured from occipital areas during wakefulness with eyes closed [57] [58]. As such, the definition of alpha wave is as old as the EEG recording technique itself. Since then, several different EEG graphoelements were introduced.

From a healthy brain, various categories of graphoelements can be recorded [48]. Regular rhythmical oscillations are mostly recorded during slow wave sleep and characterized by low frequency and high amplitude waves. Certain frequency sinusoidal waves are characterized by a single frequency and appear as a sinusoid-like wave on the recording. One of the most easily recognized certain frequency sinusoidal wave is the alpha wave. In many cases, certain frequency waves do not appear and disappear instantly but form waxing and waning oscillation snippets, called spindles. These spindles can be observed in many cases, such as sleep spindles during the deepening phase of slow wave sleep or alpha spindles during eyes closing in wakefulness. The most prevalent EEG graphoelements during a resting wakefulness with open eyes are the irregular arrhythmical EEG waves. These consist of various frequencies and reflect the ongoing activity of the wake brain. More complicated graphoelements which consist of many different frequency waves are called complexes. The most well-known complex in the EEG is the so called K-complex which can be observed during stage-2 non-REM sleep in humans [48].

In addition to the graphoelements recorded from a healthy brain, several EEG graphoelements can be indicative of pathological phenomena (Figure 5.). The most prevalent pathological graphoelements are the sharp waves, spikes, spike and wave complexes, polyspikes and polyspike and wave complexes [48]. These elements play a key role in diagnosing and localizing pathologies such as epilepsy.

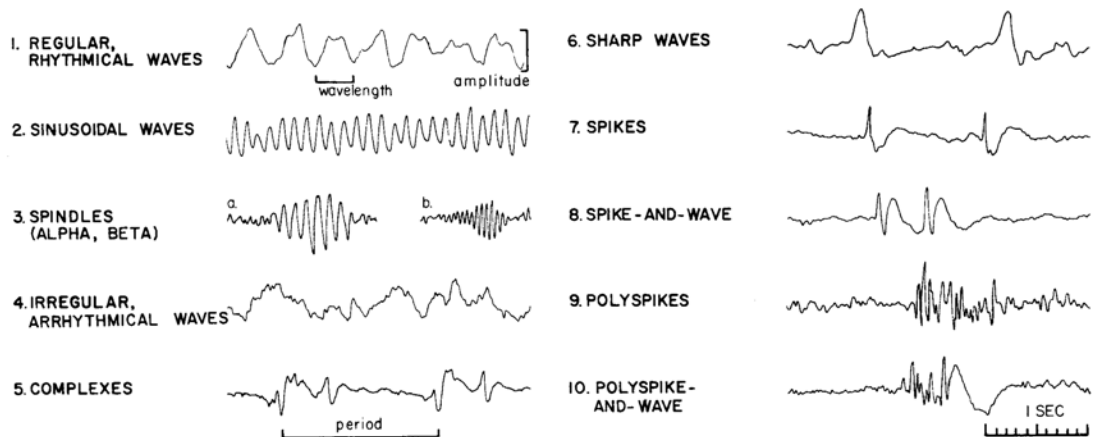


Figure 5. Examples of the above mentioned EEG graphoelements [48]

3.4 Epilepsy

Epilepsy is one of the earliest recognized neurological disorders. The Babylonians wrote down most of the seizure types, but they thought that it is some kind of evil spirit taking possession of the body.

The first person to claim that epilepsy is a kind of brain disorder was Robert Bentley Todd in 1849: he suggested that the seizures were electrical discharges from the brain.

John Hughlings Jackson was the one who had made this approach popular among the public at large, and with his guidance Victor Horsley was the first who performed craniotomy to cure epilepsy. This was the beginning of the discipline of epilepsy surgery.

The first antiepileptic medication -phenobarbital- was invented in 1912, and till now this is the most widely used medicine in the pharmacological treatment of epilepsy [3] [59] [60] [61] [62].

In 1935 Wilder Penfield and Herbert Jasper were the first who made awake EEG assisted surgeries in the Montreal Neurological Institute [63]. They stimulated different cortical areas during the surgeries and mapped the evoked responses (like movement of the mouth etc.), or what sensations the patients experienced.

Epilepsy is a frequent neurological disorder; approximately 65 million people suffer from epilepsy worldwide. Epilepsy affects seriously the quality of life of the patients and their families. Epilepsy is not curable, but large scale of antiepileptic drugs are available, which can attenuate or stop the seizures. Epilepsy is frequently accompanied by other psychiatric disease patterns like depression, psychotic symptoms, personality disorder, anxiety, cognitive failures and a higher suicide rate compared to the non-epileptic population [59] [60] [61] [62]. This can be explained either by the disease itself or by the side effects of the different antiepileptic drugs. There is an increased mortality (2-10 times higher) in the case of epileptic patients. However, this is not the consequence of the brain disorder, but the injuries connected to the seizures [64] [65].

It is important to be mentioned that an epileptic seizure is not equal to epilepsy. On one hand, a seizure can be a symptom or a momentary signal. It can be synchronous or excessive, but it is always the consequence of some pathologic activity of the brain. On the other hand, epilepsy is a long lasting susceptibility to seizures by the dysfunctional behavior of the brain.

On the neuronal network level epileptic seizures manifest as states of pathological hyperexcitability and hypersynchronous activity of large populations of neurons with concomitant synaptic reorganization of the affected brain region [2] [66].

The epileptogenicity of the different brain regions are diverse. Neocortical neuron populations are especially capable to produce excessive, synchronous firing during physiological conditions which is indispensable in several processes like formation of memory.

Therefore, they have the potential to display extensive hypersynchronous firing under pathological conditions [67].

According to the most well-known hypothesis, epilepsy is linked to an impaired balance of excitation and inhibition in the affected brain region [2]. The role of an altered GABA-mediated inhibition in epileptogenesis and seizure activity has been studied for decades, as well as the sprouting of certain excitatory pathways [8] [68].

There are a lot of syndromes of epilepsy, and the International League Against Epilepsy tried to distinguish the different types. There are two main categories: they are either separable by the seizure focus, or by the etiology of the seizures/epilepsy.

When separating by the focus, there are focal/partial seizures (the epileptogenic zone is well localized), and there are generalized seizures (both of the hemispheres are involved in the emergence). Regarding etiology, there are idiopathic, or symptomatic epilepsies. Symptomatic epilepsies occur along with other disorders of the central nervous system. There is not any other disease before the occurrence of idiopathic epilepsies; they are the result of some kind of heritable susceptibility.

The seizures which are connected to a specific brain region are called partial seizures. Partial seizures which do not involve disturbance of the consciousness are the simplex partial seizures. Seizures involving the frontal and temporal lobe are the complex seizures (mostly with loss of consciousness). If the motor cortex of both hemispheres are involved, than grand mal seizure occurs (generalized tonic-clonic-seizure). When the area of the epileptic seizure is not definable then it's a generalized seizure, with symmetrical motoric phenomenons appearing in the EEG signal, the seizure appears on systems which innervates areas on both hemispheres.

There are some generalized seizures during which no or only a few excitation signs appear (petit mal). These seizures cut off extensive areas for a few seconds with cortical spike trains [3] [59] [60] [61] [62]. Focal seizures are most often of temporal lobe origin [3] [69], but frontal, occipital or parietal lobes are also frequently the focus of the seizures.

Despite the large variety of antiepileptic drugs available, a considerable part of the patients are resistant to pharmacological treatment. In case of temporal lobe epilepsy, the percentage of drug resistant patients is extremely high [70] [71].

Nowadays, the surgical treatment emerges in some type of epilepsy. The progression of the surgeries is due to the advances of imaging techniques. With the ever growing influence and quality of the imaging techniques, there is a possibility now to gain much more insight into the localization, extension, and pathological nature of the epileptogenic brain disorder in a variety of lesion types. The vascular malformations diagnostics have improved greatly in recent years, and by the characteristic MR signals of an epileptogenic cavernome gives us the opportunity to surgically treat it. MR is good for recognizing epileptogenic sub-acute, or chronic encephalitis.

Some of the newest application of fMRI is that it can localize the motoric and speaking functions areas, so it gives the opportunity to make a surgery close to these areas.

The development of subdural electrodes allows a much better localization of the seizure onset zone, where the scalp electrodes are not sufficient enough. Using the two techniques together the seizure onset zone can be connected to a specific anatomical structure in the brain. Since the majority of partial epilepsies are of temporal lobe origin, temporal lobectomy is performed most often, during which the parts of the hippocampus and the temporal lobe are removed [3] [4] [72] [73]. After the surgery the majority of the patients is seizure free, or has seizures less frequently.

3.4.1 Tumor based epilepsies

20-45% of tumor patients have some kind of epileptic event. The age, the place of the lesion, the pathology of the tissue can all influence the seizure's appearance. The etiology of the tumor caused epilepsies are quite diverse [3] [59] [60] [61] [62] [74] [75].

- Central nervous systems disorders
 - o Primary brain tumor: glial, neuronal
 - o Increase in the number of excitatory neurotransmitters, increase of the pH
 - o Morphological alterations in the tissue (abnormal neuronal migration), receptor binding site alteration
 - o Brain metastasis (lung-, breast melanoma)
 - Toxic, metabolic effects
 - o Medicine side effect
 - o Liver- or renal failure
 - o Non-central nervous system infection
 - o Electrolyte disorder
 - Treatment caused seizures
 - o Chemotherapy
 - o Other agents
- [3] [59] [60] [61] [62] [74] [75] [76].

The tumor caused epilepsy treatment needs to be cautious, because the treatment can cause seizure as well, or the different agents can effect each other. Yet, antiepileptics are often used in case of these patients (mostly monotherapy to eliminate interactions). Surgery comes only after unsuccessful medical treatments. First, the primary brain tumor or metastasis is removed and after this the epileptogenic zone. Sometimes the chemotherapy and radiotherapy can offer solution for some of the problems.

3.4.2 Cortical dysgenesis

Cortical dysgenesis derives from a disorder in the brain's development. These alterations are hard to detect without a high-resolution MRI. 24% of the epilepsies are due to cortical dysgenesis [77] [78] [79].

The cortical cells are developed from the neuroblasts of the ventricular zone near the developing brain's midline. These cells divide, differentiate and migrate continuously before birth. More than 25% of the primer neurons will die by programmed cell death. Cortical dysgenesis is a disorder that can occur in the whole pregnancy but mostly between the 7-16th week. The pathology depends more on the occurring time of the defect, than its cause. MRI can be used for the detection of the structural difference, but not the etiology of it [77] [79].

A useable classification of the dysgenesis caused epilepsies was based on MRI, which takes into account the histological properties (many times the cause is a subependymal or subcortical heterotopy). Misplaced cell groups can be formed by abnormal migrating endpoint, excessive migrating, or the absence of the programmed cell death before birth.

3.4.3 SPA and interictal activity

For patients with pharmacoresistant focal epilepsy, resective surgery provides a good treatment alternative. The possibility of examining the removed epileptogenic zone revolutionized epilepsy research, as it raised the opportunity of measuring the activity of single neurons in a physiological or quasi-physiological state. In the experiment described in this manuscript, this is important, because our aim was not just to record and analyze LFP changes caused by the cells, we also wanted to know the underlying mechanisms involved in SPA generation. For this purpose, it was examined how all the separate cells are responding to the activity that is recorded using a laminar microelectrode. It has been shown that interictal spikes don't depend on age, gender, pathology, histology, or used antiepileptics [6].

Distinct from these pathologic interictal events, spontaneously occurring synchronous population activity could be detected in vitro in brain slices obtained from resected human epileptic neocortices, subiculum, and hippocampus [6] [80] [81] [82] [83]. The emergence of synchronized events in the neocortex is probably based on the complex interactions between and within the neural network's inhibitory and excitatory components.

The work of Köhling et al. [6] involved the investigation of human neocortical tissues resected during epilepsy surgery. They investigated the role of glutamatergic and GABAergic synaptic transmission, as well as the role of voltage gated calcium channels in the generation of the spontaneous activity they describe [6]. In their work, the extracellular field potential gradient

was measured in the cortical layers II and V. However, Köhling et.al. measured this activity only in tissue obtained from epilepsy patients. Their characteristics of the spontaneous field potentials were:

- amplitude 20-323 μV (72 \pm 13 μV)
- duration 20-200ms (151 \pm 18ms)
- repetition rate 4-108 per minute (43 \pm 4 per minute)
- monophasic [6]

While some have argued that SPA is distinct from the pathologic interictal events occurring in epilepsy patients [84], it is still controversial whether SPA is epileptic, or whether it can be found in physiological conditions.

Many studies demonstrated the importance of transmembrane calcium currents and the effects of glutamate, and GABA during spontaneous field potential transients [82] [83] [85]. It has been shown, that an increase in the Mg^{2+} concentration reduces the recurrence frequency of spontaneous population activity, but application of APV does not, which points to a calcium-antagonistic effect of Mg^{2+} . Calcium currents play a crucial role in the generation of spontaneous activity, and epileptiform activity induced in experimental models and in seizures in epilepsy patients [6]. Blocking the non-NMDA type glutamate receptors, the GABA_A receptors, or calcium channels can suppress this type of activity, but blocking the NMDA type or GABA_B receptors does not have any effect on these field potential transients [6] [80] [86] [87].

Our group's preliminary results [83] [85] [88] indicate that an activity similar to interictal spikes (as in Köhling et. al. [6]) is detectable in non-epileptic tissue (derived from deep brain tumor patients, non-epileptic part not infiltrated by the tumor (Figure 6.)).

Using current source density (CSD) analysis the flowing currents between cell compartments can be estimated. Using CSD analysis, it is possible to evaluate which neuronal populations generate the changes in the field potential. During spontaneous interictal discharges in vitro, the current sinks are mostly located in layers II. and III. (positive charges flowing into the cells) even after Mg^{2+} withdrawal. However, where spontaneous activity did not occur, the Mg^{2+} withdrawal, or Bicuculline (GABA_A receptor antagonist) application caused the sinks to spread over the whole extent of the cortex, especially in layer V. [87].

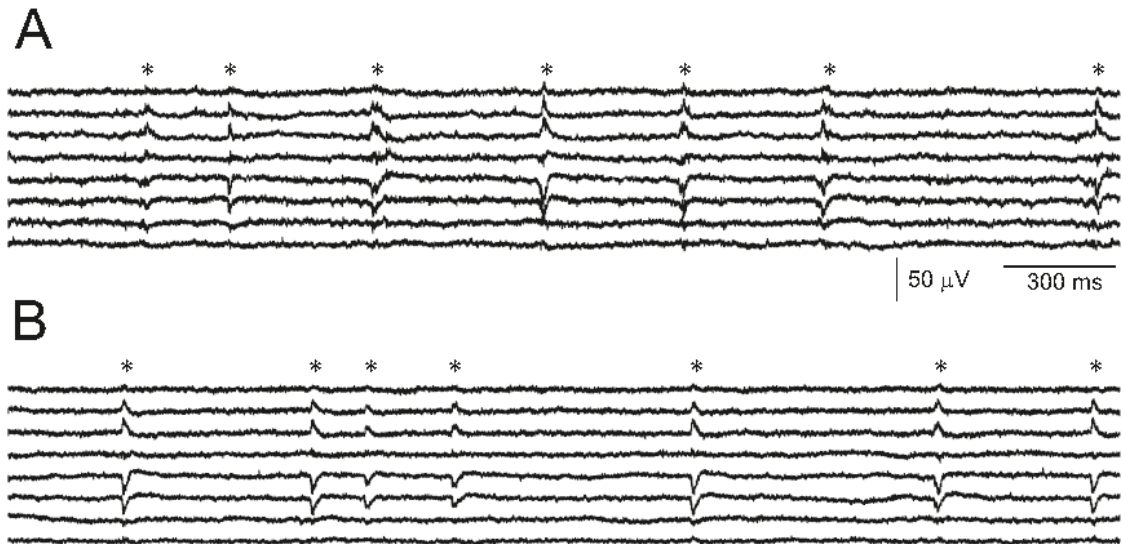


Figure 6. Example recording of SPA from an epileptic (A), and from a tumor (B) patient. The SPA discharges are marked with an asterisk (*). SPA is mostly generated in the supragranular layers, shows increased cell firing (indicated by an increase in MUA), and the occurrence of High frequency oscillations during the LFP discharge [83] [85] [88].

In the present study, we want to further investigate the origins of this SPA. Measurements performed with an extracellular laminar multielectrode provide the desired spatial information on how the different cortical layers respond.

However, this approach does not yield extensive information on single cell activity. Thus, it is difficult to address the question of cellular mechanisms, as it is not feasible to patch each of the cells to obtain cell specific information. Question addressed in the present study are: How are the cells involved in the generation of SPA? What proportion of cells is active during SPA? Which types of cells are active (neurons, interneurons, glial cells) during SPA? When are they most active (before/during/after the LFP transient)?

Since SPA can occur both in epileptic and in healthy tissues, we decided to investigate the differences in how the healthy and versus the pathological tissue generate a very similar activity. To be able to answer the questions stated above, our research group used 2-photon microscopy. In addition, histological analysis of the tissue is included (cell labeling and staining, followed by light and electron microscopy and 3D reconstruction) to address the question of morphological differences between epileptic and non-epileptic tissue.

3.5 Two-photon microscopy

Neuroscientists have become more and more interested in two-photon microscopy over the last decades because of the numerous advantages. Two-photon microscopy allows high resolution imaging in living tissue compared to confocal microscopy. Another great advantage

of this method is that it makes achievable to image even in great depths (several hundred microns 1 millimeter compared to 30-50 μm) by, solving the light scattering problem causing deterioration of optical signals. The improvements of the fluorescent staining and marking techniques in the last few years allowed the functional exploration of neuronal activity from single cell (or subcellular) activity, through cellular networks, to even the measurement of a cortical column (with 3D scanning technology). In this chapter the principles of two photon microscopy will be introduced and its application in the field of neuroimaging will also be discussed.

3.5.1 Theoretical background of two-photon microscopy

In 1931 Maria Göppert-Mayer set the theorem of two-photon absorption [89]. However, because of technological reasons it was experimentally confirmed in the 1960s. With the production of ultra-short pulsed lasers, two-photon microscopes became designable [90].

Fluorescence techniques addressed the problems of neurobiology. Currently, two-photon microscopy became an essential tool for the examination of biological tissues (living or fixed), because the fluorescent objects can be visualized selectively (even with small fluorophore concentration) with good signal-to-noise ratio. Light microscopy is able to track spatially complex dynamics [91] over a great depth, and can resolve single synapses [17] [92]. For light microscopy intact cortical tissue is challenging, but if it is possible neurons should be studied in their natural domain.

The drawback of conventional fluorescent microscopy is that in thick (over 100 μm) samples contrast and resolution are degraded because of the scattering of the tissue [93] [94]. By confocal microscopy some of the scattering effects were overcome by the pinhole detectors, because it rejects fluorescence from off-focus locations [93] [94]. However, scanning a section excites the whole specimen, and thus could damage it. Furthermore, pinhole rejects the scattered signal photons emerging from the focus. In great depth confocal microscopy loses intolerably high amount of signal photons by the scattering [93] [95]. Signal loss can be compensated by increased fluorescence excitation, but it can lead to photobleaching and phototoxicity.

The theory of two-photon excitation is based on the concept when two low-energy photons hits a fluorescent molecule causing an electronic transition to a higher-energy state. Each photon carries the half of the energy necessary to the excitation, and results in the emission of a fluorescent photon (the photon is at a higher energy than either of the excitatory ones (Figure

7.)).

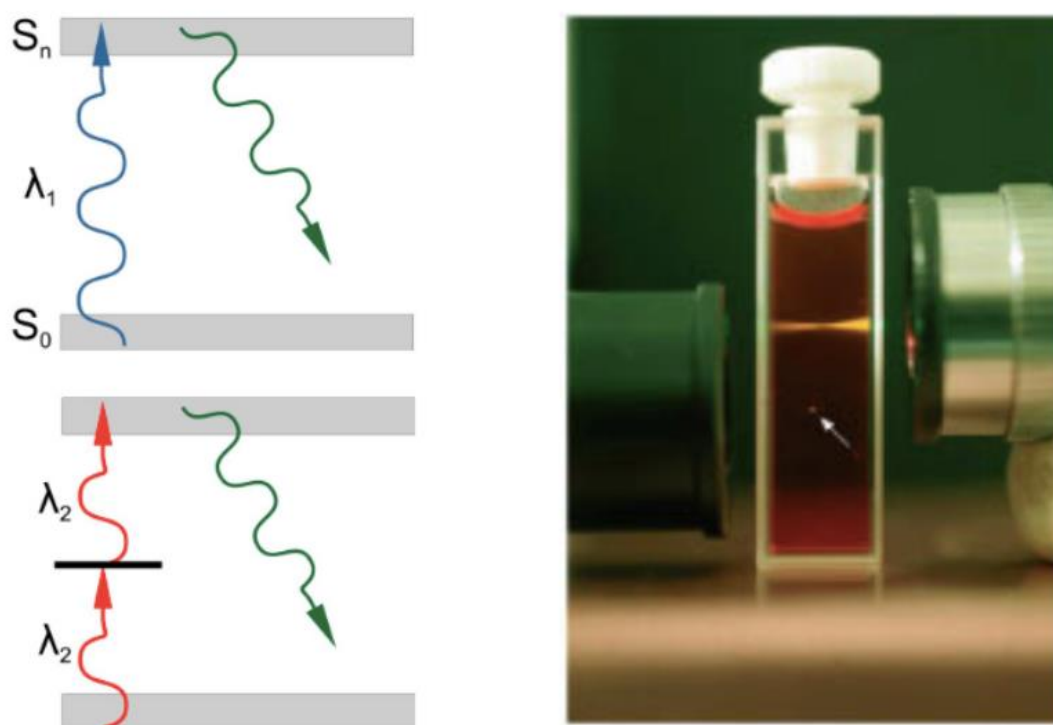


Figure 7. Left: Single and two-photon excitation of a fluorescent molecule (from the excitation it goes up to an excited energy state, and when it descends back to the original a photon is emitted). Right: the focus of the laser beam by confocal or two-photon (marked with white arrow) technology [96].

In a focused laser, the intensity is highest in the focus, and degrades quadratically by the distance. A fluorescent molecules excitation probability has a quadratic dependence on light intensity, resulting in an excitation exclusively only a small diffraction-limited focal volume (Figure 7.). If the objective (used to focus the beam) has a high numerical aperture (NA), most of the fluorescence excitation occurs in a focal volume of $\sim 0.1 \text{ mm}^3$ [97]. This way the point spread function's axial spread is significantly lower than for single-photon excitation. Photobleaching and photodamage are greatly reduced to the tissue, and no fluorescence is emitted from out of focus locations (automatic optical sectioning), so there is no need for out of focus rejection strategy (like in confocal microscopy). The signal to noise ratio (SNR) is greatly increased by the collection of scattered photons, in contrast to confocal microscopy where they are rejected.

The most commonly used fluorophores have excitation spectra in the 400–500 nm range, whereas the laser used to excite the two-photon fluorescence lies in the $\sim 700\text{--}1000$ nm (infrared) range. The living tissue scatters light more in the visible wavelengths than in the infrared, thus fluorescent objects in living tissue can be examined in greater depth [98] [99]. Nowadays it ranges from hundreds of micrometers to a millimeter.

For its above mentioned advantages two-photon microscopy became a unique tool for imaging samples in depth (especially *in vivo*), or in local photochemistry. However, on transparent or very thin slices two-photon microscopy is not as effective as confocal or wide field fluorescence microscopy since the achievable spatial resolution is reduced by the longer wavelengths.

Two-photon functional imaging, and calcium imaging have an extensive background [100], either focusing on its technical aspects [97] [99] [101] [102], on its applications [103] [104] [105] [106], or on its place in the wider context of the various recent technological developments, which provide tools for the "reverse engineering" of the brain [107].

3.5.2 Hardware of a two photon microscope

Two-photon microscopy is typically implemented in a simple laser scanning microscope. The setup consist of the following main elements: laser source, scanner, objective and detectors (Figure 8.).

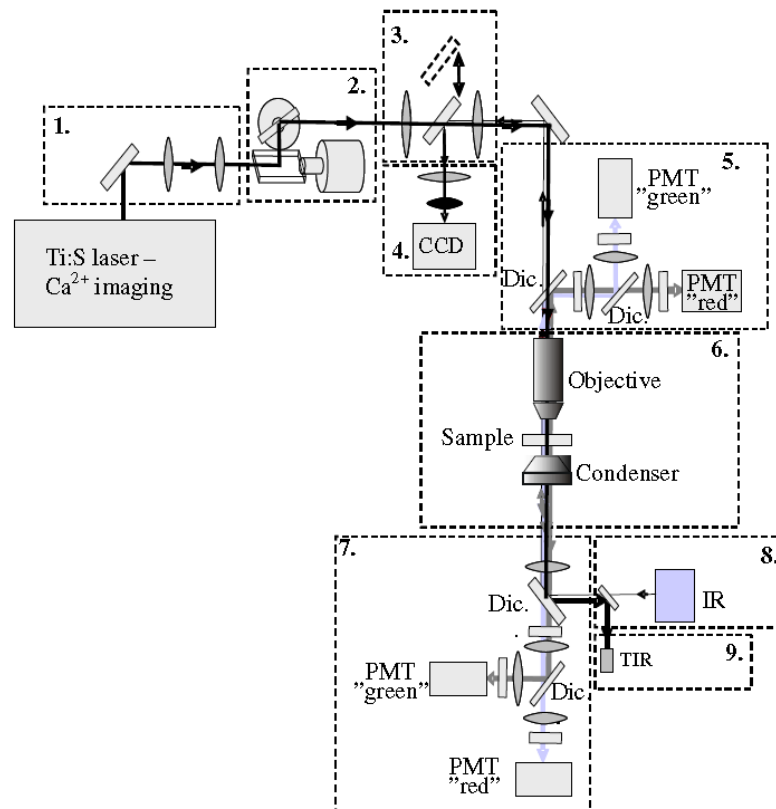


Figure 8. Schematic drawing showing the optical design and modular nature of the 2P microscope used. Modules: 1 - Dispersion compensation. 2 - Laser beam positioning. 3 - CCD/2P switcher. 4 - CCD camera. 5 - Upper detectors (PMT - photomultiplier; Dic. - dichroic mirror). 6 - Perfusion chamber and focusing. 7 - Lower detectors. 8 - Infrared lamp (IR). 9 - Transmission infrared detector (TIR). Dic: Dichroic mirror. Source: [108].

The typical differences between two-photon and confocal microscopes are the laser (see below) and the fluorescence detection path. In two-photon microscopy, all useful fluorescence photon collected by the objective. The optimal solution is to project the objective back-aperture onto the photosensitive area of the photodetector [109] [110]. Fluorescence photons can appear to originate from a large effective field of view because the multiple scattering before exiting the tissue [108]. In confocal microscopy, the epifluorescent light passes back through the scan mirrors and through a pinhole before detection [93].

In two-photon microscopy the laser beam is directed into the microscope through an epifluorescent light path. To focus in the specimen, the excitation light is passed through a dichroic mirror to the microscope objective. Two-photon induced fluorescence occurs only at the focal spot. By scanning the fluorescent volume with a galvanometer-driven scanner, the images can be constructed. The emission signal is collected by the same objective and reflected to the detector by the dichroic mirror. A barrier filter is also needed to attenuate the scattered excitation light. To ensure maximal detection efficiency high-sensitivity detectors and electronics are used.

3.5.3 Laser Sources

Opposed to confocal microscopy (continuous wave emitting lasers) two photon microscopy requires pulsed lasers (for precise technical details see the corresponding part of the methods section).

Two-photon excitation efficiency increases with the inverse of the pulse duration, if the average pulse repetition rate, and power are constant. The most commonly employed lasers for two photon microscopy are mode-locked Ti:sapphire lasers. Mostly the excitation light is tunable between 700-1000nm [112].

Pulse rates should balance the onset of saturation and the fluorophore's excitation efficiency. This criterion is met by the used laser for most common molecules (e.g. Ti:sapphire laser), that is fortunate because mode-locked lasers pulse rate is difficult to change. For stable excitation rate, it is essential that a constant number of pulses arrives on a pixel. More than 100 pulses arrive on a pixel, assuming a pulse rate of 100 MHz and 1 μ s dwell time, so the number of pulses per pixel will be stable at the 1% level [112].

The imaging depth is determined by scattering: with increasing depth, a smaller fraction of the incident photons are delivered to the focus. Since rays entering the brain at higher angles have longer paths to reach the focus they are more likely to be scattered, causing a loss of resolution with imaging depth [105]. SNR is also worsened with depth, because extensive scattering and absorption occurs on the lower wavelength emitted light.

The contrast and the localized excitation worsen with increasing depth. Because of the out of focus fluorescence generated on the surface, a depth limit is imposed on imaging. In gray matter it is ~ 1mm [112].

3.5.4 Scanning Methods (x-y plane)

The most widespread solution is the use of mirrors moved by galvanometers. Galvanometric mirrors allow rapid, arbitrary positioning of the focus in the focal plane (x-y) [113] [114]. In raster scanning application, galvanometric mirrors, allow zooming, image rotation and have excellent optical properties. Their major drawback is their relatively slow speed (>1 ms per line); raster scanning of a typical image requires ~1 s. Speed can only be increased at the cost of the spatial resolution and the extent of covered area [113] [114]. Since many neurophysiological processes take place on the millisecond time scale, faster scanning methods are required.

“Line scan” is an alternative scanning method. The laser does not scan through the whole 2D plane (like in raster scan), instead the laser scans only the lines which were specified by the user on the structure of interest. For example multiple dendritic spines can be imaged within 1 ms [115]. However, it has to be mentioned that the cost of scanning speed is the loss of spatial information. During the experiment the selection and adjustment of the trajectories should efficiently be made. This can be problematic, because only one fixed z plane at a time can be used, while the neural structures do not necessarily fall in the same plane. Another way to accelerate the scanning is to jump between regions of interests (ROIs) by maximal scanning speed between ROIs of the mirrors. With this method no time is wasted for the extracellular structures. Still line scans can be wasteful when the ROIs are sparsely distributed. The scanning speed depends on the acceleration/deceleration rate of the motors. All ROI based scanning method, such as line scan, need extensive software support which is not always provided by the microscope manufacturer.

An attractive alternative is presented by acousto-optic (AO) deflector. AO scanning technology is another solution for rapidly change beam focusing excluding mechanical movement, and AO technology is adapted in many two-photon applications [116] [117] [118] [119] [120] [121] [122] [123]. Acousto-optic deflectors are transparent crystals, in which an optical grating is created by applying sound waves to them. Periodic change in the refractive index of the medium is caused by sound-generated pressure fluctuations, and the changes behaves like optical grating (the light diffracts according to the period-and the wavelength of the light). The frequency of the sound wave determines the spacing of the grating, and thus the angle of diffraction of the laser beam. Since the laser beam can be diverted without mechanical

movements, speed of the positioning is vastly enhanced compared to the galvanometric approach. These optical materials are dispersive, leading to temporal and angular dispersion, which, worsens the excitation efficiency, point spread function and image quality for typical pulse durations (< 1 ps) [118]. With gratings, prisms and/or additional acousto-optic devices the compensation can be made [124] [125] [126]. Acousto-optic deflectors have also been proposed [117] for tackling scanning also along the z axis [102] [121] [122] [123] [127].

3.5.5 Objectives

The objective is a very important part of the microscope, because it generates the laser focus required for localization of excitation. There is a wide range of available choices from objectives in the market which are suitable for a two-photon microscope.

Important criterias are:

1. Numerical aperture, has to be large because it determines the resolution and the angle for fluorescence light collection
2. Magnification, according to the desired field of view;
3. Large working distance (2 mm is ideal), especially in in vivo applications and simultaneous electrophysiology measurements;
4. Excellent transmission efficiency in visible wavelengths and the near-infrared.

The laser beam should expand to “fill” the microscope objective’s back aperture, this way it focuses the light into the sample. Since the laser beam has a Gaussian radial intensity profile, laser beam is said to “overfill” the back aperture of the objective when the latter accepts the central part of the beam up to the radius at which its intensity decays to 13.7% ($1/e^2$). In this case, 84% of the beam’s power is transmitted and lateral and axial resolution [97] are nearly as good as with a uniform excitation beam (92 and 96%, respectively). Using a narrower beam increases the amount of power transmitted, but reduce the effective numerical aperture (NA) leading to a loss of resolution [97] [99].

It is important to note that increasing depth leads to reduced effective NA: large angle photons travel longer distances than those near to the optical axis and often they are scattered or absorbed. Underfilling the objective might be a good solution, if the observed objects are large enough and their detectability does not suffer by the reduced accuracy. As the size of the focal volume grows with decreasing effective NA, the peak intensity decreases, resulting a decrease in photobleaching and photodamage.

3.5.6 Detectors

Two-photon microscopy demands large photosensitive areas (can be millimeters) [111], so avalanche photodiodes are excluded. Important factors are gain, quantum efficiency, dark noise, absorption spectra, and absorption angle of the detector. Photomultiplier tubes (PMTs) are the best for two-photon microscope applications (the different type's performance comparison can be found in [97]).

In two-photon microscopy, with spatially ultra-selective excitation, optical partitioning can be achieved. So all photons should be collected, even the scattered ones, emitted by an excited fluorescent molecule. The excitation light has larger wavelength than the fluorescence, so from lower depths the fluorescent photons are greatly scattered thus photons appearing on the surface are negligible below several hundred μm . Thus, large NA and low magnification objectives (for example 20x at a NA of 1.0) are the best choice to catch as many photons as possible. Moreover, large sensitive area photomultipliers (PMTs) are positioned to detect as much as possible. In our in vitro experiments all excited photons can be useful (and can be detected) either scattered in the backward ("epi"- collection geometry) or forwards ("trans"- collection geometry) direction.

3.6 Neuronal calcium signals

Tissues can be considered as semi-infinite by in vivo imaging, therefore forward-collection blocked, which makes an effective backward-detection really important. "Whole-area" configuration is used in most cases. It means that to the PMT's sensitive area the objective's back is projected and this way it allows all objective collected photons to end up on a detector [128].

The role of Ca^{2+} dynamics in neuronal signaling has ever growing interest by neuroscientists during the last decade. There are basically two types of Ca^{2+} imaging techniques. One there are the classical chemical fluorescent Ca^{2+} indicators, the other is the genetically encoded protein-based Ca^{2+} indicators. In this study (in human) only the Ca^{2+} indicators can be used in vitro [11].

Calcium ions generate versatile intracellular signals for many functions in almost every cell type [129]. Intracellular calcium signals (in the nervous system) regulate processes from the time scale of neurotransmitter release (microsecond) to gene transcription, (minutes/ hours) [130]. For the function of these signals the amplitude, the time course, and the local action site are essential. There are many types of neuronal Ca^{2+} signaling, sources of Ca^{2+} influx are Ca^{2+} -permeable α -amino-3-hydroxy-5-methyl-4-isoxazolepropionic acid (AMPA) and N-methyl-D-aspartate (NMDA) glutamate- type receptors, voltage-gated Ca^{2+} channels (VGCC), nicotinic acetylcholine receptors (nAChR), and transient receptor potential type C (TRPC) channels [11].

Ryanodine receptors (RyR) and inositol trisphosphate receptors (IP3R) mediates the Ca^{2+} release from internal stores is mediated. Metabotropic glutamate receptors (mGluR) can generate inositol trisphosphate [11]. Sodium-calcium exchanger (NCX), plasma membrane calcium ATPase (PMCA) and sarco-/endoplasmic reticulum calcium ATPase (SERCA) can mediate Ca^{2+} efflux. Mitochondria is important for neuronal Ca^{2+} homeostasis [11].

In this research understanding the connection between the AP and the Ca^{2+} is very important the theoretical background will be shortly summarized in this paragraph. There are many researches, showing the connection between the AP and the Ca^{2+} inflow, especially in the neurotransmitter release to the synaptic cleft, the dendritic Ca^{2+} transients, backpropagating AP, etc... [131] [132] [133] [134] [135] [136].

When we speak about the importance of Ca^{2+} dynamics in the neuronal signals we should speak about axonal- somatic-, and dendritic Ca^{2+} response.

Neurotransmitter molecules are stored in vesicles in the presynaptic terminal of neurons. Ca^{2+} inflow plays a key role in neurotransmitter release. It is inhibited when Ca^{2+} channels are blocked. Upon the arrival of AP to the axon terminal voltage dependent Ca^{2+} channels open and Ca^{2+} flows from the extracellular fluid into the presynaptic neuron's cytosol via the concentration gradient this sudden Ca^{2+} influx is followed by the docking and fusion of neurotransmitter vesicles to the presynaptic neuron's cell membrane through SNARE proteins resulting in a rapid neurotransmitter release. So it can be said that in the axon when there is an action potential, then an inward Ca^{2+} concentration change follows it [131].

We need to speak about dendritic Ca^{2+} transients, because in two-photon microscopy the cells soma, and the dendritic tree is what can be easily imaged by scanning methods (like it was described before in the scanning methods). Dendritic Ca^{2+} transients can be related to passive somatic depolarization propagation or active AP propagation.

By somatic voltage-clamp, dendritic Ca^{2+} imaging and somatic excitation experiments, high Ca^{2+} transients were detected in both the initial, and the distal dendrites (backpropagating action potential). But when the Na^+ -dependent AP propagation was blocked, then the Ca^{2+} transients degraded in the initial and vanished in the distal dendrites. So the local Ca^{2+} entry mediated by action potentials was reflected in the Ca^{2+} transients [131] [132] [133] [134] [135].

It was also shown, that the intracellular dendritic Ca^{2+} rise could influence the synaptic integration by the downreguation of the NMDA receptor-mediated responses [133].

Based on the literature it can be assumed, that whenever there is a Ca^{2+} response in the cell: if it is measured from the soma it probably reports an AP, if it measured in the dendrites then it refers to a postsynaptic response or an AP [131] [132] [133] [134] [135] [136] (Figure 9.).

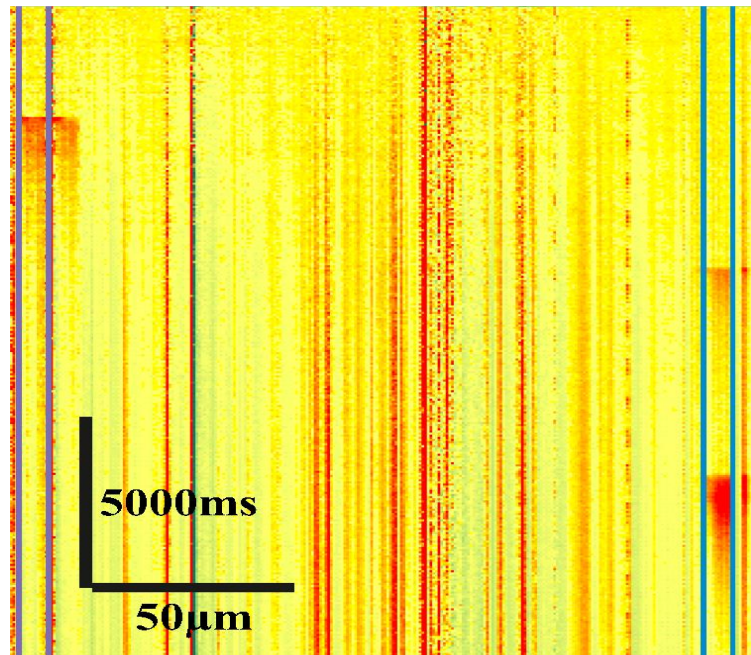


Figure 9. Representative Ca^{2+} responses recorded by two-photon Ca^{2+} imaging. 16 bulk loaded (OGB-1-AM, SR101) human neocortical neuron/interneuron were selected by line scan for spontaneous recording, the scanning time were 20 s. The vertical axis is time, the horizontal is how the laser go through the placed lines in the line-scan, and the more red the color is, the higher the Ca^{2+} fluorescence response. Two of the cells responded in this case (two of the ROI-s are marked by purple and blue).

3.6.1 Calcium indicators

The first generation of fluorescent calcium indicators consisted of quin-2, fura-2, indo-1, and fluo-3. Quin-2 can be excited by ultraviolet light (339 nm). Quin-2 was the first of this group to be used in biological experiments [137] [138]. However, to overcome cellular autofluorescence, Quin-2 needs to be used at high intracellular concentrations [139]. Fura-2 became very popular among neuroscientists [140], is in many ways superior to quin-2 and Fura-2 is excited at $\sim 350 - 380$ nm and shows significantly larger calcium-dependent fluorescence than quin-2. Furthermore, fura-2 allows more quantitative calcium measurements [141]. Nowadays Oregon Green BAPTA and fluo-4 dye families [142] are widely used in neuroscience. They provide a large signal-to-noise ratio and are relatively easy to implement. The introduction of protein-based genetically encoded calcium indicators (GECIs) was the next great breakthrough [143].

3.6.2 Calcium Imaging

Two-photon imaging started after the bulk loading, and/or whole cell configuration achieved on the two-photon laser scanning system. Spatially normalized and projected Ca^{2+} response can be calculated by the raw line-scan, $F(d,t)$ using the

$$\frac{\Delta F}{F} = \frac{(F(d, t) - F_0(d))}{F_0(d)}$$

formula where d denote to the distance along the curve and t to time. $F_0(d)$ is the average/background-corrected prestimulus fluorescence as a function of distance along the curve. Ca^{2+} responses are projected as function of t and d and K_d color coded (yellow to red show increasing Ca^{2+} responses, 0–63 % $\Delta F/F$). In the experiments the relative fluorescence value was converted to Ca^{2+} concentration [144] [145] [146]

$$\frac{\Delta[\text{Ca}^{2+}]}{K_d} = \frac{f_{max}}{f_0} \left(1 - \frac{1}{R_f}\right) \frac{\delta f}{(\delta f_{max} - \delta f)\delta f_{max}}$$

[147], where $\Delta[\text{Ca}^{2+}]$ is the change in the intracellular calcium concentration, δf denotes $\Delta F/F$, $R_f (= f_{max}/f_{min})$ is the dynamic range of the dye and K_D is the affinity of the indicator.

4 Materials and methods

First of the main goals (and Thesis I.: A method has been developed for the two-photon Ca^{2+} imaging of human neocortical tissue) of this research was to make the methodology that permits the deeper understanding of the events behind SPA. This was not an easy task, because not just the methodology should be made, but organizing the teamwork of the different research groups, and the surgeons, were a big portion of the work.

First the contact with the surgeons and the ever refreshing information of the surgeries (of the National Institute of Clinical Neuroscience, Budapest, Hungary) and the patient's approval of the research should be organized. Then the preparing the solutions, and the experimental design should be made for every experiment.

The experimental work with the Two-photon microscope should be learned (from the research group of the Femtonics Ltd (Budapest Hungary) lab in the Pázmány Péter Catholic University, Budapest, Hungary), the experimental time of the different groups in the same lab were organized. The preparation of the two-photon microscope for the experiment were made (the set-up of the laser, the preparation of the ACSF circulation system (with a double flow chamber) in the two-photon microscope, the setup of the laminar electrode recording system (the data transmission system, and the recoding electrode integration to the two-photon microscope), the preparation of the micropipettes, and the imaging dyes). And all the used programs should be learned, not just for the experiments, but for the analysis as well.

The preparation of the slices for histological analyses were included, too. The possibility of the microscope usage for light- transmission electron microscopy, and 3D reconstruction were organized.

Organizing all these people and all these pre setting should be together to make the preparation of this methodology possible.

The training of our research group (Hungarian Academy of Sciences, Research Centre for Natural Sciences, Institute of Cognitive Neuroscience and Psychology, research group of Comparative Psychophysiology, Budapest Hungary) for the experiment were prepared and made for the future work as well.

From now on this methodology will be described.

4.1 Patients

In the present study – investigating human neocortical tissue slices – we included 3 patients with therapy resistant focal epilepsy (Pts 4, 5, 7, age: 26-52 years) and 3 patients with brain tumor but without epilepsy (Pts 1, 2, 6, age: 64-78 years). Additionally, there were two patients who had tumor associated epilepsy (Pt 3, 8, age: 27, 71 years). Tissue samples derived from the temporal (Pts 2, 4, 5, 6, 7, 8), parietal (Pt 1) and frontal (Pt 3) lobes [148]. The seizure focus was identified by multimodal studies including video-EEG monitoring, magnetic resonance imaging. Brain tumor was diagnosed by computed tomography and/or magnetic resonance imaging. The patients had subcortical tumors. We examined the neocortex above the tumor, which needed to be removed for surgical technical reasons. Patients underwent their surgery in the National Institute of Clinical Neuroscience in Budapest, Hungary. All patients gave written consent approved by the Regional and Institutional Committee of Science and Research Ethics of Scientific Council of Health (ETT TUKEB 20680-4/2012/EKU) in accordance with the Declaration of Helsinki.

Neocortical samples were obtained from a total of 45 patients (age range: 19-83 years mean±SD: 53±17 years; n=9 epileptic patients, age range: 19-53 years, mean±standard deviation (SD): 32±10 years; n=8 tumor associated epileptic patients, age range: 27-71 years, mean±standard deviation (SD): 48±18 years; and n=28 tumor patients, age range: 27-83 years, mean±SD: 60±14 years) [148].

We could not achieve satisfactory recordings in several cases (in n=17 cases the slices seemed dead, and there was no activity in any type of recording, n=6 the cells looked intact, but after the bulk loading they seemed dead, in n=6 cases some SUA, or MUA were detectable in the laminar recordings, but in the two-photon there was not any detectable Ca^{2+} response from the cells)(n=2 epileptic, n=6 tumor associated epileptic and n=21 tumor patients), and therefore these patients were excluded from the data analysis. We always followed our standardized protocol (see below) but the tissue quality was unacceptable in these latter cases [148]. Criteria for acceptable tissue quality were the following 1) cellular and/or population activity on the LFPg or LFP recordings, 2) at least 25% of the cells looked healthy on the picture acquired with the transmission infrared mode of the two-photon microscope [148].

4.2 Tissue preparation

Tissue was transported from the operating room to the laboratory in a cold, oxygenated solution containing (in mM) 248 D-sucrose, 26 NaHCO₃, 1 KCl, 1 CaCl₂, 10 MgCl₂, 10 D-glucose and 1 phenol red, equilibrated with 5% CO₂ in 95% O₂. Neocortical slices of 500 μm thickness were cut with a vibratome (Leica 1000 S). They were transferred into a dual perfusion chamber mounted (Figure 10.) on a two-photon microscope. In this type of chamber artificial cerebrospinal fluid (ACSF) is allowed to flow both above and below the slice, resulting in a better oxygen supply, and in a better maintained network oscillations (Hájos et al., 2009; Chiovini et al., 2010; Chiovini et al., 2014). Slices were perfused with a warm (36°C) ACSF containing (in mM) 124 NaCl, 26 NaHCO₃, 3.5 KCl, 1 MgCl₂, 1 CaCl₂, and 10 D-glucose, equilibrated with 5% CO₂ in 95% O₂. High flow rate of the bathing medium was used to maintain the optimal oxygenation level of the tissue [108] [148] [149].

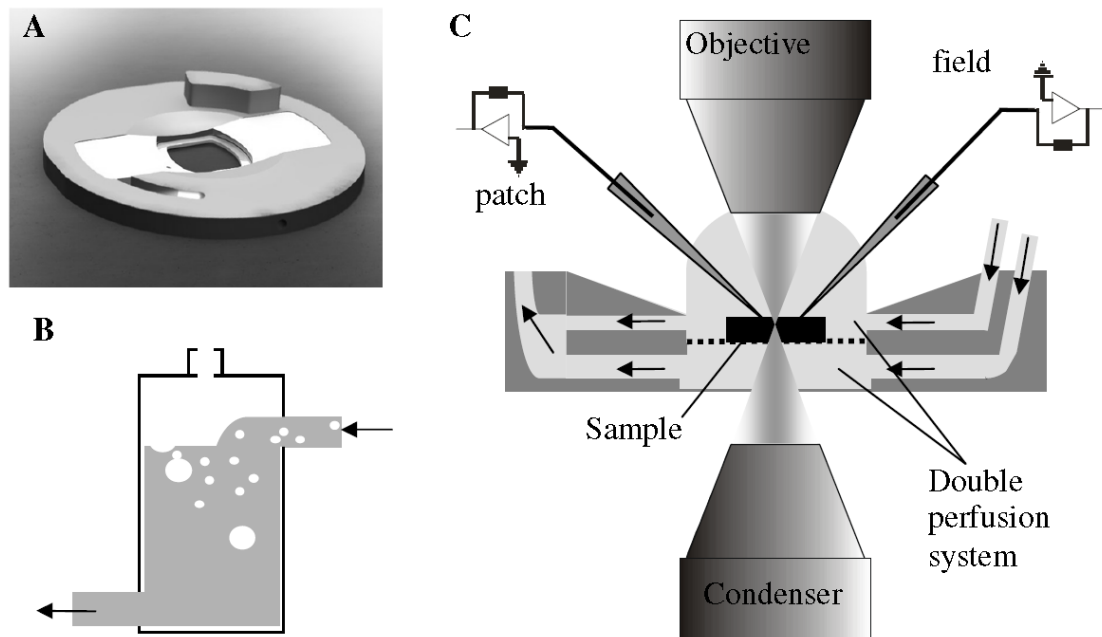


Figure 10. A) The schematic of the double perfusion chamber. B) The bubble catcher's schematic (it is connected in the tubes between the oxygenated ACSF bottle, and the double flow chamber). C) The sectional picture of the double perfusion system, and how it fit in to the two-photon microscope system [105].

Bulk loading of 1.75 mM Oregon Green 488 BAPTA-1 AM (OGB-AM), 350 μM sulforhodamine 101 (SR-101) and 20% Pluronic F-127 in DMSO was applied on the tissue (Invitrogen, Carlsbad, CA) to visualize neurons and glial cells, respectively [148] [150] [151] [152] (Figure 11).

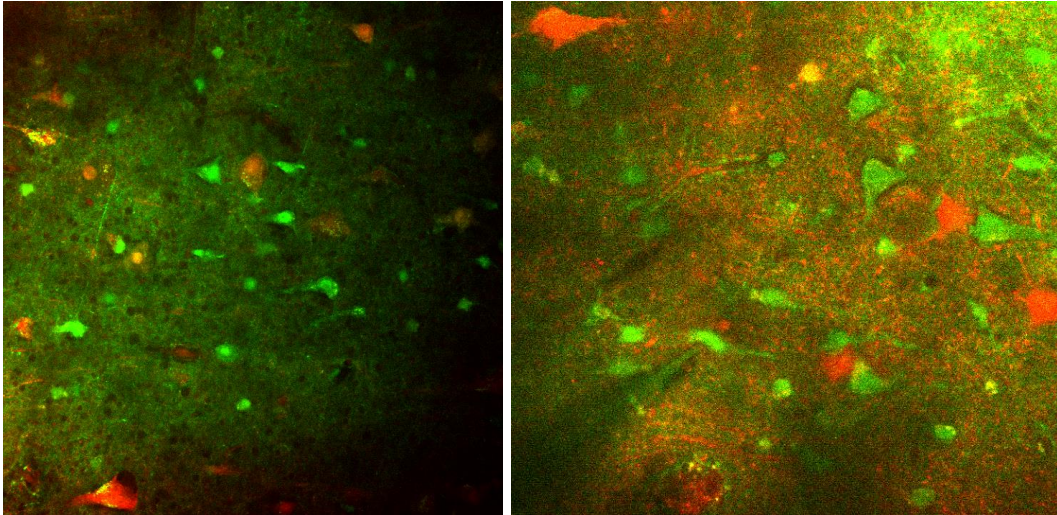


Figure 11. Two-photon image of bulk loaded human tissue. OGB-1-AM (green), SR-101 (red) were applied into the tissue. The neurons, and interneurons take up the OGB-1-AM, the glial cells (mostly astrocytes) take up the SR-101 (the dead cells are red as well).

4.3 Electrophysiology recordings

4.3.1 Laminar recordings

The extracellular local field potential gradient (LFPg) was recorded with a laminar multielectrode array (24 channels, distance between contacts: 100 or 150 μm , [56] [83] [153] [154] using a custom made voltage gradient amplifier (pass-band 0.01 Hz to 10 kHz). The 24 channel laminar probe was connected to the data transmission system's head stage. The electrode was fixed to the 2-photon microscopes built-in micromanipulator, to maneuver the probe above the slice (Figure 12.) [148].

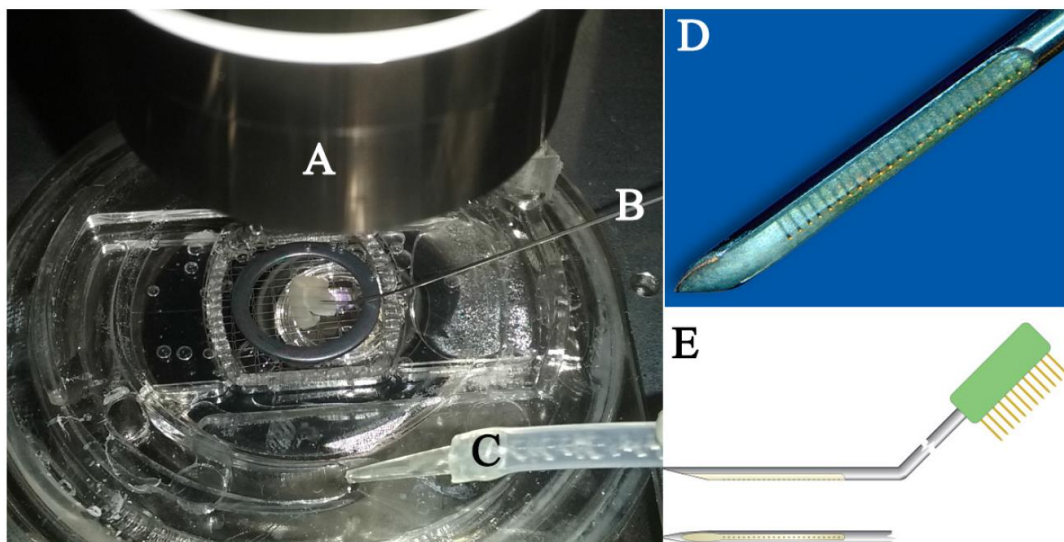


Figure 12. An example of how the laminar electrode is placed on a slice (this slice is just for the example from a rat). A) the objective, B) 24 channel laminar electrode, C) the suction of the ASCF circulation, the double flow chamber is visible too and on the slice there is a holder grid preventing the slice from floating away, D) the 24 contact of the

laminar electrode, E) the schematic of the electrode design (<http://www.neuronelektrod.hu/elektrod-tipusok/acelcso-alapu-elektrodok/agyszelet-elektrod-hajlitott.html>).

The laminar multielectrode was placed on the surface of the neocortical slice, perpendicularly to the pial surface. This way, the whole extent of the examined region was covered by the array, so that extracellular recordings were made from each neocortical layer.

4.3.2 Data transmission systems

In the experiments two types of data transmission systems were used, which both fulfilled the necessary requirements for the measurements.

In the beginning of the experiments a National Instruments (NI) device based data transmission system were used. The signals were digitized with a 32 channel, 16-bit resolution analog-to-digital converter (National Instruments, Austin, TX) at 20 kHz sampling rate (using home made routines for Lab View7 (National Instruments, Austin, TX))(Figure 13.) [148].



Figure 13. Left NI usb-6353 X series data acquisition device. Right. Gefen USB 400 FO (Gefen, LLC, Chatsworth, CA).

The data transmission system (Figure 14.) consists of a Head Stage (Gain 10x, Dc, 24 channel + reference), that connects with the Main Amplifier through ribbon cable (Gain 100x, 0.1 Hz-6kHz band, ± 3.2 V Lithium battery). After the amplification the next step is the A/D conversion with the above mentioned NI device (24 channel, 16 bit/ 20-40kHz/ channel), the A/D converter is supplied by a +14.4 V Lithium battery. The A/D converter sends a +5 V power supply and the digital signals to the Gefen USB 400 FO Optical USB links sender side (Figure 13.) (USB to optical conversion in the sender side, send the data through fiber optic cables and its back conversion happened on the receiver side). The optical USB receiver sends the signals to a computers USB port, and we can save the signals with a home made LabWiev software (.cnt format) [148].

In the second half of the experiments an Intan RHD2000 Evaluation System (Figure 14.) was used. The Intan RHD2000 Evaluation System has open-source hardware and software to record biopotential signals from up to 256 low-noise amplifier channels using RHD2000 series of digital electrophysiology chips (for detailed information check

<http://www.intantech.com/>). Here we use only 24 channel because of the electrodes, and the system fulfills the expectations for this research.

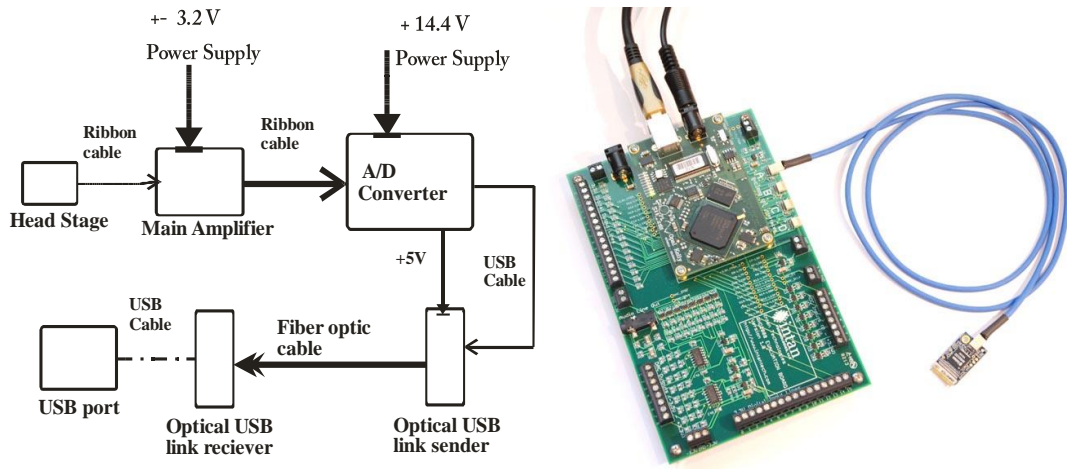


Figure 14. Left) The sketch of the NI data transmission system. Right) The Intan RHD2000 evaluation system, the interface cable, and the 2132 amplifier board (Intan Technologies, LLC., Los Angeles, California).

4.4 Micropipettes

4.4.1 Local field potential

Local field potential (LFP) signals were recorded with an additional glass patch clamp electrode (Sutter Instruments BF120-69-10) filled with ACSF on the sites where the largest SPA was detected with the laminar multielectrode (Figure 15.) [148].

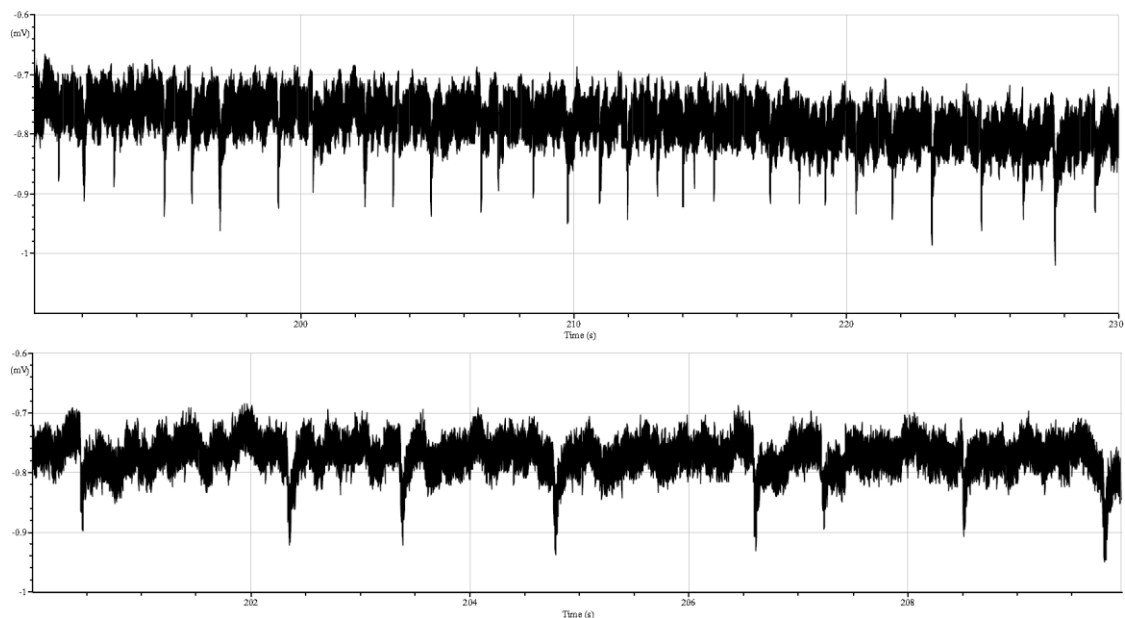


Figure 15. An example of SPA in a LFP extracellular micropipette recording (bottom zoomed in to a 10s section).

4.4.2 Intracellular

Intracellular recording in human tissue is not an easy task. Compared to the young (some days old) rodents, which are usually used in *in vitro* measurement, in human tissue it is much harder to make a good patch. Because the wide variety of age (26-78 year old), the glial cells around the neurons which are not visible on the camera pictures, etc...

Intracellular patch-clamp recordings were made with glass electrodes (5-9 M Ω) (Sutter Instruments BF120-69-10) filled with (in mM) 125 potassium gluconate, 20 KCl, 10 HEPES, 10 Di-Tris-salt phosphocreatine, 0.3 Na-GTP, 4 Mg-ATP, 10 NaCl, 0.008 biocytin, completed with 0.06 Oregon green BAPTA-1 (OGB-1) and 0.1 Alexa594 (Invitrogen, Carlsbad, CA). Electrophysiological recordings were made using a MultiClamp 700B Amplifier (Axon Instruments, Foster City, CA), and Digidata 1440 digitizer (Axon Instruments, Foster City, CA). Data acquisition was performed by using pClamp8 (Axon Instruments, Foster City, CA) and a custom made program written in MATLAB (The MathWorks, Natick, MA). Cells were held at -65 mV in current clamp recordings. Ramp test was made of the patched cells (Figure 16.) [148]. The LFP, LFPg and whole cell current clamp recording was simultaneously registered with Ca²⁺ line scans (Figure 17.) [148].

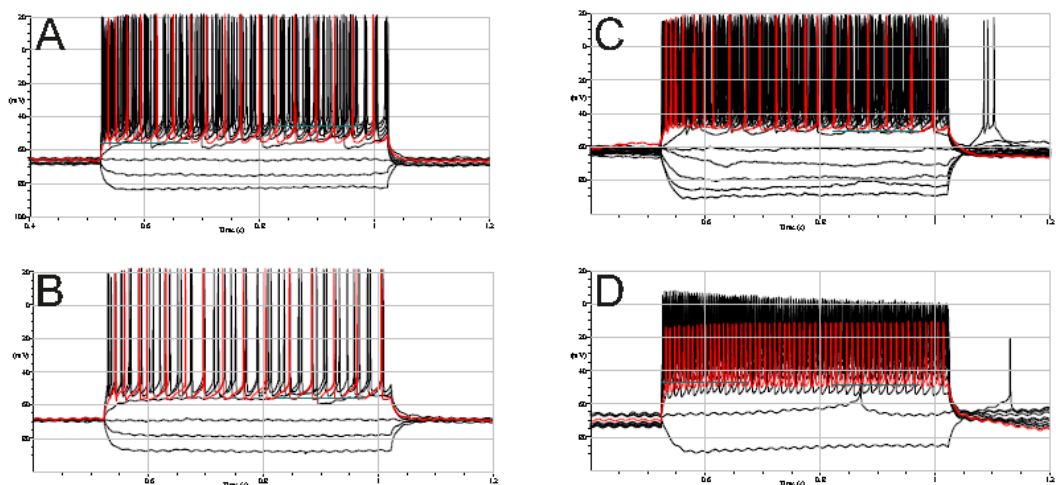


Figure 16. After a successful patch there were a ramp test to see whether the cell is active, and if so then what type of cell we have. A,B) two typical pyramidal cells. C) bursting pyramidal cell. D) interneuron.

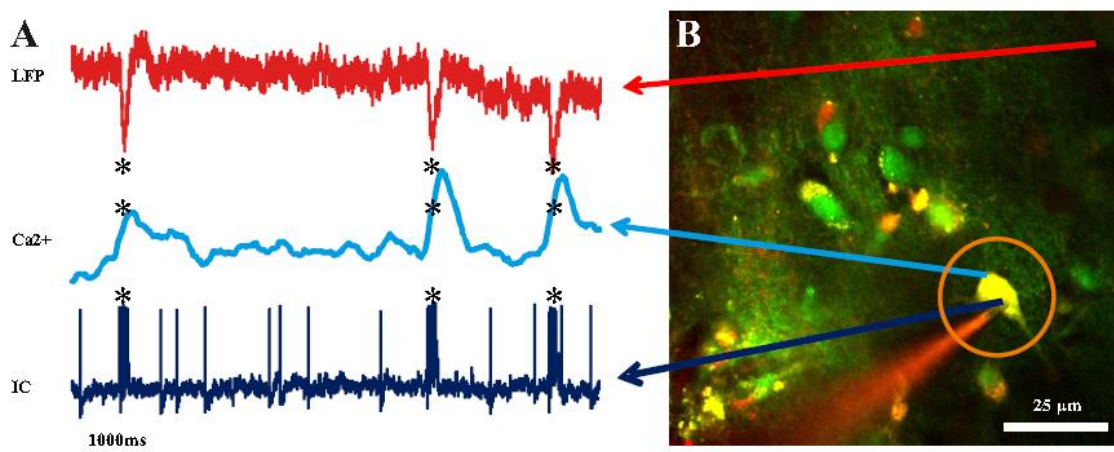


Figure 17. A) Simultaneous recording of LFP, Ca²⁺ imaging, and IC from the same slice and time. * marks the SPA. B) The bulk loaded slice and the patched cell.

4.5 Multiphoton imaging

Two-photon imaging was performed using a laser scanning system Femto2D-uncage (Femtonics, Budapest, Hungary). The imaging laser wavelength was set to 800 nm and to 840 nm in the uncaging experiments (Mai Tai HP Deep See, SpectraPhysics, Santa Clara, CA or Chameleon, Coherent, Santa Clara, CA). To minimize photodamage, the laser intensity was always kept at the minimum required to attain sufficient signal-to-noise ratio [145]. We injected bulk loading of OGB-1-AM (green) and sulforodamine-101 in the tissue, for differentiating the neuron and interneurons from the glial cells, and in half an hour the cells have taken up the cell permeable dyes. Free line scans were placed on the somata to check whether the cells have Ca²⁺ responses, or later following the curvature of long dendritic segments to monitor the backpropagating action potentials (AP) and uncaging induced Ca²⁺ signals [127] (Figure 18.). To measure population activity, neuronal somata were scanned with constant speed using lines which slightly extended the somata to decrease scanning-induced noise artifacts, while intermediate sections were jumped over within 100 μs using a spline interpolated path [155]. As all unnecessary background areas were avoided in this way, the method provided an increased signal-to-noise ratio and higher measurement speed. The scanning time of about 6 ms allowed us to analyze the spatiotemporal properties of Ca²⁺ compartments along long dendritic segments [148].

For single cell recordings we used additional OGB-1 (green) and Alexa594 (red) in the patch pipette for several reasons. First, the amount of OGB-1 taken by the cells is usually enough to mark only the cell body. Therefore, additional OGB-1 was injected through the pipette which is diffused into the dendrites within a few minutes. This allowed us to perform dendritic Ca²⁺ recordings. Second, transmission infrared mode of the microscope is usually used to perform patch clamp recordings in slice preparations, which has its visibility limits around 50 μm from

the surface of the slice. The fluorescent mode of the two-photon microscope was used to reach the bulk loaded cells located in deeper regions of the slice, which does not allow seeing unfilled electrodes. Alexa594 is used for further technical reasons. The green detector is usually earlier saturated than the red detector. Our recording system has its own safety switch shutting down the detector before getting damaged, which results in the loss of the picture in the green channel, while the red is still available. Furthermore, in some cases, we increased the signal-to-noise ratio of our recordings by subtracting the red channel signal from the green channel signal. At the end of each experiment, z-stack images of the area of interest were taken. To monitor recording conditions and the potential photodamage we repetitively measured Ca^{2+} responses induced by a burst of five action potentials (900 pA, 5ms, 50Hz) (Figure 19.) [148].

We used a Femto2D microscope in a combination with Axon amplifiers (see above). Both the microscope and the electrophysiological equipment were shielded, therefore no electric artifact was observed during scanning. We used an external shutter to switch on and off the laser which generated a small artifact at the beginning and at the end of the imaging and lines scanning. These artifacts could be easily recognized and were removed from the recordings.

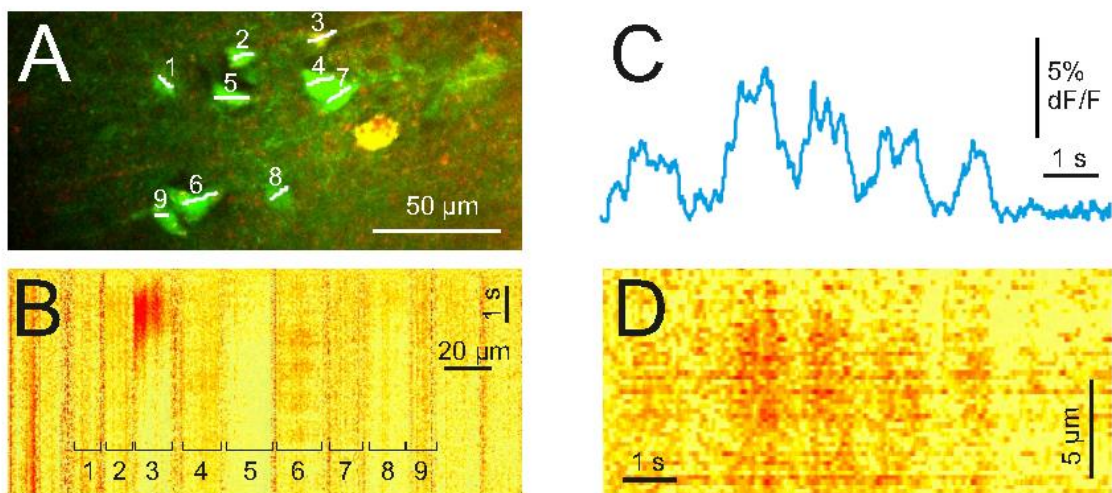


Figure 18. A) Maximum intensity z-projection of a neuronal population from a human neocortical slice loaded with OGB-1-AM Ca^{2+} indicator and sulforhodamine. White lines and numbers indicate regions of interest selected for multiple line scanning, and are covering nine neurons. B) Ca^{2+} response of 9 out of 13 cells recorded along the white lines, in top panel. C) Spatial average of Ca^{2+} response in region (=cell) #6. D) Ca^{2+} response in region #6 as in A, but recorded with a higher spatial discretization.

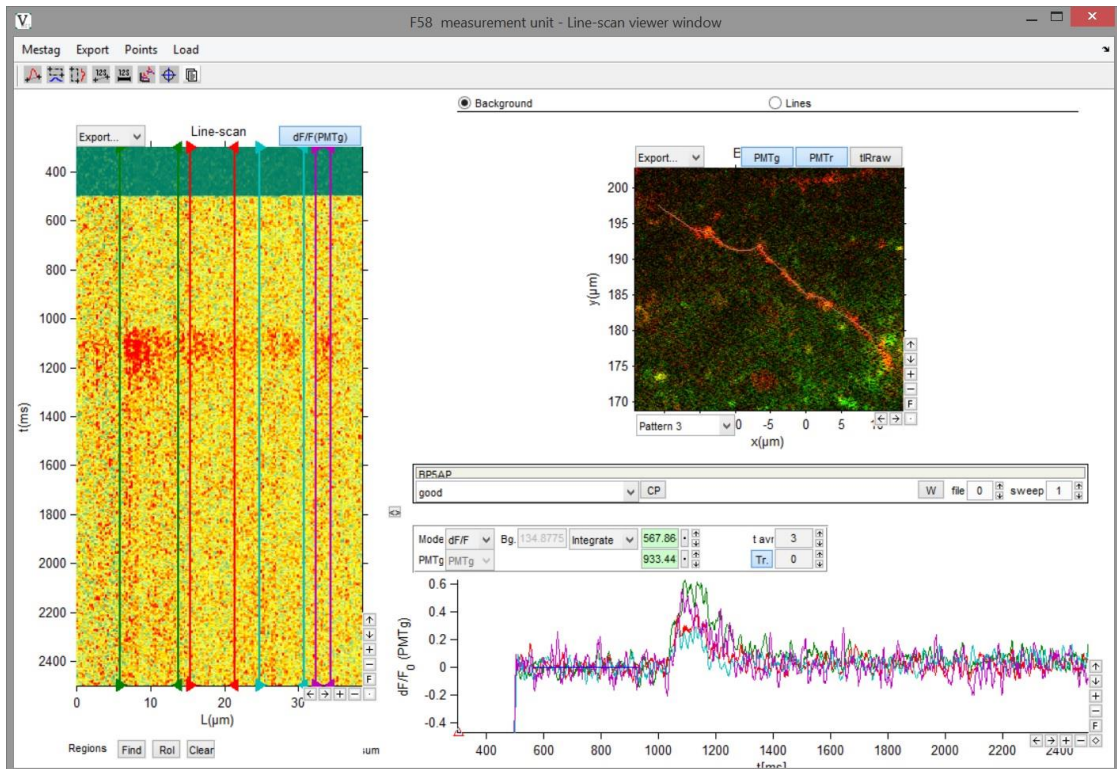


Figure 19. Ca^{2+} response in the dendrite for a BP5AP excitation protocol (the picture shows the MES software line-scan viewer window, the two-photon image and the scanning line in the right top, the Ca^{2+} response in the left, and the different ROIs on Ca^{2+} responses in the right bottom).

4.6 Multiphoton glutamate uncaging

In uncaging experiments the bath solution was exchanged to ACSF containing 4-Methoxy-7-Nitroindolyl (MNI)-caged L-glutamate trifluoroacetate (MNI-glutamate TFA; 2.5 mM; Femtonics, Budapest, Hungary). Fast photolysis of caged glutamate was performed with ultrafast, pulsed lasers at 720 nm. Laser intensity was controlled with an electro-optical modulator in the Femto2D-uncage microscope. A motorized beam stabilization unit provided 100 nm radial and 300 nm axial overlap of the imaging and uncaging point spread functions. The overlap was monitored by the transmitted infrared detector. Chromatic aberration was compensated for at the focal plane. Free line scanning of the dendritic segments was interleaved with uncaging periods when galvano mirrors jumped to the pre-selected locations (within 60-80 μ s jump time) and returned back to the scanning trajectory thereafter (Figure 20.). The distance of uncaging locations from the activated dendritic segments was also monitored by measuring the fluorescence artifact and keeping it below a given critical value (\sim 2000 analog-to-digital converter unit at 90% photomultiplier (PMT) saturation) during photostimulations. The uncaging evoked artifact was relatively small due to the strong infrared filtering before detectors and we also used the motion artifact correction program module of the Femto2D microscope. With the use of this program module we were able to correct for the sample drift during measurements as well as to keep the relative distance between dendrite and uncaging locations [148]. Therefore the overlap between uncaging locations and the dendritic segment was minimal which decreased the fluorescent artifact. In the uncaging measurements we used BPAP or BP5AP protocols:

- At 1000ms the shutter of the uncaging laser opens for 0.1-1ms. The laser goes through each uncaging point with \sim 100 Hz, but this is based on ROI-s in the process, because we need an EPSP excitation not an AP. With an EPSP it is easier to quantify the Ca^{2+} response, by deleting the uncage excitation points one by one.
- At 2500ms one or five (depends on the protocol) action potential evoked by somatic current injection through the micropipette (900 pA, 5ms, 50Hz) (see in Figure 27.).

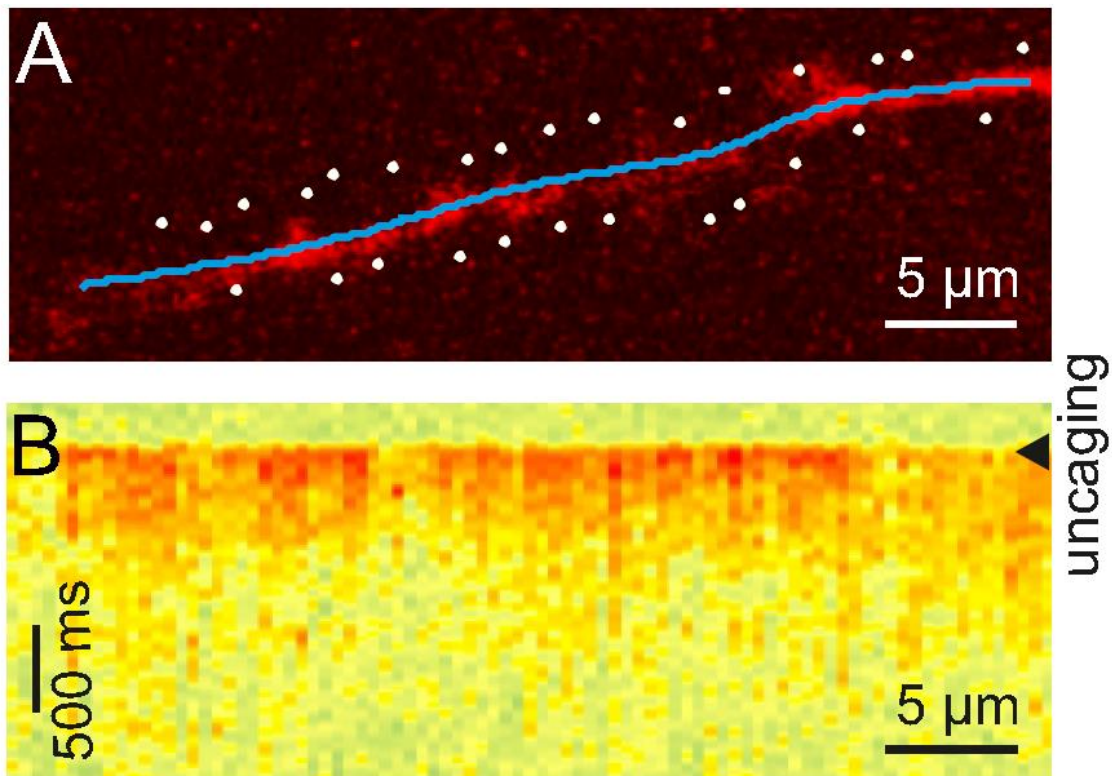


Figure 20. A) Dendritic segment with the uncaging locations (white spots). Blue line indicates the scanning path of free line scanning. B) Dendritic Ca²⁺ response, recorded along the blue line in the middle, was normalized to the background fluorescence level and plotted as a function of dendritic distance and time. Ca²⁺ response was evoked by two-photon glutamate uncaging in the white points. Uncaging time is indicated by black arrowhead.

4.7 Data analysis

LFPg data analysis was performed with Neuroscan Edit 4.5 program (Compumedics Neuroscan, Charlotte, NC), LFP and patch clamp recordings were analyzed using the pClamp 8, or MES (Femtonics) program. Home written programs for Matlab were used to analyze data of two-photon imaging (MES (Femtonics)). MES program was written to control the two-photon microscope in the measurement, and has lots of features for that (camera mode two-photon mode, linescan, z-stack, etc...) [96] [119], but on top of that it has an analysis program part as well. MES analysis handle well the Ca²⁺ imaging data and the recordings from the micropipettes (extracellular, or intracellular) can be imported.

The MES analysis software is very good in event related studies, like uncaging experiments, or episodic stimulation, they are easy to handle (for example: all of the episodes can be loaded, and preprocessed at the same time with one command, because one can set the event time, and on these signals, use a loads of built in filtering, averaging, etc...) [148].

The spontaneous recordings are a little bit harder to handle, because you need to search your signal for each event to preprocess (like in this research for the average of the signals one need to search for every event (SPA peak), and set a new window for it (and on all the connected

Ca²⁺ signals or patch) to prepare it for further analysis), but one can easily get the amplitudes, and the latencies of the events.

The LFP signal was band pass filtered between 1 and 30 Hz to determine the peak of the SPA. The peak of the SPA was set as time zero for further event related analyses.

During intracellular Ca²⁺ signal detection, the baseline was set for each cell at 120-80 ms before the peak of each SPA. The Ca²⁺ transient was considered to be significantly increased when it passed two times the standard deviation (SD) of the baseline interval. We determined for each cell, during each SPA event, whether its Ca²⁺ signal passed this significance level.

So to summarize the steps of the signal preprocessing:

- import the LFP signal from the .abf files to the Ca²⁺ responses in MES program
- low pass filter the LFP recording (Bessel 30Hz)
- filter the Ca²⁺ signals (Gaussian filtering)
- SPA peakdetection
- windowing the signals (around the SPA events) and aligning the SPA peaks
- baselining the Ca²⁺ responses
- gathering the amplitudes, and the latencies of the events
- defining the 2SD threshold
- separating the cells which datacluster (see below in Table 1.) it fits

After these steps the more complex analyses can take place (averaging, comparisons, statistics, etc...).

4.8 Cell morphology

Biocytin was passively diffused into the cell through the patch pipette, during intracellular recording. After recording, slices were maintained for at least 30 minutes in the recording chamber, and then fixed overnight in 4% paraformaldehyde with 15% picric acid in 0.1 M phosphate buffer (PB, pH 7.4) at 4°C. The slices were resectioned (Leica 1200 S) at 60 µm and freeze-thawed above liquid N₂ in 0.1 M PB containing 30% sucrose. Endogenous peroxidase activity was blocked by 1% H₂O₂ in Tris-buffered saline for 10 min. Cells containing biocytin were revealed with the ABC reaction (avidin-biotinylated horseradish complex, Vector, 1.5 h, 1:250) using 3,3'-diaminobenzidine-tetrahydrochloride (DAB, Sigma, St. Louis, MO, 0.05 M in Tris-buffer pH 7.6) as the chromogen. Sections were osmicated (20 min, 0.5% OsO₄), dehydrated in ethanol, and mounted in Durcupan (ACM; Fluka, Buchs, Switzerland).

One biocytin-filled neuron was chosen to be digitally reconstructed in three dimensions using the NeuroLucida system (MicroBrightField Inc. Williston, VT). Shrinkage correction factor of 1.33 was used in x and y dimensions [156]. Shrinkage in z dimension was measured in 10 randomly chosen points in the section containing the cell body, and was averaged. A shrinkage correction factor of 1.41 was applied in z dimension [148].

4.9 Electron microscopy

After light microscopic examination (and three dimensional reconstruction of the chosen filled cell) areas of interest were re-embedded and sectioned for electron microscopy with a Leica ultramicrotome (Leica EM UT7). Ultrathin (~60 nm) serial sections were collected on Formvar-coated single slot grids, stained with lead citrate, and examined with a Hitachi 7100 (Hitachi, Tokyo, Japan) transmission electron microscope [148].

5 Results

In the following the new scientific results will be presented. Let there be a summary of the theses again, but the results will be shown in an arrangement of the steps of the measurement, because it is easier to describe the results by that way.

Thesis I: A method has been developed for the two-photon Ca^{2+} imaging of human neocortical tissue (see in the Materials and methods section).

Thesis II: The extracellular recording system was successfully combined with the two-photon microscope system. This way the epileptic and non-epileptic human neocortical neurons Calcium responses during SPA was compared.

Thesis III: The functional coupling of LFP, Calcium responses and intracellular activity in human neocortical interneurons and pyramidal cells during SPA will be demonstrated.

Thesis IV: The electrophysiological and imaging measurements were successfully combined with anatomical reconstruction of the intracellularly loaded cells, to gain more information of the morphology of the loaded cells.

Thesis V: The electron microscopic ultrastructure of the filled and reconstructed pyramidal cell will be described at electron microscopic level.

5.1 Recording the spontaneous network activity by simultaneous Ca^{2+} imaging and field-potential measurements

The local field potential (LFP) was recorded in 69 human neocortical slices from 17 patients (32 slices from 8 tumor patients, 17 slices from 5 epileptic patients, and 20 from 4 tumor associated epileptic patients). SPA was detected in 15 slices (9 slices from 4 tumor patients, 4 slices from 3 epileptic patients, and 2 slices from 1 tumor associated epileptic patient) by using the following procedure. The multielectrode was placed on the surface of the slice, perpendicular to the pial surface, allowing electrophysiological recording from all neocortical layers. The slices were mapped to localize the areas generating SPA by recording every 300-400 μm from one end of the slice to the other end (Figure 21.) [148].

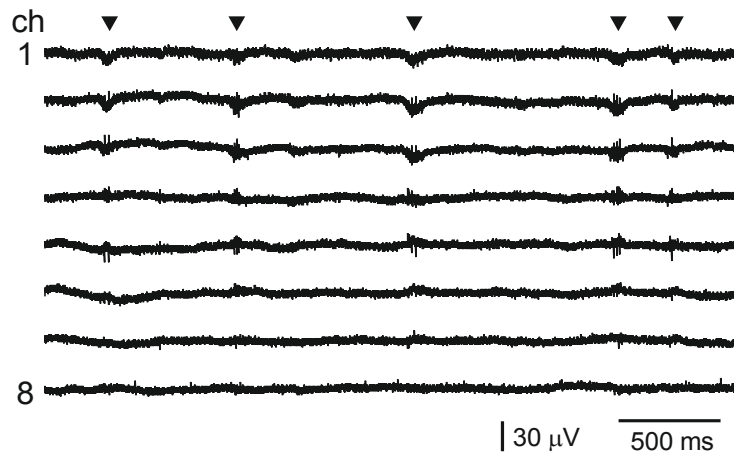


Figure 21. Laminar recordings were made in the human neocortex in vitro. The 24 channel multielectrode array was placed perpendicularly to the pial surface and covered the whole width of the neocortex, permitting recordings from each layer. LFPg recordings from 8 channels are shown on this figure. Spontaneous population activity (SPA, marked with black triangles) emerged in layer I-III in the neocortex of Pt 1.

After mapping the neocortical slices with the laminar multielectrode, regions where SPA could be detected with LFPg recording were chosen for further two-photon Ca^{2+} imaging and intracellular patch clamp recordings. Bulk loading was performed on the sites where SPA had the largest LFPg amplitude, and additional extracellular local field potential (LFP) signals were recorded with a glass patch pipette filled with ACSF at the site of the bulk loaded cells. This way we could effectively record the SPA generation associated Ca^{2+} signals with two-photon imaging in human neuronal populations (Figure 22.). The multielectrode array measured neuronal activity in the entire width of the examined neocortical region, near the site of the bulk loading. We simultaneously recorded the LFP signal of SPAs and the Ca^{2+} signals of the loaded neurons in 6 slices. In the remaining 4 slices SPA could not be detected after bulk loading. In the slices with detectable SPA a frame scan was taken after bulk loading, then cells were selected for fast measurement (Figure 23.) and were measured using the multiple line scanning method [127] [148].

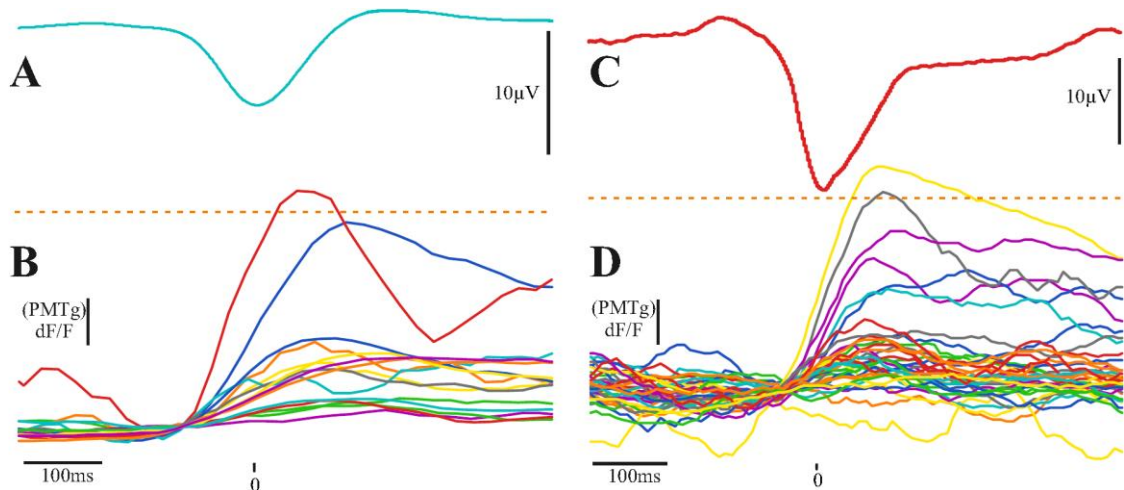


Figure 22. A) Average of LFP from a whole measurement of a tumor patient. B) The connected cells Ca^{2+} responses, from a whole measurement of a tumor patient. There are two of the cells that had good responses in the whole experiment. The LFP is filtered (Bessel 30 Hz low pass), and the Ca^{2+} responses are smoothed (Gaussian average). Dashed orange line is the 2SD. Because of the averaging the second cell seems here not to pass the 2SD limit, but by the reliably responding cell definition below, the cell was in this group.

C) Average of LFP from a whole measurement of an epileptic patient. D) The connected cells Ca^{2+} responses, from a whole measurement of an epileptic patient. There are 3 cells that had good responses in the whole experiment. The LFP is filtered (Bessel 30 Hz low pass), and the Ca^{2+} responses are smoothed (Gaussian average). Dashed orange line is the 2SD. Because of the averaging the third cell seems here not to pass the 2SD limit, but by the reliably responding cell definition below, the cell was in this group.

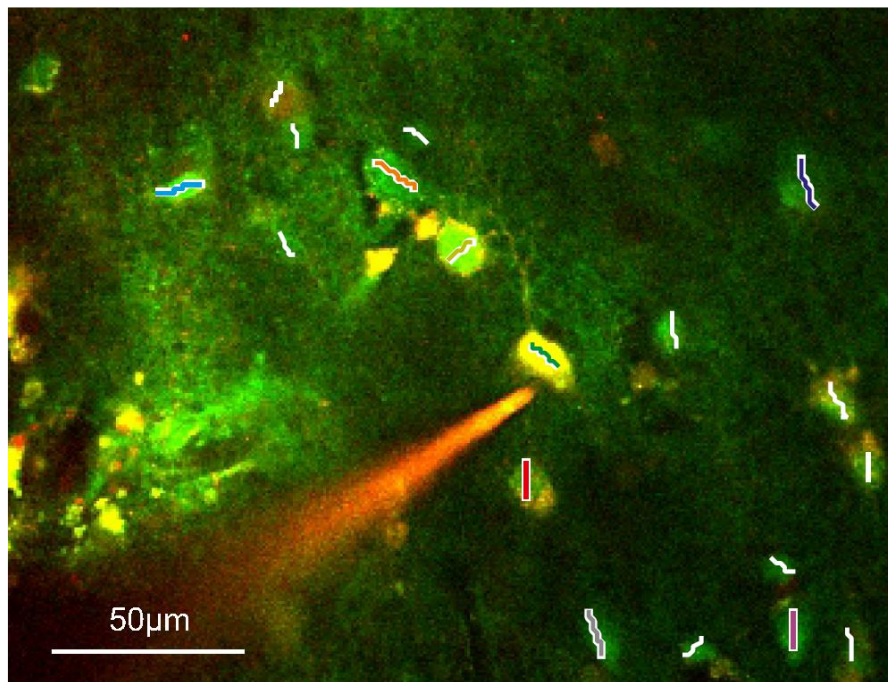


Figure 23. Two-photon image of a human neuronal population loaded with OGB-1-AM Ca^{2+} dye for population imaging. A pyramidal neuron was patch-clamped (IC, intracellular recording) and filled with OGB-1 (60 μM) and Alexa594 (100 μM) through the recording pipette. Neuronal somata were scanned with constant speed along the white lines while intermediate sections were jumped over within 100 μs using a spline interpolated path (multiple line scanning).

The advantage of this method is that it increases the product of measurement speed and signal collection efficiency [119] resulting in high measurement speed and an increased signal-to-noise ratio (Figure 23, 24). We simultaneously recorded the LFP signal of SPAs and the somatic Ca^{2+} signal of 31 neurons in 2 slices from tumor patients, and 55 neurons in 4 slices from epileptic patients (Table 1).

A relative increase in Ca^{2+} signal from the baseline larger than 2x standard deviation (SD) of the baseline was taken as significant Ca^{2+} response. Baseline was measured from -120 to -80 ms before the peak of every SPA event. The neurons showing at least one significant Ca^{2+} response were taken as responding cells. Occasionally responding cells showed increased Ca^{2+} signal during <20% of the SPA events, non-reliably responding cells responded to 20-40% of the SPA events, whereas reliably responding cells showed Ca^{2+} responses to >40% of the SPA events. With this method, we identified 21 silent cells (68%), 4 occasionally (13%), 1 non-reliably (3%) and 5 reliably responding (16%) cells in the tumor tissue. The distribution of the responding cells was considerably different in epileptic tissue: we found 19 silent cells (35%), 20 occasionally (36%), 11 non-reliably (20%) and 5 reliably (9%) responding cells (Table 1) [148].

Table 1.

Examination of cellular activity during SPA with two-photon Ca²⁺ imaging in epileptic and non-epileptic tissue.

| Patient/Slice | Number of SPAs | Number of recorded cells | Number of silent cells (0%) | Number of occasionally responding cells (<20%) | Number of non-reliably responding cells (20-40%) | Number of reliably responding cells (≥40%) |
|-------------------------------|----------------|--------------------------|-----------------------------|--|--|--|
| Pt 1 (tumor) slice 1 | 8 | 13 | 7 | 2 | 1 | 3 |
| Pt 2 (tumor) slice 1 | 15 | 18 | 14 | 2 | 0 | 2 |
| Pt 4 (epileptic) slice 2 | 79 | 26 | 4 | 16 | 3 | 3 |
| Pt 4 (epileptic) slice 3 | 13 | 15 | 5 | 3 | 6 | 1 |
| Pt 5 (epileptic) slice 1 | 15 | 4 | 2 | 0 | 2 | 0 |
| Pt 5 (epileptic) slice 2 | 12 | 10 | 8 | 1 | 0 | 1 |
| Pt 8 (t associated e) slice 4 | 7 | 23 | 11 | 6 | 3 | 3 |
| Tumor | | 31 | 21 (68%) | 4 (13%) | 1 (3%) | 5 (16%) |
| Epileptic | | 55 | 19 (35%) | 20 (36%) | 11 (20%) | 5 (9%) |
| T associated E | | 23 | 11 (48%) | 6 (26%) | 3 (13%) | 3 (13%) |

5.2 Intracellular recordings

Based on the Ca^{2+} responses of the cells within region of interest, we chose non-reliably or reliably responding neurons for further intracellular recording. Whole cell ($n=7$ neurons) or loose patch clamp ($n=2$ neurons) recordings were made to reveal the electrophysiological activity of the given cell. In these cases LFP, intracellular recordings and Ca^{2+} signals of the patched and the neighboring cells were simultaneously detected (Figure 21, 23, 24). Based on the morphology revealed by the fluorescent dyes, electrophysiological recording was made from 3 pyramidal cells and 6 interneurons.

We examined the somatic and dendritic Ca^{2+} responses of both interneurons ($n=4$, Figure 25.) and pyramidal cells ($n=3$, Figure 26.), together with their somatic electrophysiological activity [148].

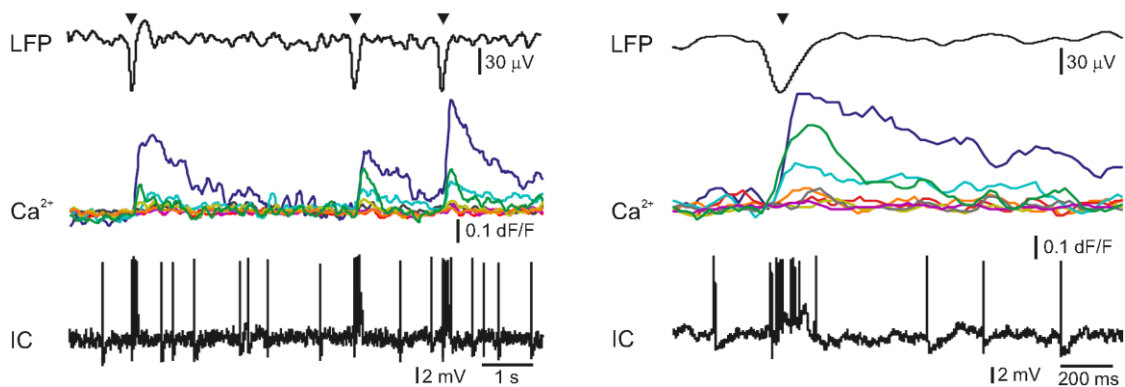


Figure 24. Left) Simultaneous LFP, Ca^{2+} signal (Ca^{2+}) and loose patch clamp recording during three successive spontaneous SPA events (black triangles). Ca^{2+} transients show the responses of eight neurons from the eighteen recorded shown Figure 23. Different colors of the Ca^{2+} signals represent different cells. Note that three cells were responding to SPAs, but the other cells did not show increased Ca^{2+} levels. The intracellularly recorded cell (IC), shown in Figure 23 was burst firing during SPA, which is also reflected in a simultaneous increase in the intracellular Ca^{2+} level (green line). Note the trial-to-trial variability in relative Ca^{2+} responses between neurons.

Right) LFP signal of a SPA event (black triangle) on an enlarged view with the corresponding Ca^{2+} responses recorded from the neuronal population shown in Figure 23. and the simultaneously recorded loose-patch signal. Note the large Ca^{2+} signal during the somatic AP burst associated to the SPA event (green line in the middle).

As it has been described in animal tissue [157] [158] positive correlation between the number of somatic action potentials and the amplitude of the dendritic Ca^{2+} signal was observed. Briefly, bursts of action potentials generated in pyramidal cells ($n=2$ cells) and multiple action potentials detected in interneurons ($n=2$ cells) resulted in larger dendritic Ca^{2+} increase than single action potentials. A detailed future study is needed to exactly correlate somatic electrophysiological recording with the somatic and dendritic Ca^{2+} signal of both human pyramidal cells and interneurons (Figure 25, 26).

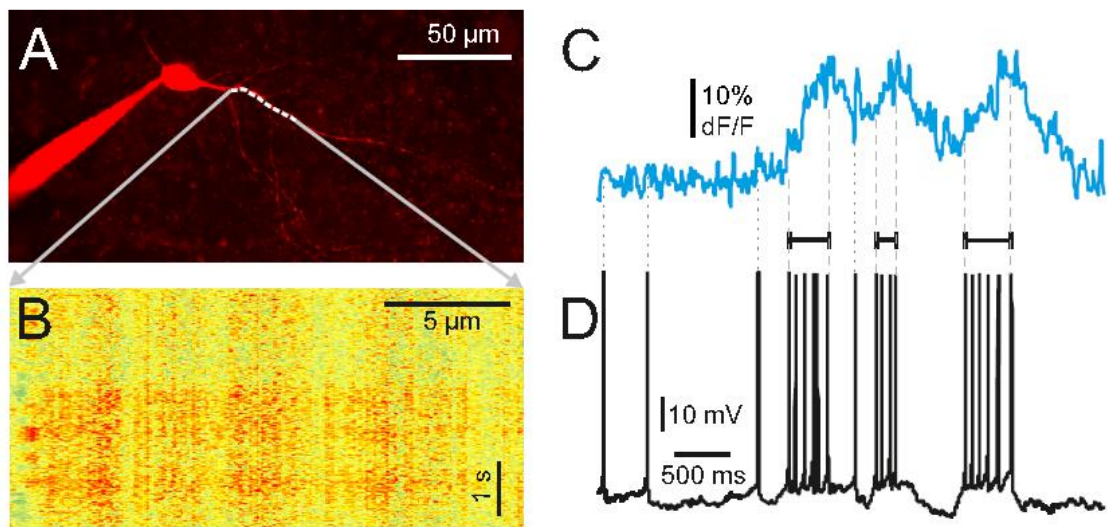


Figure 25. A) Maximum intensity z-projection image of a human aspiny neocortical interneuron with a dendritic segment selected for free line scanning (white dashed line). Only the red PMT channel data are shown. B) Ca^{2+} response measured along the white dashed line plotted as a function of distance along the dendrite and time. Responses were spatially normalized to the background fluorescence level. C) Spatial integral of the dendritic Ca^{2+} response shown B. D) Simultaneously recorded somatic membrane potential. Dashed gray lines mark the initiation and termination of short temporal intervals with high AP number and dotted lines mark single APs. Note the synchronous increase in average dendritic Ca^{2+} response during the multiple APs.

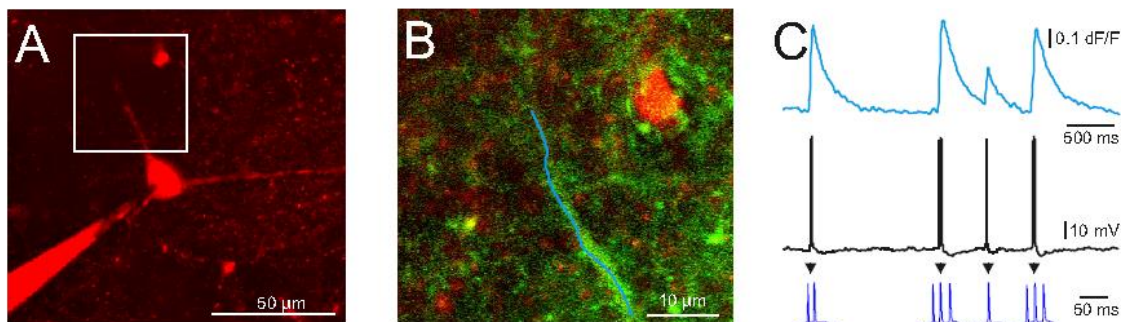


Figure 26. A) Maximum intensity z-projection image of a human neocortical pyramidal cell, red channel data. B) Enlarged view of the dendritic segment shown in the white box in Left. Blue line indicates free line scan. C) Dendritic Ca^{2+} responses (cyan line) averaged along the blue line in B. Simultaneously recorded somatic membrane potential responses. Enlarged view of AP bursts (blue). The amplitude of the Ca^{2+} signal shows correspondence to the number of APs recorded in the cell body. Note, that the rising phase of the pyramidal cell dendritic Ca^{2+} signal is steeper than that of the interneuron shown on Figure 25.

Measurement of input-output functions of cortical pyramidal cells and interneurons is important to understand dendritic integration and neuronal computation [115] [127] [159] [160] [161]. As human neurons have more complex dendritic branching compared to animals, (see the dendritic length of our reconstructed pyramidal cell, [162], we expect a more complex human dendritic arithmetic. Two-photon uncaging is widely used to investigate neuronal input-output functions and postsynaptic signal integration. As in animal models [127] [163], we could use

spatially and temporally clustered input pattern to activate short dendritic segments via glutamate uncaging and measured the postsynaptic Ca^{2+} response using free line scanning and somatic whole cell recording (Figure 27) [148].

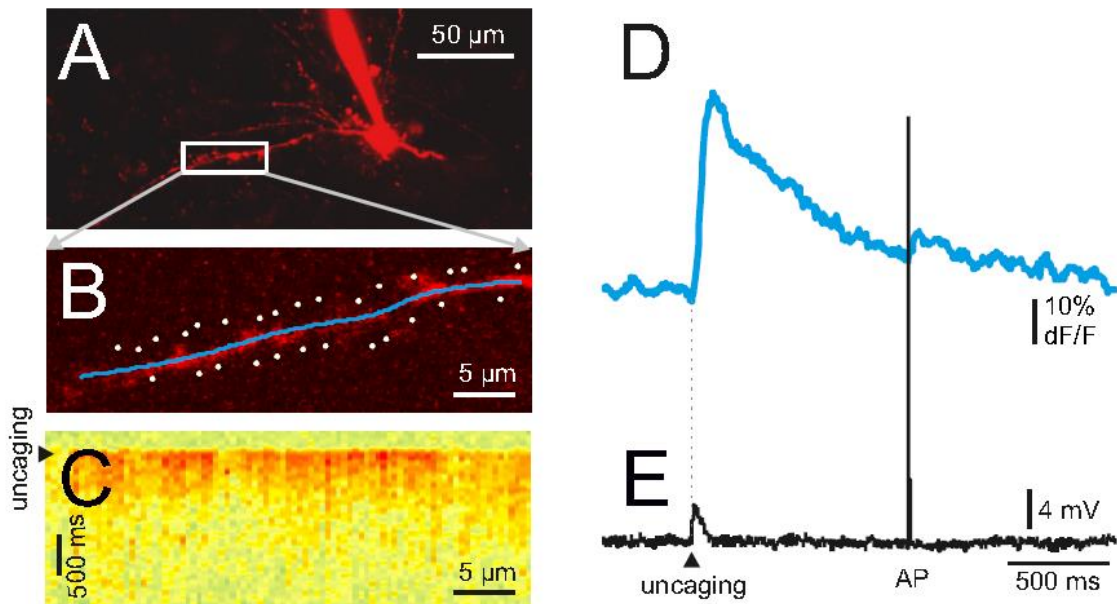


Figure 27. A Maximum intensity z-projection image of a human neocortical interneuron. Only the red channel data are shown. B) Dendritic segment with the uncaging locations (white spots). Blue line indicates the scanning path of free line scanning. C) Dendritic Ca^{2+} response, recorded along the blue line in the middle, was normalized to the background fluorescence level and plotted as a function of dendritic distance and time. Ca^{2+} response was evoked by two-photon glutamate uncaging in the white points. Uncaging time is indicated by black arrowhead. D) Spatial average of five Ca^{2+} responses detected in the dendrite shown in C. E) Simultaneously recorded somatic membrane potential. Note that both the uncaging evoked EPSP (black arrowhead) and the somatic current injection induced AP was associated with an increase in dendritic Ca^{2+} level.

5.3 Anatomy

Intracellularly recorded cells were filled with biocytin ($n=6$) and were processed for anatomy. The successfully filled neurons showed the morphology of either pyramidal cells ($n=2$) or interneurons ($n=2$). The pyramidal cells displayed a long and thick apical dendrite and numerous thin basal dendrites (Figure 28), the interneurons appeared as small multipolar cells with shorter smooth dendrites (Figure 30). The whole dendritic and axonal arbor of one well filled neocortical layer III. pyramidal cell was chosen to be reconstructed in three dimensions (from Pt 7, Figure 29.). Out of the 4 filled cells, this was the only neuron having an apparently complete (and well filled) dendritic arbor, as well as filled axons. Two other cells were not completely filled, i.e. they possessed pale dendritic segments and had no filled axons. The cell body of one neuron was close to the surface of the slice (within $50\ \mu\text{m}$) and part of its dendritic tree was cut during slice preparation.

The apical dendrite of the reconstructed cell was 4310 μm long, the sum of the length of its basal dendrites was 13478 μm and the length of all the axonal segments was 3875 μm long. It far exceeds the dendritic length of pyramidal cells in monkey temporal cortex, even though they were labelled *in vivo* [148] [164]. Pyramidal cells of the rodent neocortex also possess considerably shorter dendritic lengths (see www.neuromorpho.org, [165] [166] [167]).

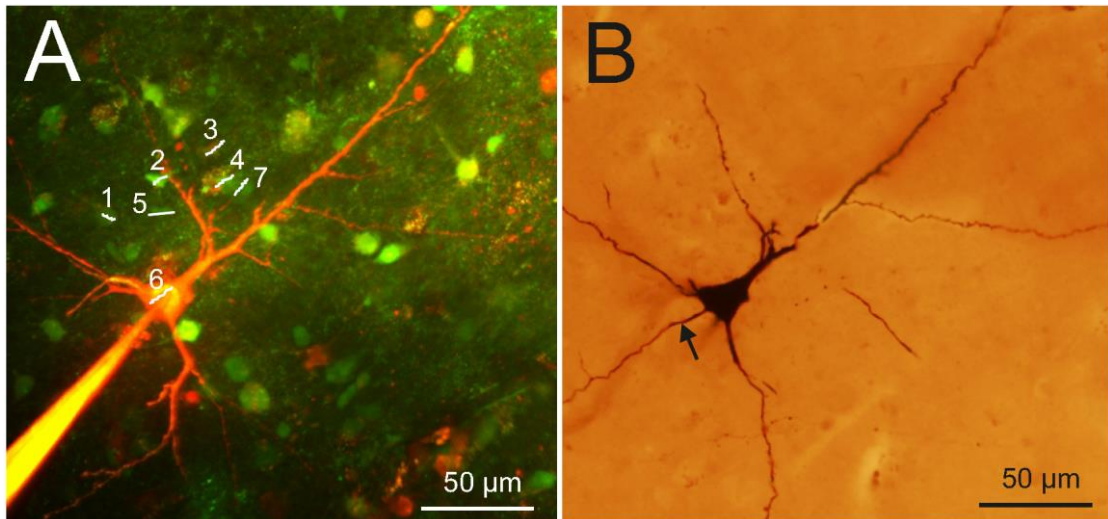


Figure 28. A) Maximum intensity z-projection of a population of human neurons loaded with OGB-1-AM dye. The neuron corresponding to region #6 (also shown in Figure 18) was whole-cell recorded and loaded through the recording pipette with the green Ca^{2+} dye OGB-1, the red Alexa594 and biocytin.

B) Light micrograph of the cell #6 shown left, processed for anatomy. The axon initial segment is marked with arrow.

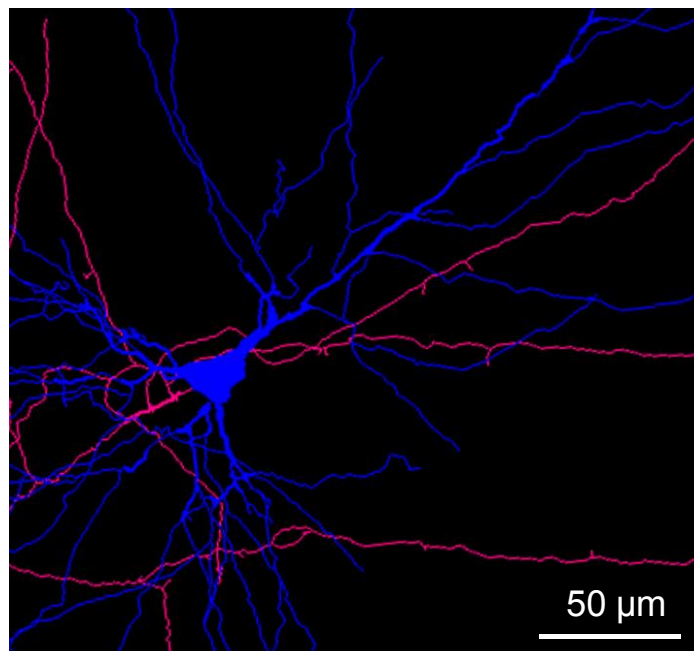


Figure 29. The dendritic (blue) and axonal (pink) arbor of the pyramidal cell #6 in Figure 28 was reconstructed in three dimensions.

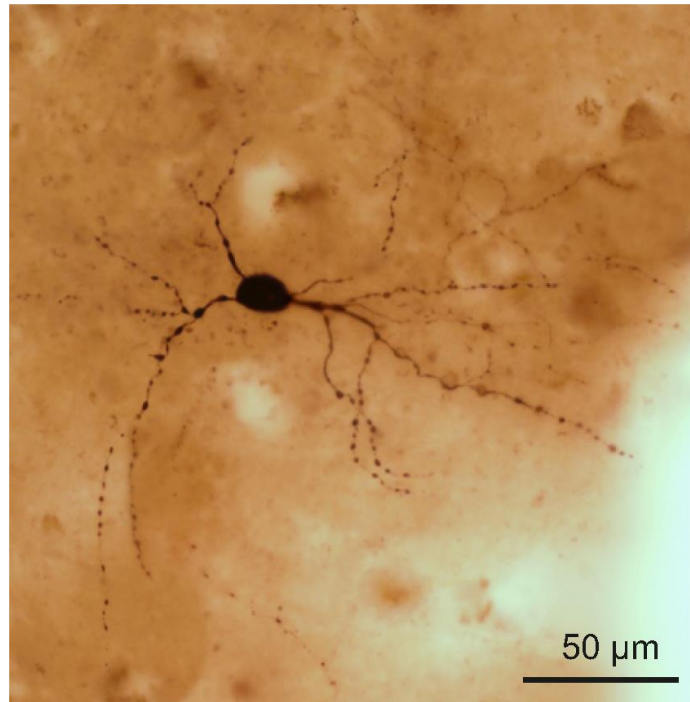


Figure 30. Light microscopy image of an interneuron shown in Figure 25. The cell was filled with biocytin and was processed for anatomy following the two-photon experiment.

5.4 Electron microscopy

We examined the filled and reconstructed pyramidal cell at electron microscopic level. Large vacuoles were found in the cell body and the dendrites of the cell (Figure 31), while outside these areas mitochondria and other organelles such as endoplasmic reticulum seemed to be intact. We found numerous axon terminals forming either asymmetrical (presumably excitatory) or symmetrical (presumably inhibitory) synapses on the dendrites of the filled cell. We could not find synapses innervating the cell body of this pyramidal cell, but we observed several symmetrical synapses terminating on its axon initial segment. The axon terminals of the filled cell formed asymmetrical synapses with non-stained dendrites and spines [148].

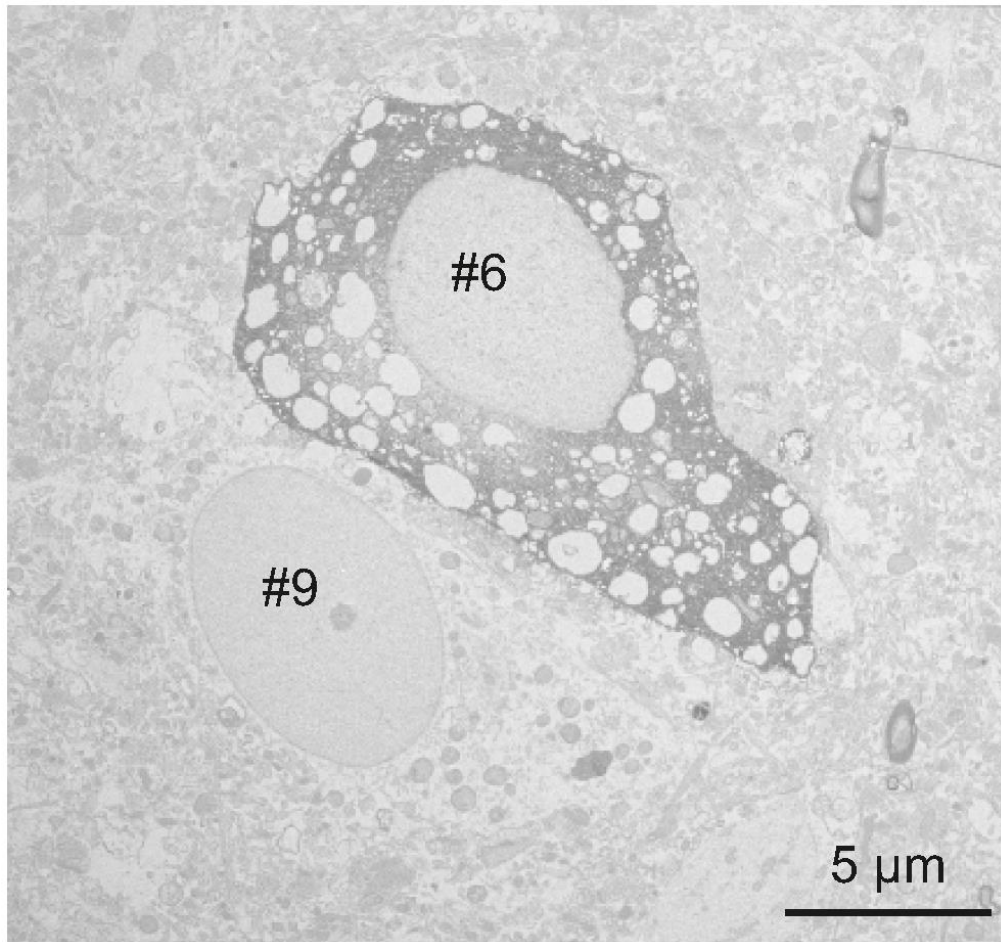


Figure 31. The electron microscopic investigation of the same cell (Figure 18, 28 #6) showed large empty spaces (vacuoles) in the cell body. The neighboring neuron (identified on Figure 18 as #9) is a healthy pyramidal cell without large somatic vacuoles.

We hypothesized that the presence of vacuoles is the result of our methodological procedure. First, applying OGB-AM and SR-101 for bulk loading may change the structure of the neurons. Second, the long time (several hours) spent in the recording chamber might also affect the survival of the cells. And third, patch clamp procedure (mechanical damage caused by the pipette, as well as the intracellular use of a high concentration of the fluorophores Alexa594 and OGB-AM) might also trigger changes in cellular ultrastructure. To test these hypotheses we made further electron microscopic examinations. First, we examined 62 non-filled cells (45 neurons and 17 glial cells) in the vicinity of the biocytin-filled cell. Based on the low magnification frame scan taken during the two-photon experiment, these cells were located within the region of bulk loading. We could not see large vacuoles in any of the bulk loaded cells. Next, we checked 61 cells (43 neurons and 18 glial cells) in the same slice, in a region where bulk loading was not performed. Both blocks were re-embedded from neocortical layer III. of Pt. 7, with a distance of ~5mm between them. None of the non-loaded cells displayed similar vacuoles in their somata. We made further experiments to test the hypothesis that several

hours of in vitro conditions might induce the formation of somatic vacuoles. We therefore re-embedded one block from Pt. 4, from a slice which spent 6 hours in the recording chamber and an other block from the same tissue sample (from the same part of the gyrus) which was fixed immediately after the cutting procedure. We examined 35 neurons and 22 glial cells from the recorded tissue slice and 43 neurons and 25 glial cells from the immediately fixed tissue sample. Large vacuoles were not observed in these cells [148].

6 Conclusion

Two-photon Ca^{2+} imaging is widely used to reveal sub- and suprathreshold neuronal activity in rodent neocortical and hippocampal slice preparations [11]. Somatic, dendritic and axonal Ca^{2+} signals were also correlated with somatic electrophysiological and local field potential recordings in these animal models [108] [168], but nothing is known about the intracellular Ca^{2+} signaling of single human neurons and neuronal populations. The aim of the present technical report is to demonstrate that these fundamental measurements can be achieved in human neurons following similar methodological procedures to those used in animals. Furthermore, we wished to show that combining different electrophysiological and optical methods in human neocortical slice preparations can give valuable information about cellular and network properties of cortical synchronization processes.

Recording in human brain tissue is very valuable in order to gain information about characteristics of human neurons and relate it to animal models. The present study is the first to show that Ca^{2+} dynamics of human neurons is comparable to those found in animals. We demonstrate that the use of appropriate methodological procedures provide high quality data about the somatic and dendritic Ca^{2+} signals of individual neurons and populations of human neocortical cells. During our experiments we noticed the high variability of tissue quality, even though we followed our standardized protocol. Several reasons might account for this phenomenon, usually not reported in studies using animals. The age of the patients varied from young adults to elderly (19 to 83 years), while research groups working on animal models usually use young animals of the same age group. Furthermore, we cannot exclude the possibility that differences in the pathology and in surgery conditions of our patients might also account for the considerable variance of tissue quality. We concluded that valuable electrophysiological, two-photon Ca^{2+} imaging and anatomical results could be obtained if the tissue quality was acceptable. Here we have adopted and used an improved version of dual perfusion chamber [108] [149], which provided excellent tissue oxygenation to maintain network activity and allowed simultaneous imaging and two-photon uncaging experiments during population activity. The high signal-to-noise ratio obtained in our measurements has not only been enhanced by the high numerical aperture of the water-immersion objectives but also by the use of our multiple line scanning method.

The techniques used in our study are complementary in several ways: two-photon Ca^{2+} imaging records the activity of large populations of neighboring neurons although at low temporal scale, whereas multiple channel electrophysiology records the activity of a few cells distributed along the entire width of the cortex and at high temporal scale. This allows us to examine larger and more complex neuronal populations than any of the mentioned technique alone. In summary, one of the main advantages of our combined method is that it allows

simultaneous optical and electrophysiological examination of human neurons and neuronal assemblies with high spatial and temporal resolution. Subsequent anatomy is a useful tool to reveal differences in the fine structure of the human cortex related to the pathology of the patient, or to the capability of SPA generation. Anatomical examination of intracellularly filled human neurons could reveal possible differences between cells participating vs. not participating in the generation of SPA, between cells located in regions where SPA is present vs. regions outside of SPA, as well as between cells derived from epileptic vs. tumor patients.

Our study reported a technical difficulty associated to Ca^{2+} imaging of living cells. Although our intracellularly labeled cells looked healthy under light microscope, we observed large autophagic vacuoles in the somatodendritic compartment of the examined neuron at electron microscopic level (see also supplementary material of [169]). Our electron microscopic studies suggest that this phenomenon is attributed to photodamage. Oxygen radicals generated during illumination and photobleaching of intracellular fluorophores [170] [171] induce ultrastructural changes in the cell, such as inactivation of proteins [170] [172] [173] and formation of autophagic vacuoles [174]. This phenomenon is exploited in a developing powerful technique called Chromophore-Assisted Laser Inactivation (CALI), used as a potent cell biology technique and as a therapeutic tool in cancer research (for review see [173]). At the same time, Ca^{2+} imaging caused photodamage has never been directly addressed in neuronal tissue. We tried to minimize photodamage by using line scans and by keeping laser intensity at the minimum required to attain sufficient signal-to-noise ratio. We could not see changes in the physiology of the neurons during recordings, neither signs of cell degeneration at the light microscope, but photodamage became evident when examined with electron microscopy.

We performed simultaneous correlated somatic whole-cell, local field potential and intracellular Ca^{2+} measurements during conditions when the network of human neurons showed synchronous discharges. Electrophysiological recordings of synchronous population events in the human neocortex were already performed in vitro, describing the responses of single neurons [6]. Our multimodal approach allows us to record the simultaneous activity of large neuronal populations together with the intracellular response of selected single neurons. In addition, Ca^{2+} imaging of neuronal populations revealed the relatively high percentage of silent cells (35% of the cells in epileptic and 67% in tumor tissue) which were unnoticeable in electrophysiological recordings. We demonstrated that higher proportions of neurons participate in the generation of SPA in slices from epileptic (65% of the cells) than from tumor (32% of the cells) patients (Table 1). The ratio of cells responding to >20% of the SPA events is also higher in epileptic tissue (29% vs. 19% in epileptic vs. tumor tissue), even if the proportion of reliably responding cells was lower in epileptic tissue. This suggests that in the human epileptic neocortex more neurons are contributing to network synchrony, although with a lower precision. This network phenomenon is similar to the cellular properties observed in epileptic rats [175], where an

enhanced synaptic activity and a lower spike-timing reliability have been shown to induce synchronies related to epilepsy (fast ripples).

The epilepsies are a serious health problem affecting large percentage of human populations during their lifetime. Our multi-modal and multi-scale approach could help to clarify the abnormalities in cellular and network properties that underlie this pathology, providing both a better understanding of the disease and, eventually, contributing to better therapeutic approaches to the treatment of neocortical epilepsies. Future therapeutic strategies that consider data from human neural tissue will better facilitate the development of new, more efficient drugs or other treatments that prevent epileptic seizures and/or alleviate epilepsy caused damage. The detailed analysis of human epileptic tissue is required to promote pharmaceutical research, but also crucial for the development of new, more realistic animal models. Animal models are necessary to better understand the mechanisms, causes and consequences of epilepsy. However, results derived from animal models must be compared and contrasted with human data if they are to provide valuable information about human disease.

7 Future plans

We want to move forward with these experiments and have more informations of the mechanisms behind SPA. For this we need more successful simultaneous LFP, Ca²⁺ imaging, and intracellular recordings.

There are two ways we are developing the laminar electrode: - polyimid based, and silicon based. We want to test and use these newer versions of the electrode in our future experiments.

For the exact and precise statistics we need more simultaneous recordings (and enough events) from each patient groups (we think that at least 5-5 patient from each group will be enough but 10-10 would be much more precise), avoiding the misinterpretation of the statistical results. We want to make correlation from the Ca²⁺ signals and the SPA events between the different patient groups, coherence, and causality investigation, and some statistical tests.

We want to further investigate the above mentioned vacuoles detected with Transmission Electron Microscopy, and how they occurred. We will study the different parts of our experimental methodology which is the responsible for it. We will investigate laser effect on simple tissue, on bulk loaded tissue, and on filled cells, on different laser energy levels, and on different laser exposure times. With this investigation we want to know if there is a limit of the laser energy and exposure time for our research.

We want to have more informations of the morphological differences of the cells of different patients groups (if there are any) so we need more filled cells to reconstruct, and investigated under Transmission Electron Microscope.

For more informations from the human neurons behaviour, we want to investigate the dendritic integration of the spontaneous, and induced (uncaging, or electrical stimulated) signals.

8 Acknowledgements

I would like to acknowledge here the people who made this work possible: first of all my supervisor István Ulbert for all the guidance, instructions to learn the different electrophysiological measurements and imaging methods and the possibilities he gave me during this years.

I would like to thank the Group of Comparative Psychophysiology in the Institute of Cognitive Neuroscience and Psychology, Research Centre for Natural Sciences, Hungarian Academy of Sciences, (for the advices, and answers during this research, and this thesis would be much more disorganized without their constructive criticism), especially Lucia Wittner for introducing me to the field, and the principles of this study, and Kinga Tóth for training me the slice preparation techniques, and histology.

I would like to thank Balázs Rózsa and the researchers (of company Femtonics, and Institute of Cognitive Neuroscience and Psychology, Research Centre for Natural Sciences, Hungarian Academy of Sciences, Budapest, Hungary) Attila Kaszás, Dénes Pálfi, and Balázs Chiovini, who taught me the use of the Two-photon microscope, and Calcium imaging techniques.

I would like to acknowledge the surgeons (of National Institute of Clinical Neuroscience, Budapest, Hungary) especially Loránt Eröss, and Attila Bagó for the surgeries to this research.

Last, but not least, I would like to thank my family for all the support they gave me in these years.

Supported by:

Hungarian-French grant TÉT_10-1-2011-0389, GOP-1.1.1-08/1-2008-0085, Swiss-Hungarian grant SH/7/2/8, KTIA (KMR_12-1-2012-0214), Hungarian grant OTKA PD91151, Bolyai Research Fellowship (to L.W.), KTIA_NAP_13 and TÁMOP 4.2.1.B11/2/KMR2011-0002.

9 References

- [1] J. Corsellis and B. S. Meldrum, *The pathophysiology of epilepsy*, London: Edward Arnold, 1976.
- [2] R. S. Fisher, W. v. E. Boas, W. Blume, C. Elger, P. Genton, P. Lee and J. J. Engel, "Epileptic seizures and epilepsy: definitions proposed by the International League Against Epilepsy (ILAE) and the International Bureau for Epilepsy (IBE)," *Epilepsia*, vol. 46, pp. 470-472, 2005.
- [3] M. J. Morell, "Epilepsia," *Orvostudomány*, vol. 8(1), pp. 1-18, 1997.
- [4] D. D. Spencer and S. S. Spencer, "Surgery for epilepsy.," *Neurol Clin*, pp. 313-30, 1985.
- [5] P. A. Schwartzkroin, "Cellular electrophysiology of human epilepsy.," *Epilepsy Res*, pp. 185-92, 1994.
- [6] R. Kohling, A. Lucke, H. Straub, E. J. Speckmann, I. Tuxhorn, P. Wolf, H. Pannek and F. Ooppel, "Spontaneous sharp waves in human neocortical slices excised from epileptic patients.," *Brain*, pp. 121 (Pt 6):1073-1087., 1998.
- [7] D. D. Spencer and S. S. Spencer, "Hippocampal resections and the use of human tissue in defining temporal lobe epilepsy syndromes.," *Hippocampus*, pp. 243-9, 1994.
- [8] Z. Maglóczy and T. F. Freund, "Impaired and repaired inhibitory circuits in the epileptic human hippocampus.," *Trends Neurosci*, pp. 334-40, 2005.
- [9] P. A. Schwartzkroin and W. D. Knowles, "Intracellular study of human epileptic cortex: in vitro maintenance of epileptiform activity?," *Science*, pp. 223:709-712, 1984.
- [10] A. K. Roopun, J. D. Simonotto, M. L. Pierce, A. Jenkins, C. Nicholson, I. S. Schofield, R. G. Whittaker, M. Kaiser, M. A. Whittington, R. D. Traub and M. O. Cunningham, "A nonsynaptic mechanism underlying interictal discharges in human epileptic neocortex.," *Proc Natl Acad Sci U S A*, vol. 107, pp. 338-343, 2010.
- [11] C. Grienberger and A. Konnerth, "Imaging calcium in neurons.," *Neuron*, vol. 73, pp. 862-885, 2012.
- [12] G. S. Belinsky, M. T. Rich, C. L. Sirois, S. M. Short, E. Pedrosa, H. M. Lachman and S. D. Antic, "Patch-clamp recordings and calcium imaging followed by single-cell PCR reveal the developmental profile of 13 genes in iPSC-derived human neurons.," *Stem Cell Res*, vol. 12, pp. 101-118, 2014.
- [13] W. Boesmans, M. A. Martens, N. Weltens, M. M. Hao, J. Tack, C. Cirillo and P. V. Berghe, "Imaging neuron-glia interactions in the enteric nervous system.," *Front Cell Neurosci*, vol. 7, p. 183, 2013.
- [14] M. Navarrete, G. Perea, L. Maglio, J. Pastor, R. G. de Sola and A. Araque, "Astrocyte calcium signal and gliotransmission in human brain tissue.," *Cereb Cortex*, pp. 23:1240-1246., 2013.
- [15] C. Economo and G. N. Koskinas, *Die Cytoarchitektonik der Hirnrinde des erwachsenen Menschen.*, Berlin: J. Springer, 1925.
- [16] C. Economo and L. C. Triarhou, *Cellular structure of the human cerebral cortex.*, Basel: Karger Publishers, 2009.
- [17] R. Y. Cajal, *Histology of the Nervous System*, two volumes [1909-1911], Oxford University Press, 1995.
- [18] G. J. Tortora and B. Derrickson, *Principles Of Anatomy And Physiology*, 13th ed, Hoboken: John Wiley & Sons, 2012.

- [19] J. Szentágothai and M. Réthelyi, *Funkcionális anatómia*, Budapest: Medicina Könyvkiadó, 2002.
- [20] K. Brodman, *Vergleichende Lokalisationslehre der Groshirnrinde*, Leipzig: Verlag von Johann Ambrosius Barth, 1909.
- [21] J. Talairach and P. Tournoux, *Co-planar Stereotaxic Atlas of the Human Brain*, New York: Thieme Medical, 1988.
- [22] L. Triarhou, "A proposed number system for the 107 cortical areas of Economo and Koskinas, and Brodmann area correlations," *Stereotact Funct Neurosurg*, vol. 85, pp. 204-215, 2007.
- [23] P. Roland and K. Zilles, "Structural divisions and functional fields in the human cerebral cortex," *Brain Research Reviews*, vol. 26, pp. 87-105, 1998.
- [24] J. Szabadics, C. Varga, G. Molnar, S. Olah, P. Barzo and G. Tamas, "Excitatory effect of GABAergic axo-axonic cells in cortical microcircuits," *Science*, vol. 311, pp. 233-235, 2006.
- [25] B. W. Connors, M. J. Gutnick and D. A. Prince, "Electrophysiological properties of neocortical neurons in vitro.," *J Neurophysiol*, vol. 48, pp. 1302-1320, 1982.
- [26] B. W. Connors and M. J. Gutnick, "Intrinsic firing patterns of diverse neocortical neurons.," *Trends Neurosci*, vol. 13, pp. 99-104, 1990.
- [27] A. Nunez, F. Amzica and M. Steriade, "Electrophysiology of cat association cortical cells in vivo: intrinsic properties and synaptic responses.," *J Neurophysiol*, vol. 70, pp. 418-430, 1993.
- [28] M. Steriade, I. Timofeev and F. Grenier, "Natural waking and sleep states: A view from inside neocortical neurons.," *J Neurophysiol*, vol. 85, pp. 1969-1985, 2001.
- [29] M. Steriade and I. Timofeev, "Neuronal plasticity in thalamocortical networks during sleep and waking oscillations.," *Neuron*, vol. 37, pp. 563-576, 2003.
- [30] Y. Chagnac-Amitai, H. J. Luhmann and D. A. Prince, "Burst generating and regular spiking layer 5 pyramidal neurons of rat neocortex have different morphological features.," *J Comp Neurol*, vol. 296, pp. 598-613, 1990.
- [31] Y. Nishimura, H. S. K. Kitagawa, M. Asahi, K. Itoh, K. Yoshioka, T. T. T. Asahara and T. Yamamoto, "The burst firing in the layer III and V pyramidal neurons of the cat sensorimotor cortex in vitro.," *Brain Res*, vol. 727, pp. 212-216, 1996.
- [32] M. Steriade and R. W. McCarley, *Brainstem control of wakefulness and sleep.*, New York: Plenum Press, 2005.
- [33] M. Abeles, *Corticonics : neural circuits of the cerebral cortex.*, Cambridge: Cambridge University Press, 1991.
- [34] E. M. Kasper, A. U. Larkman, J. Lubke and C. Blakemore, "Pyramidal neurons in layer 5 of the rat visual cortex. I. Correlation among cell morphology, intrinsic electrophysiological properties, and axon targets.," *J Comp Neurol*, vol. 339, pp. 459-474, 1994.
- [35] J. Lubke, V. Egger, B. Sakmann and D. Feldmeyer, "Columnar organization of dendrites and axons of single and synaptically coupled excitatory spiny neurons in layer 4 of the rat barrel cortex.," *J Neurosci*, vol. 20, pp. 5300-5311, 2000.
- [36] C. D. Gilbert and T. N. Wiesel, "Morphology and intracortical projections of functionally characterised neurones in the cat visual cortex.," *Nature*, vol. 280, pp. 120-125, 1979.
- [37] H. Markram, M. Toledo-Rodriguez, Y. Wang, A. Gupta, G. Silberberg and C. Wu, "Interneurons of the neocortical inhibitory system.," *Nat Rev Neurosci*, vol. 5, pp. 793-807, 2004.

- [38] P. Somogyi, G. Tamas, R. Lujan and E. H. Buhl, "Salient features of synaptic organisation in the cerebral cortex.," *Brain Res Brain Res Rev*, vol. 26, pp. 113-135, 1998.
- [39] A. Peters and E. G. Jones, *Cerebral cortex*, New York: Plenum Press, 1984.
- [40] I. N. G. Petilla, G. A. Ascoli, L. Alonso-Nanclares, S. A. Anderson, G. Barrionuevo, R. Benavides-Piccione, A. Burkhalter, G. Buzsaki, B. Cauli, J. Defelipe, A. Fairen, D. Feldmeyer, G. Fishell, Y. Fregnac, T. F. Freund, D. Gardner, E. P. Gardner and J. Goldberg, "Petilla terminology: nomenclature of features of GABAergic interneurons of the cerebral cortex.," *Nat Rev Neurosci*, vol. 9, pp. 557-568, 2008.
- [41] M. Nelson and J. Rinzel, *The Hodgkin-Huxley Model*, New York: Springer, 1990.
- [42] E. Lábos, "Az Elektrofiziológia Fejlődésének Állomásai," *Fiz. Szle*, vol. 6, p. 195, 1996.
- [43] J. A. Kiernan and M. L. Barr, *Barr's the Human Nervous System: An Anatomical Viewpoint 9th ed*, Lippincott Williams & Wilkins, 2009.
- [44] L. Sherwood, *Human Physiology: From Cells to Systems*, Cengage Learning, 2010.
- [45] F. Bezanilla, "Review: The action potential: From voltage-gated conductances to molecular structures," *Biol. Res.*, vol. 39, p. 425-435, 2006.
- [46] S. Sanei and J. A. Chambers, *EEG Signal Processing*, John Wiley & Sons, 2007.
- [47] J. Kropotov, *Quantitative EEG, Event-Related Potentials and Neurotherapy.*, London: Academic Press, 2008.
- [48] E. Niedermeyer and F. H. L. da Silva, *Electroencephalography: Basic Principles, Clinical Applications, and Related Fields 5th edition*, Philadelphia: Lippincott Williams & Wilkins, 2005.
- [49] S. Sanei, *Adaptive Processing of Brain Signals*, Chichester: John Wiley & Sons, 2013.
- [50] F. Bretschneider and J. R. de Weille, *Introduction to Electrophysiological Methods and Instrumentation.*, Oxford: Elsevier Ltd, 2006.
- [51] R. Cooper, J. W. Osselton and J. C. Shaw, *EEG technology*, Butterworth-Heinemann, 1974.
- [52] C. Gold, D. A. Henze, C. Koch and G. Buzsáki, "On the Origin of the Extracellular Action Potential Waveform: A Modeling Study," *Journal of Neurophysiology*, vol. 95, no. 5, pp. 3113-3128, 2006.
- [53] M. Carter and J. C. Shieh, *Guide to Research Techniques in Neuroscience*, Oxford: Elsevier Inc, 2010.
- [54] S. Veitinger, *The Patch-Clamp Technique: An Introduction*, Science Lab, 2011.
- [55] R. Cserscsa, D. B. D. Fabo, L. Wittner, L. Eross, L. Entz, A. Solyom, G. Rasonyi, A. Szucs, A. Kelemen, R. Jakus, V. Juhos, L. Grand, A. Magony, P. Halasz, T. F. Freund, Z. Maglóczy, S. S. Cash, L. Papp, G. Karmos and E. Halgren, "Laminar analysis of slow wave activity in humans.," *Brain*, vol. 133, pp. 2814-29, 2010.
- [56] D. Fabó, Z. Maglóczy, L. Wittner, A. Pék, L. Eröss, S. Czirják, J. Vajda, A. Solyom, G. Rasonyi, A. Szűcs, A. Kelemen, V. Juhos, L. Grand, B. Dombovári, P. Halász, T. F. Freund, E. Halgren, G. Karmos and I. Ulbert, "Properties of in vivo interictal spike generation in the human subiculum.," *Brain*, vol. 131, pp. 485-499, 2008.
- [57] P. Gloor, "Hans Berger on Electroencephalography," in *American Journal of EEG Technology*, 1969, pp. 1-8.
- [58] H. Berger, "Über das Elektrenkephalogramm des Menschen.," *Arch. Psychiat. Nervenkr.*, vol. 87, p. 527-570, 1929.
- [59] P. Halász and A. Fogarasi, *Epilepszia esetkönyv: Sikerek, kudarcok, tanulságok*, Budapest: GARBO Kiadó, 2010.

- [60] P. Halász, *Epilepszia: ablak az agyra*, Budapest: GARBO KIADÓ, 2007.
- [61] P. Halász, *Epilepszia*, Budapest: Medicina könyvkiadó ZRT., 2008.
- [62] P. Halász and P. Rajna, *A felnőttkori epilepszia EEG atlasza - The EEG of adulthood epilepsy*, Innomark, 1990.
- [63] W. Penfield and H. Jasper, *Epilepsy and the functional anatomy of the human brain*, Oxford, England: Little, Brown & Co, 1954.
- [64] A. T. B. David, J. Thurman, E. Beghi, C. E. Begley, W. A. H. Jeffrey, R. Buchhalter, D. Ding, D. C. Hesdorffer, K. L. L. Kazis, R. Kobau, B. Kroner, D. Logroscino, M. T. Medina, C. R. Newton, A. S. A. Pascal, P. M. Preux, J. W. Sander, T. T. W. Theodore and S. Weibe, "Standards for epidemiologic studies and surveillance of epilepsy," *Epilepsia*, 2011.
- [65] P. Shackleton and R. G. J. Westendorp, "Mortality in patients with epilepsy: 40 years of follow up in a Dutch cohort study," *J. Neurol. Neurosurgery, Psychiatry*, vol. 66, p. 636-640, 1999.
- [66] R. C. Green, "Neuropathology and behavior in epilepsy.," in *Epilepsy and Behavior*, Wiley-Liss, Inc, 1991, pp. 345-359.
- [67] L. M. de la Prida and A. J. Trevelyan, "Cellular mechanisms of high frequency oscillations in epilepsy: on the diverse sources of pathological activities.," *Epilepsy Res*, vol. 97, pp. 308-17, 2011.
- [68] Z. Maglóczy, "Sprouting in human temporal lobe epilepsy: excitatory pathways and axons of interneurons.," *Epilepsy Res*, vol. 89, pp. 52-59, 2010.
- [69] J. H. Margerison and J. A. Corsellis, "Epilepsy and the temporal lobes. A clinical, electroencephalographic and neuropathological study of the brain in epilepsy, with particular reference to the temporal lobes.," *Brain*, vol. 89, pp. 499-530, 1966.
- [70] H. J. Meencke and G. Veith, "Hippocampal sclerosis in epilepsy," in *H. Luders (Ed.), Epilepsy Surgery*, New York, Raven Press, 1991, pp. 705-715.
- [71] L. A. Miller, D. G. Munoz and M. Finmore, "Hippocampal sclerosis and human memory," *Arch Neurol*, pp. 391-394, 1993.
- [72] N. Nakasato, M. F. Lévesque and T. L. Babb, "Seizure outcome following standard temporal lobectomy: correlation with hippocampal neuron loss and extrahippocampal pathology.," *J Neurosurg*, pp. 194-200, 1992.
- [73] T. H. Swanson, "The pathophysiology of human mesial temporal lobe epilepsy," *J Clin Neurophysiol*, pp. 2-22, 1995.
- [74] E. K. Avila, "Tumor Associated Epilepsy," in *Clinical Management and Evolving Novel Therapeutic Strategies for Patients with Brain Tumors*, T. Lichter, Ed. InTech, 2013.
- [75] K. F. Rajneesh and D. K. Binder, "Tumor-associated epilepsy," *Neurosurg. Focus*, vol. 27, p. E4, 2009.
- [76] J. Grewal, H. K. Grewal and A. D. Forman, "Seizures and epilepsy in cancer: etiologies, evaluation, and management," *Curr. Oncol. Rep.*, vol. 10, pp. 63-71, 2008.
- [77] A. A. Raymond, M. Cook, D. R. Fish and S. D. Shorvon, "Cortical dysgenesis in adults with epilepsy," in *Magnetic Resonance Scanning and Epilepsy*, vol. 264, Plenum Press, 1994, pp. 89-94.
- [78] J. Janszky, "Az epilepszia diagnózisa," *Idegyogy. Sz.*, vol. 57, p. 157-164, 2004.
- [79] S. Shorvon, "I of Cortical Dysgenesis," *Epilepsia*, vol. 38, p. Suppl. 13-18, 1997.

- [80] I. Cohen, V. Navarro, S. Clemenceau, M. Baulac and R. Miles, "On the origin of interictal activity in human temporal lobe epilepsy in vitro.," *Science*, vol. 298, pp. 1418-1421, 2002.
- [81] C. Wozny, A. Knopp, T. N. Lehmann, U. Heinemann and J. Behr, "The subiculum: a potential site of ictogenesis in human temporal lobe epilepsy.," *Epilepsia*, vol. 46, pp. 17-21, 2005.
- [82] G. Huberfeld, L. Wittner, S. Clemenceau, M. Baulac, K. Kaila, R. Miles and C. Rivera, "Perturbed chloride homeostasis and GABAergic signaling in human temporal lobe epilepsy.," *J Neurosci*, vol. 27, p. 9866–9873, 2007.
- [83] L. Wittner, G. Huberfeld, S. Clémenceau, L. Eross, E. Dezaamis, L. Entz, I. Ulbert, M. Baulac, T. F. Freund, Z. Maglóczy and R. Miles, "The epileptic human hippocampal cornu ammonis 2 region generates spontaneous interictal-like activity in vitro.," *Brain*, vol. 132, p. 3032–3046, 2009.
- [84] M. R. Karlócai, Z. Kohus, S. Káli, I. Ulbert, G. Szabo, Z. Máté, T. F. Freund and G. A. I, "Physiological sharp wave-ripples and interictal events in vitro: what's the difference?," *Brain*, vol. 137, pp. 463-85, 2014.
- [85] L. Wittner, Z. Jakab, P. Vaci and I. Ulbert, "Patterns of sharp-wave ripple complexes in the rat hippocampus in vitro," *J. Neurosci*.
- [86] R. Köhling, J. M. Höhling, H. Straub, D. Kuhlmann, U. Kuhnt, I. Tuxhorn, A. Ebner, P. Wolf, H. W. Pannek, A. Gorji and E. J. Speckmann, "Optical monitoring of neuronal activity during spontaneous sharp waves in chronically epileptic human neocortical tissue.," *J. Neurophysiol*, vol. 84, pp. 2161-2165, 2000.
- [87] R. Köhling, M. Qü, K. Zilles and E. J. Speckmann, "Current source density profiles associated with sharp waves in human epileptic neocortical tissue," *Neuroscience*, vol. 94, p. 1039–1050, 1999.
- [88] K. T. Hofer, Á. Kandrás, I. Ulbert, I. Pál, C. Szabó, L. Héja and L. Wittner, "The hippocampal CA3 region can generate two distinct types of sharp wave-ripple complexes, in vitro.," *Hippocampus*, vol. 25, p. 169–186, 2015.
- [89] M. Göppert-Mayer, "Über Elementarakte mit zwei Quantensprüngen.," *Annalen der*, vol. 401, pp. 273-294, 1931.
- [90] W. Denk, J. H. Strickler and W. W. Webb, "Two-photon laser scanning fluorescence microscopy," *Science*, vol. 248, pp. 73-76, 1990.
- [91] A. Grinvald and R. Hildesheim, "Vsd: a New Era in Functional Imaging of Cortical Dynamics," *Nature Reviews Neuroscience*, vol. 5, pp. 874-885, 2004.
- [92] W. Müller and J. A. CONNOR, "Dendritic spines as individual neuronal compartments for synaptic Ca²⁺ responses," *Nature*, vol. 354, pp. 73 - 76, 1991.
- [93] J. A. Conchello and J. W. Lichtman, "Optical sectioning microscopy," *Nature Methods*, vol. 2, pp. 920-931, 2005.
- [94] W. Denk and K. Svoboda, "Photon upmanship: why multiphoton imaging is more than a gimmick," *Neuron*, vol. 18, p. 351–357, 1997.
- [95] V. E. Centonze and J. G. White, "Multiphoton excitation provides optical sections from deeper within scattering specimens than confocal imaging.," *Biophys J*, vol. 75, p. 2015–2024, 1998.
- [96] B. Rózsa, *Hippokampális interneuronok dendritikus Ca²⁺ szignalizációjának mérése 2-foton pásztázó mikroszkóp technológiával (Doktori értekezés (Ph.D.))*, 2006.
- [97] W. R. Zipfel, R. M. Williams and W. W. Webb, "Nonlinear magic: multiphoton microscopy in the biosciences," *Nat Biotechnol*, vol. 21, pp. 1369-1377, 2003.

- [98] B. A. Flusberg, E. D. Cocker, W. Piyawattanametha, J. C. Jung, E. L. Cheung and M. J. Schnitzer, "Fiber-optic fluorescence imaging," *Nat Methods*, vol. 2, pp. 941-950, 2005.
- [99] F. Helmchen and W. Denk, "Deep tissue two-photon microscopy," *Nat Methods*, vol. 2, pp. 932-940, 2005.
- [100] R. D. Frostig, *In Vivo Optical imaging of brain function*, Boca Raton: FL: CRC Press, 2009.
- [101] H. J. Koester, D. Baur, R. Uhl and S. W. Hell, "Ca²⁺ fluorescence imaging with pico- and femtosecond two-photon excitation: signal and photodamage," *Biophys J*, vol. 77, p. 2226-2236, 1999.
- [102] W. Göbel and F. Helmchen, "In vivo calcium imaging of neural network function," *Physiology*, vol. 22, pp. 358-365, 2007.
- [103] M. Hubener and T. Bonhoeffer, "Visual cortex: two-photon excitement," *Curr. Biol.*, vol. 15, p. R205-R208, 2005.
- [104] O. Garaschuk, R. I. Milos, C. Grienberger, N. Marandi, H. Adelsberger and A. Konnerth, "Optical monitoring of brain function in vivo: from neurons to networks," *Pflugers Arch*, vol. 453, pp. 385-396, 2006.
- [105] K. Svoboda and R. Yasuda, "Principles of two-photon excitation microscopy and its applications to neuroscience," *Neuron*, vol. 50, pp. 823-839, 2006.
- [106] J. N. Kerr and W. Denk, "Imaging in vivo: watching the brain in action," *Nat. Rev. Neurosci.*, vol. 9, pp. 195-205, 2008.
- [107] D. H. O'Connor, D. Huber and K. Svoboda, "Reverse engineering the mouse brain," *Nature*, vol. 461, pp. 923-929, 2009.
- [108] B. Chiovini, G. F. Turi, G. Katona, A. Kaszás, F. Erdélyi, G. Szabó, H. Monyer, A. Csákányi, E. S. Vizi and B. Rózsa, "Enhanced dendritic action potential backpropagation in parvalbumin-positive basket cells during sharp wave activity," *Neurochem Res*, vol. 35, pp. 2086-2095, 2010.
- [109] W. Denk, J. R. Holt, G. M. Shepherd and D. P. Corey, "Calcium imaging of single stereocilia in hair cells: Localization of transduction channels at both ends of tip links," *Neuron*, vol. 15, p. 1311-1321, 1995.
- [110] Z. F. Mainen, R. Malinow and K. Svoboda, "Synaptic calcium transients in single spines indicate that NMDA receptors are not saturated," *Nature*, vol. 399, pp. 151-155, 1999.
- [111] M. Oheim, E. Beaurepaire, E. Chaigneau, J. Mertz and S. Charpak, "Two-photon microscopy in brain tissue: parameters influencing the imaging depth," *J Neuroscience Methods*, vol. 111, p. 29-37, 2001.
- [112] P. Theer, M. T. Hasan and W. Denk, "Two-photon imaging to a depth of 1000 micron in living brains by use of a Ti:Al₂O₃ regenerative amplifier," *Opt Lett*, vol. 28, p. 1022-1024, 2003.
- [113] G. Y. Fan, H. Fujisaki, A. Miyawaki, R. K. Tsay, R. Y. Tsien and M. H. Ellisman, "Video-rate scanning two-photon excitation fluorescence microscopy and ratio imaging with cameleons," *Biophys J*, vol. 76, pp. 2412-2420, 1999.
- [114] Q. T. Nguyen, N. Callamaras, C. Hsieh and I. Parker, "Construction of a two-photon microscope for video-rate Ca(2+) imaging," *Cell Calcium*, vol. 30, pp. 383-393, 2001.
- [115] A. Losonczy and J. C. Magee, "Integrative properties of radial oblique dendrites in hippocampal CA1 pyramidal neurons," *Neuron*, vol. 50, pp. 291-307, 2007.
- [116] A. Kaplan, N. Friedman and N. Davidson, "Acousto-optic lens with very fast focus scanning," *Opt Lett*, vol. 26, pp. 1078-1080, 2001.

- [117] G. D. Reddy and P. Saggau, "Fast three-dimensional laser scanning scheme using acousto-optic deflectors," *J Biomed Opt*, vol. 10(6), p. 064038, 2005.
- [118] V. Iyer, T. M. Hoogland and P. Saggau, "Fast functional imaging of single neurons using random-access multiphoton (RAMP) microscopy," *J Neurophysiol*, vol. 95, pp. 535-545, 2006.
- [119] B. Rózsa, G. Katona, E. S. Vizi, Z. Varallyay, A. Saghy, L. Valenta, P. Maak, J. Fekete, A. Banyasz and R. Szipocs, "Random access three-dimensional two-photon microscopy," *Appl Opt*, vol. 46, pp. 1860-1865, 2007.
- [120] D. Vucinic and T. J. Sejnowski, "A compact multiphoton 3D imaging system for recording fast neuronal activity," *PLoS One*, vol. 2(8), pp. e699. 1-12, 2007.
- [121] G. Duemani Reddy, K. Kelleher, R. Fink and P. Saggau, "Three-dimensional random access multiphoton microscopy for functional imaging of neuronal activity," *Nat Neurosci*, vol. 11, pp. 713-720, 2008.
- [122] B. F. Grewe, F. F. Voigt, M. van 't Hoff and F. Helmchen, "Fast two-layer two-photon imaging of neuronal cell populations using an electrically tunable lens," *Biomed Opt Express*, vol. 2, pp. 2035-2046, 2011.
- [123] P. A. Kirkby, K. M. S. Nadella and R. A. Silver, "A compact Acousto-Optic Lens for 2D and 3D femtosecond based 2-photon microscopy," *Opt Express*, vol. 18, pp. 13720-13744, 2010.
- [124] B. K. Ngoi, K. Venkatakrishnan, L. E. Lim and B. Tan, "Angular dispersion compensation for acousto-optic devices used for ultrashort-pulsed laser micromachining," *Opt Express*, vol. 9, pp. 200-206, 2001.
- [125] J. D. Lechleiter, D. T. Lin and I. Sieneart, "Multi-photon laser scanning microscopy using an acoustic optical deflector," *Biophys J*, vol. 83, p. 2292-2299, 2002.
- [126] V. Iyer, B. E. Losavio and P. Saggau, "Compensation of spatial and temporal dispersion for acousto-optic multiphoton laser-scanning microscopy," *J Biomed Opt*, vol. 8(3), pp. 460-471, 2003.
- [127] G. Katona, A. Kaszas, G. F. Turi, N. Hajos, G. Tamas, E. S. Vizi and B. Rozsa, "Roller Coaster Scanning reveals spontaneous triggering of dendritic spikes in CA1 interneurons," *Proc Natl Acad Sci*, vol. 108, p. 2148-2153, 2011.
- [128] C. A. Combs, A. Smirnov, D. Chess, D. B. McGavern, J. L. Schroeder, J. Riley, S. S. Kang, M. Lugar-Hammer, A. Gandjbakhche, J. R. Knutson and R. S. Balaban, "Optimizing multiphoton fluorescence microscopy light collection from living tissue by noncontact total emission detection (epiTED)," *J Microsc*, vol. 241, pp. 153-161, 2011.
- [129] M. J. Berridge, P. Lipp and M. D. Bootman, "The versatility and universality of calcium signalling," *Nat Rev Mol Cell Biol*, vol. 1, pp. 11-21, 2000.
- [130] M. J. Berridge, M. D. Bootman and H. L. Roderick, "Calcium signalling: Dynamics, homeostasis and remodelling," *Nat Rev Mol Cell Biol*, vol. 4, pp. 517-529, 2003.
- [131] G. Stuart, N. Spruston, B. Sakmann and M. Häusser, "Action potential initiation and backpropagation in neurons of the mammalian CNS," *Cell Press Trends in Neuroscience*, vol. 20, p. 125-131, 1997.
- [132] B. R. Christie, J. C. Magee and D. Johnston, "The role of dendritic action potentials and Ca²⁺ influx in the induction of homosynaptic long-term depression in hippocampal CA1 pyramidal neurons," *Learning and Memory*, vol. 3, pp. 160-169, 1996.
- [133] J. C. Magee and D. Johnston, "A synaptically controlled, associative signal for Hebbian plasticity in hippocampal neurons," *Science*, vol. 275, pp. 209-213, 1997.

- [134] D. B. Jaffe, D. Johnston, N. Lasser-Ross, J. E. Lisman, H. Miyakawa and W. N. Ross, "The spread of Na⁺ spikes determines the pattern of dendritic Ca²⁺ entry into hippocampal neurons," *Nature*, vol. 357, pp. 244 - 246, 1992.
- [135] H. Markram, P. J. Helm and S. B. "Dendritic calcium transients evoked by single back-propagating action potentials in rat neocortical pyramidal neurons," *Journal of Physiology*, vol. 485, pp. 1-20, 1995.
- [136] F. Helmchen, K. Imoto and B. Sakmann, "Ca²⁺ buffering and action potential-evoked Ca²⁺ signaling in dendrites of pyramidal neurons," *Cell Press Biophysical journal*, vol. 70(2), p. 1069–1081., 1996.
- [137] T. Pozzan, P. Arslan, R. Y. Tsien and T. J. Rink, "Anti-immunoglobulin, cytoplasmic free calcium, and capping in B lymphocytes," *Cell Biol*, vol. 94, pp. 335-340 , 1982.
- [138] R. Y. Tsien, T. Pozzan and T. J. Rink, "Calcium homeostasis in intact lymphocytes: cytoplasmic free Ca²⁺ monitored with a new, intracellularly trapped fluorescent indicator," *Cell biol*, vol. 94, pp. 325-334 , 1982.
- [139] R. Y. Tsien and T. Pozzan, "Measurement of cytosolic free Ca²⁺ with quin-2 practical aspects," *Methods Enzymol*, vol. 172, p. 230–261, 1989.
- [140] G. Grynkiewicz, M. Poenie and R. Y. Tsien, "A new generation of Ca²⁺ indicators with greatly improved fluorescence properties," *J. Biol. Chem.*, vol. 260, pp. 3440-3450., 1992.
- [141] E. Neher, "The use of fura-2 for estimating Ca²⁺ buffers and Ca²⁺ fluxes," *Neuropharmacology*, vol. 34, p. 1423–1442, 1995.
- [142] R. M. Paredes, J. C. Etzler, L. T. Watts, W. Zheng and J. D. Lechleiter, "Chemical calcium indicators.," *Methods*, vol. 46, p. 143–151, 2008.
- [143] A. Miyawaki, J. Llopis, R. Heim, J. M. McCaffery, J. A. Adams, M. Ikura and R. Y. Tsien, "Fluorescent indicators for Ca²⁺ based on green fluorescent proteins and calmodulin," *Nature*, vol. 388, pp. 882-887 , 1997.
- [144] G. Tamas, A. Lorincz, A. Simon and J. Szabadics, "Identified sources and targets of slow inhibition in the neocortex," *Science*, vol. 299 , pp. 1902-1905, 2003.
- [145] B. Rozsa, T. Zelles, S. E. Vizi and B. Lendvai, "Distance-dependent scaling of calcium transients evoked by backpropagating spikes and synaptic activity in dendrites of hippocampal interneurons," *J Neurosci*, vol. 24, p. 661– 670, 2004.
- [146] B. Rozsa, G. Katona, A. Kaszas, R. Szipocs and S. E. Vizi, "Dendritic nicotinic receptors modulate backpropagating action potentials and long-term plasticity of interneurons.," *Eur J Neurosci*, vol. 27, p. 364–377, 2008.
- [147] M. Maravall, Z. F. Mainen, B. L. Sabatini and K. Svoboda, "Estimating intracellular calcium concentrations and buffering without wavelength ratioing.," *Biophys. J.*, vol. 78, p. 2655–2667, 2000.
- [148] B. P. Kerekes, K. Tóth, A. Kaszás, B. s Chiovini, Z. Szadai, G. Szalay, D. Pálfi, A. Bagó, K. Spitzer, B. Rózsa, I. Ulbert and L. Wittner, "Combined two-photon imaging, electrophysiological, and anatomical investigation of the human neocortex in vitro.," *Neurophotonics*, vol. 1, pp. 011013-1-10, 2014.
- [149] N. Hájos, T. J. Ellender, R. Zemankovics, E. O. Mann, R. Exley, S. J. Cragg, T. F. Freund and O. Paulsen, "Maintaining network activity in submerged hippocampal slices: importance of oxygen supply," *Eur J Neurosci*, vol. 29, p. 319–327, 2009.
- [150] A. Nimmerjahn, F. Kirchhoff, J. N. Kerr and F. Helmchen, "Sulforhodamine 101 as a specific marker of astroglia in the neocortex in vivo.," *Nat Methods*, vol. 1, pp. 31 - 37, 2004.
- [151] J. N. Kerr, D. Greenberg and F. Helmchen, "Imaging input and output of neocortical networks in vivo," *Proc Natl Acad Sci*, vol. 102, p. 14063–14068, 2005.

- [152] G. Katona, G. Szalay, P. Maák, A. Kaszás, M. Veress, D. Hillier, B. Chiovini, E. S. Vizi, B. Roska and B. Rózsa, "Fast two-photon in vivo imaging with three-dimensional random-access scanning in large tissue volumes," *Nat Methods*, vol. 9, p. 201–208, 2012.
- [153] I. Ulbert, E. Halgren, G. Heit and G. Karmos, "Multiple microelectrode-recording system for human intracortical applications.," *J Neurosci Methods*, vol. 106, pp. 69–79, 2001.
- [154] I. Ulbert, Z. Maglóczy, L. Erőss, S. Czirják, J. Vajda, L. Bognár, S. Tóth, Z. Szabó, P. Halász, D. Fabó, E. Halgren, T. F. Freund and G. Karmos, "In vivo laminar electrophysiology co-registered with histology in the hippocampus of patients with temporal lobe epilepsy," *Exp Neurol*, vol. 187, p. 310–318, 2004.
- [155] A. Lőrincz, B. Rózsa, G. Katona, E. S. Vizi and G. Tamás, "Differential distribution of NCX1 contributes to spine-dendrite compartmentalization in CA1 pyramidal cells.," *Proc Natl Acad Sci*, vol. 104, p. 1033–1038, 2007.
- [156] L. Wittner, D. A. Henze, L. Záborszky and G. Buzsáki, "Three-dimensional reconstruction of the axon arbor of a CA3 pyramidal cell recorded and filled in vivo.," *Brain Struct Funct*, vol. 212, pp. 75–83, 2007.
- [157] N. L. Rochefort, O. Garaschuk, R. I. Milos, M. Narushima, N. Marandi, B. Pichler, Y. Kovalchuk and A. Konnerth, "Sparsification of neuronal activity in the visual cortex at eye-opening.," *Proc Natl Acad Sci*, vol. 106, p. 15049–15054, 2009.
- [158] H. Lutcke, M. Murayama, T. Hahn, D. J. Margolis, S. Astori, S. M. Z. A. Borgloh, W. Gobel, Y. Yang, W. Tang, S. Kugler, R. Sprengel, T. Nagai, A. Miyawaki, M. E. Larkum, F. Helmchen and M. T. Hasan, "Optical recording of neuronal activity with a genetically-encoded calcium indicator in anesthetized and freely moving mice.," *Front Neural Circuits*, vol. 4, pp. 1–12, 2010.
- [159] M. E. Larkum, T. Nevian, M. Sandler, A. Polsky and J. Schiller, "Synaptic integration in tuft dendrites of layer 5 pyramidal neurons: a new unifying principle," *Science*, vol. 325, pp. 756–760, 2009.
- [160] T. Abrahamsson, L. Cathala, K. Matsui, R. Shigemoto and D. A. DiGregorio, "Thin dendrites of cerebellar interneurons confer sublinear synaptic integration and a gradient of short-term plasticity.," *Neuron*, vol. 73, p. 1159–1172, 2012.
- [161] K. Vervaeke, A. Lőrincz, Z. Nusser and R. A. Silver, "Gap junctions compensate for sublinear dendritic integration in an inhibitory network.," *Science*, vol. 335, pp. 1624–1628, 2012.
- [162] G. N. Elston, R. Benavides-Piccione, A. Elston, B. Zietsch, J. Defelipe, P. Manger, V. Casagrande and J. H. Kaas, "Specializations of the granular prefrontal cortex of primates: implications for cognitive processing," *Anat Rec A Discov Mol Cell Evol Biol*, 2006.
- [163] B. Chiovini, G. F. Turi, G. Katona, A. Kaszás, D. Pálfi, P. Maák, G. Szalay, M. F. Szabó, G. Szabó, Z. Szadai, S. Káli and B. Rózsa, "Dendritic Spikes Induce Ripples in Parvalbumin Interneurons during Hippocampal Sharp Waves," *Neuron*, vol. 82, p. 908–924, 2014.
- [164] H. Duan, S. L. Wearne, J. H. Morrison and P. R. Hof, "Quantitative analysis of the dendritic morphology of corticocortical projection neurons in the macaque monkey association cortex," *Neuroscience*, vol. 114, p. 349–359, 2002.
- [165] T. P. Wong, G. Marchese, M. A. Casu, A. Ribeiro-da-Silva, A. C. Cuello and Y. De Koninck, "Loss of presynaptic and postsynaptic structures is accompanied by compensatory increase in action potential-dependent synaptic input to layer V neocortical pyramidal neurons in aged rats.," *J Neurosci*, vol. 20(22), pp. 8596–8606, 2000.

- [166] M. Marx and D. Feldmeyer, "Morphology and physiology of excitatory neurons in layer 6b of the somatosensory rat barrel cortex," *Cereb Cortex*, vol. 23 (12), pp. 2803-2817, 2013.
- [167] K. I. van Aerde and D. Feldmeyer, "Morphological and Physiological Characterization of Pyramidal Neuron Subtypes in Rat Medial Prefrontal Cortex," *Cereb Cortex*, vol. 25, pp. 788-805, 2013.
- [168] H. J. Koester and B. Sakmann, "Calcium dynamics associated with action potentials in single nerve terminals of pyramidal cells in layer 2/3 of the young rat neocortex," *J Physiol*, vol. 529, p. 625—646, 2000.
- [169] N. Holderith, A. Lőrincz, K. G. B. Rózsa, A. Kulik, M. Watanabe and Z. Nusser, "Release probability of hippocampal glutamatergic terminals scales with the size of the active zone.," *Nat Neurosci*, vol. 15, p. 988-997, 2012.
- [170] D. G. Jay, "Selective destruction of protein function by chromophore-assisted laser inactivation," *Proc Natl Acad Sci*, vol. 85, p. 5454-5458, 1988.
- [171] M. Grabenbauer, W. J. Geerts, J. Fernandez-Rodriguez, A. Hoenger, A. J. Koster and T. Nilsson, "Correlative microscopy and electron tomography of GFP through photooxidation.," *Nat Methods*, vol. 2, pp. 857 - 862, 2005.
- [172] F. S. Wang and D. G. Jay, "Chromophore-assisted laser inactivation (CALI): probing protein function in situ with a high degree of spatial and temporal resolution.," *Trends Cell Biol*, vol. 6, p. 442-445, 1996.
- [173] K. Jacobson, Z. Rajfur, E. Vitriol and K. Hahn, "Chromophore-assisted laser inactivation in cell biology," *Trends Cell Biol*, vol. 18, p. 443-450, 2008.
- [174] J. J. J. Reiners, P. Agostinis, K. Berg, N. L. Oleinick and D. Kessel, "Assessing autophagy in the context of photodynamic therapy.," *Autophagy*, vol. 6, pp. 7-18, 2010.
- [175] G. Foffani, Y. G. Uzcategui, B. Gal and L. M. de la Prida, "Reduced spike-timing reliability correlates with the emergence of fast ripples in the rat epileptic hippocampus," *Neuron*, vol. 55, p. 930-941, 2007.

10 Publications

10.1 Papers

Combined two-photon imaging, electrophysiological, and anatomical investigation of the human neocortex in vitro.

Bálint Péter Kerekes, Kinga Tóth, Attila Kaszás, Balázs Chiovini, Zoltán Szadai, Gergely Szalay, Dénes Pálfı, Attila Bagó, Klaudia Spitzer, Balázs Rózsa, István Ulbert, Lucia Wittner
Neurophotonics 1:(1) pp. 111. (2014)

In vivo validation of the electronic depth control probes

Balázs Dombovári, Richárd Fiáth, **Bálint Péter Kerekes**, Emília Tóth, Lúcia Wittner, Domonkos Horváth, Karsten Seidl, Stanislav Herwik, Tom Torfs, Oliver Paul, Patrick Ruther, Herc Neves and István Ulbert*

Biomed Tech, 2013, DOI 10.1515/bmt-2012-0102

A novel multisite silicon probe for high quality laminar neural recordings

Grand L, Pongrácz A, Vázsonyi E, Márton G, Gubán D, Fiáth R, **Kerekes B P**, Karmos G, Ulbert I, Battistig G

Sensors and Actuators A: Physical 166:(1) pp. 1421. (2011)

Torfs T, Aarts A A A, Erismis M A, Aslam J, Yazicioglu R F, Seidl K, Herwik S, Ulbert I, Dombovari B, Fiáth R, **Kerekes B P**, Puers R, Paul O, Ruther P, Van Hoof C, Neves H P

Twodimensional multichannel neural probes with electronic depth control

IEEE Transactions on Biomedical Circuits and Systems 5:(5) pp. 403412. (2011)

10.2 Posters

Multimodal analysis of the human cortical synchronous population activity in vitro

Kerekes B P, Kaszás A, Tóth K, Chiovini B, Szalay G, Pálfı D, Spitzer K, Ulbert I, Lucia W, Rózsa B

Magyar Idegtudományi Társaság XIV. Konferenciája, 2013. Jan. 17-19., Budapest, Magyarország

Analysis of the human cortical spontaneous synchronous population activity in vitro based on multimodal experiments

Bálint Péter Kerekes, Kinga Tóth, Attila Kaszás, Balázs Chiovini, Gergely Szalay, Zoltán Szadai, Dénes Pálfı, Klaudia Spitzer, Balázs Rózsa, István Ulbert, Lucia Wittner

8th FENS Forum of European Neuroscience, 2012. Jul. 14-18., Barcelona, Spanyolország

Spontán populációs aktivitás vizsgálata kombinált két foton és elektrofiziológiai módszerekkel

Bálint Péter Kerekes, Kinga Tóth, Attila Kaszás, Balázs Chiovini, Gergely Szalay, Zoltán Szadai, Dénes Pálfi, Attila Bagó, Balázs Rózsa, István Ulbert, Lucia Wittner

A Magyar Idegsebészeti Társaság 2014. évi Nemzeti Kongresszusa, 2014.nov.20-22 Budapest Magyarország

Simultaneous Electrophysiology and Ca-imaging of human cortical population activity in vitro

Bálint Péter Kerekes, Kinga Tóth, Attila Kaszás, Balázs Chiovini, Gergely Szalay, Zoltán Szadai, Dénes Pálfi, Klaudia Spitzer, Balázs Rózsa, István Ulbert, Lucia Wittner

Neuroscience 2013, Society for Neuroscience, 43rd Annual Meeting, 2013. Nov. 5-15., San Diego, USA

Torfs T, Aarts A, Erismis M A, Aslam J, Yazicioglu R F, Puers R, Van Hoof C, Neves H, Ulbert I, Dombóvari B, Fiath R, **Kerekes B P**, Seidl K, Herwik S, Ruther P

Two-dimensional multichannel neural probes with electronic depth control: 2010 IEEE Biomedical Circuits and Systems Conference, BioCAS 2010

10.3 Presentations

Simultaneous Electrophysiology and Ca-imaging of human cortical synchronous population activity in vitro

Kerekes BP, Kaszás A, Tóth K, Chiovini B, Szalay G, Pálfi D, Spitzer K, Ulbert I, Lucia W, Rózsa B

Neuronus 2014 IBRO & IRUN Neuroscience Forum, 2014.ápr.25-28 Krakow, Lengyelország

A method to analyze the human cortical spontaneous synchronous population activity in vitro

Kerekes BP, Kaszás A, Tóth K, Chiovini B, Szalay G, Pálfi D, Spitzer K, Ulbert I, Lucia W, Rózsa B

Kálmán Erika Doktori Konferencia 2014, 2014. december 10-12. Budapest Magyarország

Else

Multimodal analysis of the human cortical spontaneous synchronous population activity in vitro

Bálint Péter Kerekes

Pázmány Péter Catholic University PhD Proceedings 8: pp. 133136. (2013)

Towards combining cortical electrophysiology, fMR measurements and 2photon microscopy

Bálint Péter Kerekes

Pázmány Péter Catholic University PhD Proceedings pp. 8588. (2012)

Towards combining cortical electrophysiology and fMR measurements

Bálint Péter Kerekes

Pázmány Péter Catholic University PhD Proceedings pp. 912. (2011)